arXiv:cond-mat/0504703v1 [cond-mat.str-el] 27 Apr 2005

Renormalization, Conservation Laws and Transport in Correlated Electron Systems

Tilman Enss

Dissertation accepted by the University of Stuttgart[1]
for the degree of Doctor of Natural Sciences

Examiner: Prof. Dr. Walter Metzner
Co-examiner: Prof. Dr. Siegfried Dietrich

Max-Planck-Institut für Festkörperforschung
Stuttgart, Germany 2005

Abstract

This thesis comprises two parts centered around the functional renormalization-group framework: in the first part, I study the role of symmetries and conservation laws in approximate solutions, while in the second part I analyze Friedel oscillations and transport in Luttinger liquids with impurities.

The functional renormalization group (fRG) has been developed as a new computational tool in the theory of interacting Fermi systems. The effective behavior of a given microscopic model is calculated by solving coupled differential flow equations for the Green functions with an energy scale as the flow parameter. The symmetries of the microscopic model imply Ward identities between Green and response functions. It is shown that solutions of truncated flow-equation hierarchies satisfy Ward identities if the cutoff bare action is gauge invariant. However, truncations are generally not self-consistent approximations in the sense of Baym and Kadanoff.

The fRG is then applied to study Luttinger liquids. By computing the full spatial effective potential of a single impurity, long-range Friedel oscillations are observed in the density profile with the expected power laws for systems with up to 10^7 lattice sites. For a double barrier enclosing a dot region we find temperature regimes in which the conductance follows power laws with universal exponents, as well as non-universal crossover regimes in intermediate parameter regions.

[1] Version without the German summary; full version available online at
http://elib.uni-stuttgart.de/opus/volltexte/2005/2258/

Für Carmen

Contents

1 Introduction **5**

2 Functional renormalization group **9**

2.1 Functional formalism 10

2.1.1 Bare action 10

2.1.2 Partition function and connected Green functions 11

2.1.3 1PI vertex functions 12

2.1.4 Connected amputated Green functions 13

2.2 Renormalization-group flow equations 14

2.2.1 Regularization and flow parameters 15

2.2.2 Connected Green function flow 17

2.2.3 1PI vertex function flow 19

2.2.4 Connected amputated Green function flow 22

2.2.5 Wick-ordered Green function flow 23

2.3 Summary 25

3 Ward identities in the functional RG **27**

3.1 Gauge invariance and Ward identities 28

3.1.1 Gauge transformation 28

3.1.2 Minimal coupling in the continuum 29

3.1.3 Functional derivation of Ward identities 31

3.1.4 Momentum- and real-space formulation 32

3.2 Cutoff Ward identities 33

3.2.1 Modified Ward identities 34

3.2.2 Background-field method 37

3.2.3 Manifest gauge invariance 37

3.2.4 Ward identities in truncated flows 40

3.3 The role of self-consistency 41

3.3.1 Self-consistent Ward identities in truncated flows 43

3.3.2 Conserving approximations of Baym and Kadanoff 45

3.3.3 How important is self-consistency? 49

3.4 Summary 50

4 Functional RG technique in one dimension **53**
4.1 Microscopic model . . . 53
4.1.1 Projection method applied to the wire . . . 54
4.1.2 Bare vertices . . . 57
4.2 Functional RG flow equations . . . 57
4.2.1 Truncated 1PI flow equations . . . 57
4.2.2 Frequency cutoff at zero temperature . . . 60
4.2.3 Frequency cutoff at finite temperature . . . 61
4.2.4 Temperature flow . . . 64
4.2.5 Interaction flow . . . 66
4.2.6 Initial conditions for general filling . . . 67
4.2.7 Algorithm for tridiagonal matrices . . . 68
4.3 Flow of the density-response vertex . . . 69
4.4 Computation of the conductance . . . 71
4.4.1 Kubo formula . . . 71
4.4.2 Vertex corrections . . . 75
4.4.3 Different flow schemes . . . 77

5 Luttinger liquids with impurities **79**
5.1 Friedel oscillations . . . 80
5.1.1 Results . . . 82
5.2 Transport through double barriers . . . 84
5.2.1 Results . . . 89
5.3 Summary . . . 95

6 Conclusions and outlook **97**

A Heat equation **101**

B Efficient computation of tridiagonal loops in O(N) **103**
B.1 Propagator . . . 103
B.2 Bubble . . . 105

Bibliography **109**

Publications **117**

Acknowledgments **118**

Curriculum Vitae **120**

1 Introduction

In one-dimensional metals electrons can move freely in one direction but are confined in the two transverse directions. The interaction between the electrons leads to *Luttinger-liquid* behavior with unusual properties different from conventional (Fermi-liquid) metals. In particular, the low-energy behavior of Luttinger liquids is strongly affected by impurities. Already a single static impurity has a dramatic effect: for a repulsive interaction, the backscattering amplitude grows as the energy scale is lowered, until at $T = 0$ transport is inhibited and the chain is effectively cut into two pieces. The local density of states near an impurity, as well as the spatial density profile away from the impurity, obey characteristic power laws depending only on the bulk parameters. The conductance through a single impurity with varying parameters can be collapsed onto a single curve by a one-parameter scaling ansatz. A double barrier shows particularly rich behavior: it can be tuned to resonance, and additional scales are introduced by the separation of the two barriers and the detuning from the resonance. The conductance as a function of temperature is non-monotonous, exhibiting several distinct power laws, as well as a complex non-universal crossover behavior for intermediate parameter ranges.

In recent years experiments on carbon nanotubes have allowed to measure the effect of one or two impurities in an otherwise perfectly clean one-dimensional metal. While several field-theoretical predictions were confirmed, transport through a double barrier did not obey the expected asymptotic power laws. This led to a renewed theoretical interest to understand the behavior in intermediate parameter ranges accessible in experiments. Different analytical and computational methods applied to a spinless double-barrier model either supported or disagreed with the experimental data. This prompted us to investigate the problem with the functional renormalization-group method, which we have already used to treat complex multi-scale problems, such as Luttinger liquids with a single impurity.

The functional renormalization group (fRG) has been developed in recent years as a new computational tool to study interacting Fermi systems. It is particularly efficient in low dimensions. Starting from a specific microscopic model, high-energy modes are successively integrated out to obtain the effective behavior on all energy scales. The method captures universal scaling laws in certain limits, as well as non-universal crossover phenomena at intermediate scales.

Formally, the fRG flow equations constitute an infinite hierarchy of coupled dif-

ferential equations which describe the change of all Green functions as the energy scale is lowered. This hierarchy of flow equations produces the exact solution to all orders of perturbation theory at the end of the flow. In practice, however, the full hierarchy has to be truncated by neglecting the flow of some higher Green functions, which is justified perturbatively for weak renormalized interactions. In contrast to other renormalization-group methods we not only follow the flow of a few running couplings but of whole functions, such as the impurity potential.

For the 1D problems with one or two impurities, we approximate the interaction by an effective nearest-neighbor coupling but retain the full effective impurity potential. Our method is thus perturbative in the renormalized interaction but non-perturbative in the impurity strength. This already yields the expected universal scaling of the local density of states. In order to obtain the spatial density profile it is necessary to follow the flow of the density-response vertex. We treat the simpler case of spinless fermions; the more realistic modeling of electrons by spinful fermions is currently being considered. Our fRG results have been checked against numerically exact density-matrix renormalization group (DMRG) data for systems with up to 1000 sites. The computation of the conductance as a function of temperature requires several extensions of the method. We develop the flow of the full impurity potential at fixed, *finite* temperature, as well as the temperature-flow scheme with self-energy feedback. Moreover, it is shown that on the level of our approximation, no corrections to the current vertex appear in the Kubo formula for the conductance. We are thus able to compute the conductance consistently within one approximation over several orders of magnitude in temperature, for arbitrary impurity strength.

Besides the formal developments, the practical feasibility of the method depends crucially on the required computation time. Using a little-known mathematical theorem, an algorithm has been developed which scales linearly in the system size, instead of quadratically. For a lattice of 60.000 sites, the zero-temperature flow now takes minutes instead of days, and systems of up to 10^7 sites have been computed. This allows to find interesting regions in a large parameter space much more quickly.

The vanishing of current-vertex corrections to the conductance is an example of a more general topic: the role of *symmetries* and *conservation laws* in the fRG formalism. The microscopic model considered above, for instance, has a local $U(1)$ gauge symmetry which implies charge conservation. As a consequence, the exact Green functions are related by Ward identities. In particular for transport calculations it is crucial to respect these identities exactly even in approximate calculations. This raises the question whether typical approximations in the fRG, especially the truncation of the infinite hierarchy of flow equations, satisfy—or can be made to satisfy—Ward identities. This problem has been addressed ten years ago in the context of gauge theories with a fluctuating gauge field, using either modified Ward

identities or the background-field method, but simple gauge-invariant truncations remained elusive. In those cases where a gauge-invariant flow is possible, for instance if the model is regularized not by a momentum cutoff but by a finite temperature, we show that even truncated flows satisfy the Ward identities. On the other hand, we find that "self-consistency" between Green functions of different degree, a feature of the conserving approximations by Baym and Kadanoff, is generally not satisfied by common truncations of the fRG flow equations.

This thesis is organized as follows:

- In Chapter 2 the fRG formalism is introduced. After a brief review of generating functionals and their expansion in terms of Green or vertex functions, an infrared cutoff is defined which introduces a scale dependence in the generating functionals. A derivative with respect to this scale leads to functional flow equations. These are then expanded in terms of their constituent Green functions to obtain an infinite hierarchy of coupled differential flow equations for the Green functions and a diagrammatic representation of the flow equations. The merits of different schemes are compared.

- In Chapter 3 Ward identities are derived expressing the symmetry of the bare action in the functional formalism. A momentum cutoff generally modifies the Ward identities. For other flow schemes which preserve Ward identities we show that they hold even in truncated flows. Conserving approximations are reviewed as an example of self-consistent approximations. It is then shown that common truncated fRG flow equations are generally not self-consistent.

- In Chapter 4 the general fRG formalism is applied to study one-dimensional correlated fermion systems (Luttinger liquids) with impurities, in particular their single-particle and transport properties. In this technical part the precise form of the flow equations on the lattice is derived, as well as the details of the finite-temperature cutoff procedure, truncations of the flow-equation hierarchy and parametrizations of the flowing vertices. At the end of the flow we obtain the effective impurity potential (self energy) and the renormalized density profile. In order to compute transport in our approximation, we then have to solve the scattering problem of non-interacting electrons in this effective potential. It is also shown that current-vertex corrections to the conductance vanish in our approximation, in accordance with the Ward identities. The loop algorithm for nearest-neighbor interaction, which scales linearly in the system size, is derived in appendix B.

- In Chapter 5 new results are reported for the Friedel oscillations of the spatial

density profile generated by a boundary or impurity in one dimension, and the temperature-dependent conductance through a double barrier. For appropriate parameter ranges universal scaling is observed with several distinct power laws in temperature. In intermediate regions the full non-universal crossover behavior is obtained, suggesting an interpretation of recent measurements on carbon nanotubes.

The publications based on this thesis are listed on page 117.

2 Functional renormalization group

Challenging many-body problems often involve effects on many energy scales. In perturbation theory one has to perform loop integrals over all energy scales, which may lead to infrared or ultraviolet divergences. Some of these divergences have a physical origin indicating for instance a phase transition, while others are an artefact of perturbation theory. Wilson's exact renormalization group (RG) [Wilson 1971, Wilson&Kogut 1974] provides a method to deal with such problems: the different energy scales are successively taken into account by integrating out momentum shells. This can be done by introducing for example an infrared cutoff in the bare propagator which suppresses all modes with an energy below the cutoff scale Λ. Then, all correlation functions depend on the scale Λ. One follows the change (*flow*) of the correlation functions as the cutoff scale is lowered until finally the cutoff is removed and the original theory is recovered. An important advantage of this procedure is that the right-hand side (RHS) of the flow equation remains regular even if perturbation theory leads to unphysical divergences.

There are several variants of the exact functional RG flow equations. After Wilson's early review [Wilson&Kogut 1974] on the exact RG, [Polchinski 1984] derived equivalent continuum flow equations with a smooth cutoff in order to prove perturbative renormalizability of massive Euclidean φ^4 theory in $D = 4$. Keller, Kopper, and Salmhofer [KKS 1992] simplified and extended the proof and showed that these flow equations determine the connected amputated Green functions (cf. section 2.2.4). [Wegner&Houghton 1973] derived flow equations for a sharp cutoff, however there were ambiguities which they avoided by assuming discrete momenta. [Weinberg 1976] took the continuum limit and found that the flow could be formulated without ambiguity by expanding the connected amputated Green functions in trees, i.e., in terms of one-particle irreducible (1PI) vertex functions. The 1PI flow equation of the Legendre effective action, the generating functional of the 1PI vertex functions, was derived by [Nicoll&Chang 1977, Wetterich 1993, BDM 1993, Morris 1994, Salmhofer&Honerkamp 2001, Kopietz&Busche 2001]. Another scheme, obtained from the Polchinski scheme by Wick-ordering [Wieczerkowski 1988, Salmhofer 1998, Salmhofer 1999], is particularly suited for rigorous proofs because it allows strong bounds on the growth of correlation functions, even near the Fermi surface and to all orders in the renormalized interaction.

By then, several people had started to use the functional RG (fRG) for fermionic

lattice models. This introduces several problems not present in φ^4 theory, for example the determination of the Fermi surface, whose shape and position is not known *a priori*. Another problem is that even at low energies, when only momenta close to the Fermi surface are important, the two-electron interaction is a complicated function of momenta. Therefore, it needs to be parametrized by many discrete couplings, in contrast to the single renormalized coupling λ at zero external momenta for the φ^4 theory. On the other hand, the lattice provides a natural ultraviolet cutoff which leads to significant simplifications as compared to the continuum field-theoretical models. Important applications of the fRG in condensed-matter physics include the 2D Hubbard model using the Polchinski scheme [Zanchi&Schulz 1998, Zanchi&Schulz 2000], the Wick-ordered scheme [Halboth&Metzner 2000] and also the 1PI scheme [HSFR 2001], while 1D impurity problems and Luttinger-liquid physics are conveniently investigated in the 1PI scheme [MMSS 2002a, MMSS 2002b, AEMMSS 2004].

Initially, many of the flow-equation schemes have not been derived in the most straightforward way, and I found it worthwhile to derive them again in a simple and uniform notation, highlighting the relation between different schemes. While the results are not new, some derivations are much easier than those found in the literature, and I hope the reader new to this method will find them helpful. After introducing the functional formalism and several types of correlation functions in section 2.1, the most commonly used flow equations are derived in section 2.2. I compare important features of the different schemes in section 2.3.

2.1 Functional formalism

2.1.1 Bare action

A system of interacting spinless[1] fermions is described by the action

$$S[\psi,\bar\psi] = \big(\bar\psi, Q\psi\big) - V_0[\psi,\bar\psi] \tag{2.1}$$

with the kinetic (quadratic) term defined as a scalar product

$$\big(\bar\psi, Q\psi\big) = \int dx\, dy\, \bar\psi(y) Q(y,x) \psi(x) \tag{2.2}$$

$$= \sum_K (i\omega - \xi_{\boldsymbol{k}}) \bar\psi_K \psi_K \quad \text{(for translational invariance)} \tag{2.3}$$

where for a translationally invariant system (2.3), the multi-index $K = (\omega, \boldsymbol{k})$ contains space-time indices (frequency, momentum) and could be extended by internal

[1] Ultimately we aim to describe electrons which are fermions with spin; presently in the applications in Chapter 4, however, we only consider fermions without spin and, therefore, specialize to this case.

degrees of freedom like the spin projection σ. The ψ_K, $\bar{\psi}_K$ are Grassmann variables, and $Q(K) = i\omega - \xi_{\boldsymbol{k}}$ is the inverse bare propagator with $\xi_{\boldsymbol{k}} = \varepsilon_{\boldsymbol{k}} - \mu$ the dispersion around the chemical potential μ. If, however, one includes an impurity potential in the bare propagator that depends specifically on space and not just differences of positions, translational invariance is broken: then one has to use the general expression (2.2), cf. section 4.1. The bare propagator is the inverse operator of Q,

$$C := Q^{-1}. \tag{2.4}$$

The functional $V_0[\psi, \bar{\psi}]$ is the bare many-body interaction, for example in the typical case of a density-density interaction (with frequency conservation implicit):

$$\begin{aligned} V_0[\psi, \bar{\psi}] &= \int dx\, dy\, V_0(x-y)\; n(x)\, n(y) \\ &= \sum_{k_1, k_2, q} \tilde{V}_0(q)\; \bar{\psi}_{k_1} \bar{\psi}_{k_2+q} \psi_{k_2} \psi_{k_1+q}. \end{aligned} \tag{2.5}$$

2.1.2 Partition function and connected Green functions

All information about the physical system with action (2.1) is encoded in the normalized partition function

$$\mathcal{Z}[\eta, \bar{\eta}] := \frac{1}{Z_0} \int [d\psi\bar{\psi}]\, e^{S[\psi,\bar{\psi}]}\, e^{-\left(\bar{\psi},\eta\right) - (\bar{\eta},\psi)}\,, \tag{2.6}$$

a functional integral with weight e^S and coupled to Grassmann source fields η_K, $\bar{\eta}_K$. The integration measure is abbreviated as $[d\psi\bar{\psi}] := \prod_K d\psi_K\, d\bar{\psi}_K$. The partition function $\mathcal{Z}[\eta, \bar{\eta}]$ is the generating functional for the Green functions (connected and disconnected). The normalization constant Z_0 is the non-interacting partition function,

$$Z_0 := \int [d\psi\bar{\psi}]\, e^{\sum_K \bar{\psi}_K Q_K \psi_K} = \prod_K \int d\psi_K\, d\bar{\psi}_K\, e^{\bar{\psi}_K Q_K \psi_K} = \prod_K Q_K = \det(Q). \tag{2.7}$$

It is convenient to absorb the quadratic part of the action as well as the normalization factor into the measure,

$$\mathcal{Z}[\eta, \bar{\eta}] = \int d\mu_Q[\psi, \bar{\psi}]\, e^{-V_0[\psi,\bar{\psi}]}\, e^{-\left(\bar{\psi},\eta\right) - (\bar{\eta},\psi)} \tag{2.8}$$

with the normalized Gaussian path-integral measure

$$d\mu_Q[\psi, \bar{\psi}] := \frac{1}{Z_0} [d\psi\bar{\psi}]\, e^{\left(\bar{\psi}, Q\psi\right)} \qquad \text{such that} \int d\mu_Q[\psi, \bar{\psi}] = 1. \tag{2.9}$$

If there is no interaction, $V_0 = 0$, the integral is quadratic (Gaussian) and can be performed analytically by completing the square:

$$\begin{aligned}
\mathcal{Z}^{\text{nonint}}[\eta,\bar{\eta}] &= \int d\mu_Q[\psi,\bar{\psi}]\, e^{-\left(\bar{\psi},\eta\right)-(\bar{\eta},\psi)} \\
&= \frac{1}{Z_0}\int [d\psi\bar{\psi}]\, e^{\left(\bar{\psi},Q\psi\right)-\left(\bar{\psi},\eta\right)-(\bar{\eta},\psi)} \\
&= \frac{1}{Z_0}\int [d\psi\bar{\psi}]\, e^{\left([\bar{\psi}-C^t\bar{\eta}],Q[\psi-C\eta]\right)-(\bar{\eta},C\eta)} \\
&= e^{-(\bar{\eta},C\eta)}\int d\mu_Q[\psi-C\eta,\bar{\psi}-C^t\bar{\eta}] \\
&= e^{-(\bar{\eta},C\eta)}
\end{aligned}$$

where C^t is the transposed propagator.

The *connected* Green functions are generated by the functional

$$\mathcal{G}[\eta,\bar{\eta}] := -\ln \mathcal{Z}[\eta,\bar{\eta}]$$

as

$$\mathcal{G}[\eta,\bar{\eta}] = \sum_{m=0}^{\infty}\frac{1}{(m!)^2}\sum_{K_1\ldots K_m}\sum_{K'_1\ldots K'_m} G_m(K'_1,\ldots,K'_m;K_1,\ldots,K_m)\prod_{j=1}^{m}\bar{\eta}_{K'_j}\eta_{K_j}$$

and

$$\begin{aligned}
G_m(K'_1,\ldots,K'_m;K_1,\ldots,K_m) &= -\langle\psi_{K'_1}\ldots\psi_{K'_m}\bar{\psi}_{K_m}\ldots\bar{\psi}_{K_1}\rangle_{\text{conn}} \\
&= \frac{\delta^m}{\delta\eta_{K_1}\ldots\delta\eta_{K_m}}\frac{\delta^m}{\delta\bar{\eta}_{K'_m}\ldots\delta\bar{\eta}_{K'_1}}\mathcal{G}[\eta,\bar{\eta}]\Big|_{\eta=\bar{\eta}=0},
\end{aligned}$$

respectively. For the non-interacting system follows

$$\mathcal{G}^{\text{nonint}} = (\bar{\eta},C\eta) \tag{2.10}$$

such that $G_1^{\text{nonint}}(K) = C(K)$ is the bare propagator, and all other G_m^{nonint} vanish.

2.1.3 1PI vertex functions

There is another set of correlation functions that is particularly useful for describing phase transitions and fields whose expectation value does not always vanish, such as the order parameter in a symmetry-broken phase: the *one-particle irreducible* (1PI) vertex functions γ_m generated by the functional $\Gamma[\phi,\bar{\phi}]$. Γ is obtained via Legendre transformation from the connected Green functions [Zinn-Justin 2002, section 7.8],

$$\Gamma[\phi,\bar{\phi}] + \left(\bar{\phi},Q\phi\right) := \mathcal{G}[\eta,\bar{\eta}] + \left(\bar{\phi},\eta\right) - (\bar{\eta},\phi)\,. \tag{2.11}$$

This differs from the textbook definition by taking the inverse bare propagator Q out of the one-particle vertex function. The transformations between ϕ and η are

$$\begin{aligned} &\delta_\phi\Gamma - Q^t\bar\phi = \bar\eta, \quad \delta_\eta\mathcal{G} = \bar\phi, \quad \delta_\eta\delta_{\bar\eta}\mathcal{G} = (\delta_\phi\delta_{\bar\phi}\Gamma + Q)^{-1} \\ &\delta_{\bar\phi}\Gamma + Q\phi = \eta, \quad \delta_{\bar\eta}\mathcal{G} = \phi. \end{aligned} \tag{2.12}$$

Γ is expanded in $\bar\phi_K$, ϕ_K as

$$\Gamma[\phi,\bar\phi] = \sum_{m=0}^{\infty} \frac{1}{(m!)^2} \sum_{K_1\dots K_m} \sum_{K'_1\dots K'_m} \gamma_m(K'_1,\dots,K'_m;K_1,\dots,K_m) \prod_{j=1}^{m} \bar\phi_{K'_j}\phi_{K_j}.$$

Each 1PI vertex function γ_m is made up of those diagrams of G_m which cannot be split into two disconnected parts by cutting a single line. As all self-energy contributions on external legs are one-particle *reducible* with respect to the main part of the diagram, full propagators are amputated from all external legs. In the special case without interaction with $\mathcal{G}^{\text{nonint}}[\eta,\bar\eta] = (\bar\eta, C\eta)$ we obtain $\Gamma^{\text{nonint}}[\phi,\bar\phi] = 0$.

2.1.4 Connected amputated Green functions

Another way of looking at a system is by considering the generating functional of the connected amputated Green functions, the *effective interaction* $\mathcal{V}[\chi,\bar\chi]$:

$$\begin{aligned} e^{-\mathcal{V}[\chi,\bar\chi]} &:= \int d\mu_Q[\psi,\bar\psi]\, e^{-V_0[\psi+\chi,\bar\psi+\bar\chi]} \\ &= e^{-V_0[\delta_{\bar\varphi},\delta_\varphi]} \int d\mu_Q[\psi,\bar\psi]\, e^{(\bar\varphi,\psi+\chi)-(\bar\psi+\bar\chi,\varphi)}\Big|_{\varphi=\bar\varphi=0} \\ &= e^{-V_0[\delta_{\bar\varphi},\delta_\varphi]}\, e^{(\bar\varphi,C\varphi)}\, e^{(\bar\varphi,\chi)-(\bar\chi,\varphi)}\Big|_{\varphi=\bar\varphi=0} \\ &= e^{-V_0[\delta_{\bar\varphi},\delta_\varphi]}\, e^{(\delta_\chi,C\delta_{\bar\chi})}\, e^{(\bar\varphi,\chi)-(\bar\chi,\varphi)}\Big|_{\varphi=\bar\varphi=0} \\ &= e^{\Delta_C}\, e^{-V_0[\chi,\bar\chi]} \end{aligned} \tag{2.13}$$

where the *functional Laplace operator* is defined as

$$\Delta_C := \left(\frac{\delta}{\delta\chi}, C\frac{\delta}{\delta\bar\chi}\right) = \int dx\, dy\, \frac{\delta}{\delta\chi(y)} C(y,x) \frac{\delta}{\delta\bar\chi(x)} = \sum_K \frac{\delta}{\delta\chi_K} C_K \frac{\delta}{\delta\bar\chi_K}.$$

I shall use the shorthand notation Δ_C only if it is unambiguous on which Grassmann variable the derivatives act and use the explicit notation otherwise. Δ_C acts on a functional $\mathcal{F}[\chi,\bar\chi]$ in the following way: the derivatives $\frac{\delta}{\delta\chi}$ and $\frac{\delta}{\delta\bar\chi}$ pick an ingoing and outgoing leg from each diagram in $\mathcal{F}$ and connect them by a bare propagator C. In this picture, perturbation theory for $e^{-\mathcal{V}}$ may be visualized as follows: e^{-V_0}

is a collection of any number of disconnected bare interaction vertices, and $\Delta_C\, e^{-V_0}$ contains all diagrams where either V_0 is closed by one C loop to create a tadpole diagram, or two V_0's are connected by a C line to form a tree diagram. Repeating this procedure indefinitely, higher tree and loop diagrams appear, and finally $e^{-\mathcal{V}} = e^{\Delta_C}\, e^{-V_0}$ contains all Feynman diagrams. Taking the logarithm to obtain $\mathcal{V}$, only the connected diagrams are retained [Zinn-Justin 2002, section 1.2.1].

What is the relation between $\mathcal{G}$ and $\mathcal{V}$ as both generate all connected Green functions? We observe that by the substitution $\chi := C\eta$, $\bar{\chi} := C^t\bar{\eta}$,

$$\begin{aligned} e^{-\mathcal{V}[C\eta, C^t\bar{\eta}]} &= \int d\mu_Q[\psi, \bar{\psi}]\, e^{-V_0[\psi + C\eta, \bar{\psi} + C^t\bar{\eta}]} \\ &= \int d\mu_Q[\psi' - C\eta, \bar{\psi}' - C^t\bar{\eta}]\, e^{-V_0[\psi', \bar{\psi}']} \\ &= \int d\mu_Q[\psi', \bar{\psi}']\, e^{-\left(\bar{\psi}', \eta\right) - (\bar{\eta}, \psi') + (\bar{\eta}, C\eta)}\, e^{-V_0[\psi', \bar{\psi}']} \\ &= e^{(\bar{\eta}, C\eta) - \mathcal{G}[\eta, \bar{\eta}]} \end{aligned}$$

such that

$$\mathcal{V}[C\eta, C^t\bar{\eta}] = \mathcal{G}[\eta, \bar{\eta}] - (\bar{\eta}, C\eta)\,. \tag{2.14}$$

In the non-interacting case, $\mathcal{V} = 0$ because $(\bar{\eta}, C\eta)$ cancels the non-interacting part (2.10) of $\mathcal{G}$, in accordance with the name effective *interaction*. Generally, $\mathcal{V}$ generates connected amputated Green functions V_m,

$$\mathcal{V}[\chi, \bar{\chi}] = \sum_{m=0}^{\infty} \frac{1}{(m!)^2} \sum_{K_1 \ldots K_m} \sum_{K'_1 \ldots K'_m} V_m(K'_1, \ldots, K'_m; K_1, \ldots, K_m) \prod_{j=1}^{m} \bar{\chi}_{K'_j} \chi_{K_j}\,, \tag{2.15}$$

i.e., connected Green functions G_m with *bare* propagators $C(K)$ amputated from all external legs:

$$\begin{aligned} V_m(K'_1, \ldots, K'_m; K_1, \ldots, K_m) &= \frac{\delta^m}{\delta\chi_{K_1} \cdots \delta\chi_{K_m}} \frac{\delta^m}{\delta\bar{\chi}_{K'_m} \cdots \delta\bar{\chi}_{K'_1}} \mathcal{V}[\chi, \bar{\chi}]\Big|_{\chi=\bar{\chi}=0} \\ &= \frac{\delta\eta_{K_1}}{\delta\chi_{K_1}} \frac{\delta}{\delta\eta_{K_1}} \cdots \frac{\delta\bar{\eta}_{K'_1}}{\delta\bar{\chi}_{K'_1}} \frac{\delta}{\delta\bar{\eta}_{K'_1}} \big[\mathcal{G}[\eta, \bar{\eta}] - (\bar{\eta}, C\eta)\big]_{\eta=\bar{\eta}=0} \\ &= \frac{G_m(K'_1, \ldots, K'_m; K_1, \ldots, K_m)}{C^t(K'_1) \cdots C(K_1)} - \frac{\delta_{m,1}}{C(K_1)}\,. \end{aligned}$$

2.2 Renormalization-group flow equations

When computing a Green function perturbatively by summing the contributions of certain Feynman diagrams, there can be infrared divergences both as an artefact of

perturbation theory and physically as an indication of a phase transition. These can be regularized by an infrared cutoff Λ in the bare propagator which suppresses modes of low frequency or momentum close to the Fermi surface. The change of the Green functions as the cutoff scale is changed is governed by the *renormalization-group flow equation*.

Alternatively, one can regularize the problem by going to sufficiently high temperatures $T > T_c$, weak coupling $g^2U < U$, and/or a finite system size N; then one can consider the flow of the Green functions as the parameters T or g are changed.

2.2.1 Regularization and flow parameters

The flow schemes used for the functional RG are constructed by making *only* the quadratic part of the bare action depend on the cutoff scale or flow parameter. In all cases the regularization is done with respect to *energy* scales.

Frequency and momentum cutoff

The *frequency cutoff* is defined by multiplying the bare propagator in the action with a cutoff function $\chi^\Lambda(\omega)$,

$$C^\Lambda(K) = \chi^\Lambda(\omega)C(K), \tag{2.16}$$

where $\chi^\Lambda(\omega)$ cuts out modes with frequency $|\omega| < \Lambda$ in the frequency basis where $C(K)$ is diagonal. It may be either a sharp cutoff function using the step function $\Theta(x)$,

$$\chi^\Lambda(\omega) = \Theta(|\omega| - \Lambda),$$

or a smooth cutoff. Generally one would think that a smooth cutoff with a differentiable cutoff function is easier to handle. However, especially at zero temperature, a sharp cutoff can in fact be favorable (cf. section 2.2.3).

The *momentum cutoff* is defined analogously with

$$\chi^\Lambda(\boldsymbol{k}) = \Theta(|\xi_{\boldsymbol{k}}| - \Lambda). \tag{2.17}$$

Generally, the propagator is split as

$$C(K) = C^\Lambda(K) + D^\Lambda(K) \tag{2.18}$$

where $C^\Lambda(K)$ is the propagator for the high-energy (*hard*) modes, and $D^\Lambda(K)$ is the propagator for the remaining low-energy (*soft*) modes that are yet to be integrated out. As $\Lambda \to 0$, the cutoff is removed and $C^\Lambda \to C$, $D^\Lambda \to 0$.

It is simplest to define the cutoff in the basis where C is diagonal, as a function multiplying the kinetic energy eigenvalues ϵ with $\chi^\Lambda(\epsilon)$. We will later (section 3.2.2) see an example where in the presence of an external field the propagator is not diagonal in momentum space: then the cutoff can be defined by diagonalizing first.

Note that at finite Λ, the frequency cutoff leads to non-analyticities in certain correlation functions, for example in the current-current response function. This disadvantage is absent in the temperature flow.

Temperature flow

In order to use the temperature T as a flow parameter in the fRG formalism, only the quadratic part of the action may depend on T. Initially, however, the action has powers of T both in the kinetic and in the interaction part:

$$\begin{aligned} S[\psi,\bar\psi] = T\sum_{i\omega_n}\sum_{k}\bar\psi_K(i\omega_n-\xi_{\boldsymbol{k}})\psi_K \\ + \frac{1}{2}T^3\sum_{K_1,K_2,K_1'} V(K_1';K_1,K_2)\,\bar\psi_{K_1'}\bar\psi_{K_1+K_2-K_1'}\psi_{K_2}\psi_{K_1}\,. \end{aligned}$$

By rescaling the fields $\tilde\psi := T^{3/4}\,\psi$, one can shift the explicit T dependence of a *quartic* interaction into the quadratic part [Honerkamp&Salmhofer 2001]:

$$\begin{aligned} \tilde S[\tilde\psi,\bar{\tilde\psi}] = T^{-1/2}\sum_{i\omega_n}\sum_{k}\bar{\tilde\psi}_K(i\omega_n-\xi_{\boldsymbol{k}})\tilde\psi_K \\ + \frac{1}{2}\sum_{K_1,K_2,K_1'} V(K_1';K_1,K_2)\,\bar{\tilde\psi}_{K_1'}\bar{\tilde\psi}_{K_1+K_2-K_1'}\tilde\psi_{K_2}\tilde\psi_{K_1}\,. \end{aligned}$$

We can now perform the fRG flow on this action to obtain Green functions G_m^T in terms of the rescaled fields $\tilde\psi$ for a whole temperature range and rescale them back to obtain the usual Green functions[2]

$$G_m(\dots) = T^{(2-m)/2}\,G_m^T(\dots). \tag{2.19}$$

Interaction flow

There are systems which can be treated also by a much simpler method [HRAE 2004], namely by simply rescaling the propagator with a number $g \in [0,1]$. Then, all Feynman diagrams become dressed by a global factor of g for each internal line. This seemingly trivial change to weight each diagram by a power of g has the advantage

[2] This is in contrast to [Honerkamp&Salmhofer 2001] where the powers of T in the original action are considered part of the Green functions.

that the fRG flow equation for the Green functions from $g = 0$ to $g = 1$ resums infinite subclasses of Feynman diagrams which would otherwise be more tedious to do. At the same time we can rescale the fields and observe that for $g < 1$ the model is the same as one with full propagators but reduced interaction strength $g^2|U| < |U|$:

$$\begin{aligned} S &\sim \left(\bar{\psi}, [Q/g]\psi\right) - U\,\bar{\psi}\bar{\psi}\psi\psi \\ &\sim \left(\tilde{\bar{\psi}}, Q\tilde{\psi}\right) - g^2 U\,\tilde{\bar{\psi}}\tilde{\bar{\psi}}\tilde{\psi}\tilde{\psi} \end{aligned}$$

where $\tilde{\psi} = g^{-1/2}\,\psi$. Integrating from $g = 0$ to $g = 1$ thus yields a flow in the bare interaction.

2.2.2 Connected Green function flow

The above regularization and flow schemes lead to an action with a quadratic part depending on a scale parameter Λ, which for notational simplicity shall include T for the temperature flow and g for the interaction flow,

$$S^\Lambda[\psi, \bar{\psi}] := \left(\bar{\psi}, Q^\Lambda \psi\right) - V_0[\psi, \bar{\psi}]\,, \tag{2.20}$$

where the inverse bare propagator with cutoff is defined in analogy to equation (2.4),

$$Q^\Lambda := (C^\Lambda)^{-1}. \tag{2.21}$$

Generally, if $\chi^\Lambda(K) = 1$ then $C^\Lambda(K) = \chi^\Lambda(K)C(K)$ is just the original propagator while for $\chi^\Lambda = 0$, $C^\Lambda(K) = 0$ and the kinetic term $\left(\bar{\psi}, (C^\Lambda)^{-1}\psi\right)$ in the action becomes infinite, giving the cutoff modes of the fermion fields an infinite mass such that they are frozen out. By the action S^Λ all generating functionals, and thus their Green function components, depend on Λ. The generating functional $\mathcal{G}^\Lambda$ for the connected Green functions in the presence of the cutoff is defined as

$$e^{-\mathcal{G}^\Lambda[\eta,\bar{\eta}]} := \int d\mu_{Q^\Lambda}[\psi, \bar{\psi}]\, e^{-V_0[\psi,\bar{\psi}]}\, e^{-\left(\bar{\psi},\eta\right)-(\bar{\eta},\psi)} \tag{2.22}$$

$$= \frac{1}{Z_0^\Lambda} \int [d\psi\bar{\psi}]\, e^{\left(\bar{\psi},Q^\Lambda\psi\right)-V_0[\psi,\bar{\psi}]}\, e^{-\left(\bar{\psi},\eta\right)-(\bar{\eta},\psi)} \tag{2.23}$$

where Q is replaced by Q^Λ, and the normalization factor is changed accordingly to $Z_0^\Lambda = \det(Q^\Lambda)$. The flow equation for $e^{-\mathcal{G}^\Lambda}$ is obtained by taking the Λ derivative, denoted by the dot, on both sides of equation (2.23),

$$\begin{aligned} -\left(\partial_\Lambda \mathcal{G}^\Lambda\right) e^{-\mathcal{G}^\Lambda[\eta,\bar{\eta}]} = &-\frac{\partial_\Lambda \det Q^\Lambda}{\det Q^\Lambda}\, e^{-\mathcal{G}^\Lambda} + \\ &+ \int d\mu_{Q^\Lambda}[\psi, \bar{\psi}]\, \left(\bar{\psi}, \dot{Q}^\Lambda \psi\right)\, e^{-V_0[\psi,\bar{\psi}]}\, e^{-\left(\bar{\psi},\eta\right)-(\bar{\eta},\psi)} \end{aligned}$$

$$= \Big(- \mathrm{Tr}(\dot{Q}^\Lambda C^\Lambda) - \Delta_{\dot{Q}^\Lambda} \Big) \, e^{-\mathcal{G}^\Lambda[\eta,\bar{\eta}]}$$

where the first term comes from the derivative of the normalization factor, $\partial_\Lambda \ln \det(Q^\Lambda) = \mathrm{Tr}\, \partial_\Lambda \ln(Q^\Lambda) = \mathrm{Tr}(\dot{Q}^\Lambda C^\Lambda)$. Here, Tr denotes a sum over all space-time indices. Thus, the flow of $\mathcal{G}^\Lambda$ is

$$\boxed{\partial_\Lambda \mathcal{G}^\Lambda[\eta,\bar{\eta}] = \mathrm{Tr}(\dot{Q}^\Lambda \, C^\Lambda) - \mathrm{Tr}\left(\dot{Q}^\Lambda \, \frac{\delta^2 \mathcal{G}^\Lambda[\eta,\bar{\eta}]}{\delta\eta \, \delta\bar{\eta}} \right) + \left(\frac{\delta \mathcal{G}^\Lambda[\eta,\bar{\eta}]}{\delta\eta}, \dot{Q}^\Lambda \frac{\delta \mathcal{G}^\Lambda[\eta,\bar{\eta}]}{\delta\bar{\eta}} \right)}. \tag{2.24}$$

As a check, in the non-interacting case

$$\begin{aligned} \mathcal{G}^\Lambda[\eta,\bar{\eta}] &= \big(\bar{\eta}, C^\Lambda \eta\big) \\ G_1^\Lambda &= \frac{\delta^2 \mathcal{G}^\Lambda}{\delta\eta \, \delta\bar{\eta}} = C^\Lambda \\ \dot{\mathcal{G}}^\Lambda &= \mathrm{Tr}(\dot{Q}^\Lambda \, C^\Lambda) - \mathrm{Tr}(\dot{Q}^\Lambda \, C^\Lambda) + \Big(-\bar{\eta}, C^\Lambda \, \dot{Q}^\Lambda \, C^\Lambda \eta \Big) = \Big(\bar{\eta}, \dot{C}^\Lambda \eta \Big) . \end{aligned}$$

Two technical notes are in order. Naively, the $\dot{Q}^\Lambda$ appearing in the flow equation (2.24) for $\mathcal{G}^\Lambda$ looks ill-defined:

$$\dot{Q}^\Lambda_K = - \frac{\dot{\chi}^\Lambda(K)}{[\chi^\Lambda(K)]^2} Q(K)$$

contains a division by zero for the cutoff modes where $\chi^\Lambda(K) = 0$. But all Green functions G^Λ_m have C^Λ on their external legs so only the combination

$$S^\Lambda(K) := C^\Lambda \, \dot{Q}^\Lambda \, C^\Lambda = -\dot{C}^\Lambda = -\dot{\chi}^\Lambda(K) C(K) \quad (\textit{single-scale propagator}) \tag{2.25}$$

appears. This quantity is well-defined and, for a sharp cutoff, has support only on the scale Λ since $\dot{\chi}^\Lambda$ is a δ function. The other seemingly ill-defined contribution is

$$\mathrm{Tr}(\dot{Q}^\Lambda C^\Lambda) = - \sum_K \frac{\dot{\chi}^\Lambda(K)}{\chi^\Lambda(K)}, \tag{2.26}$$

but this is canceled by the bare part of the second term in the flow equation (2.24),

$$\begin{aligned} \mathrm{Tr}(\dot{Q}^\Lambda C^\Lambda) - \mathrm{Tr}\Big(\dot{Q}^\Lambda \, \frac{\delta^2 \mathcal{G}^\Lambda}{\delta\eta \, \delta\bar{\eta}} \Big)\Big|_{\eta=\bar{\eta}=0} &= \mathrm{Tr}(\dot{Q}^\Lambda [C^\Lambda - G^\Lambda]) \\ = - \sum_{k=1}^\infty \mathrm{Tr}(\dot{Q}^\Lambda \, C^\Lambda [\Sigma^\Lambda \, C^\Lambda]^k) \end{aligned}$$

which again contains only the well-defined combination $S^\Lambda = C^\Lambda \, \dot{Q}^\Lambda \, C^\Lambda$. On the second line, the full propagator G^Λ has been expanded into a geometric series via the Dyson equation $(G^\Lambda)^{-1} = (C^\Lambda)^{-1} - \Sigma^\Lambda$.

2.2.3 1PI vertex function flow

From the flow equation (2.24) of the connected Green functions it is simple to derive the flow of the 1PI generating functional Γ^Λ. We use the Legendre transformation (2.12) but all functionals and Q are taken at scale Λ,

$$\Gamma^\Lambda[\phi,\bar\phi] + \big(\bar\phi, Q^\Lambda\phi\big) := \mathcal{G}^\Lambda[\eta,\bar\eta] + \big(\bar\phi,\eta\big) - (\bar\eta,\phi)\,. \tag{2.27}$$

We express $\mathcal{G}^\Lambda$ and its derivatives by Γ^Λ,

$$\begin{aligned}
\partial_\Lambda\Gamma^\Lambda[\phi,\bar\phi] &= \partial_\Lambda\mathcal{G}^\Lambda[\eta,\bar\eta] - \Big(\bar\phi,\dot Q^\Lambda\phi\Big) \\
&= \Big(\frac{\delta\mathcal{G}^\Lambda[\eta,\bar\eta]}{\delta\eta}, \dot Q^\Lambda\frac{\delta\mathcal{G}^\Lambda[\eta,\bar\eta]}{\delta\bar\eta}\Big) - \operatorname{Tr}\dot Q^\Lambda\Big[\frac{\delta^2\mathcal{G}^\Lambda[\eta,\bar\eta]}{\delta\eta\,\delta\bar\eta} - C^\Lambda\Big] - \Big(\bar\phi,\dot Q^\Lambda\phi\Big) \\
&= \Big(\bar\phi,\dot Q^\Lambda\phi\Big) - \operatorname{Tr}\dot Q^\Lambda\Big[\Big(\frac{\delta^2\Gamma^\Lambda[\phi,\bar\phi]}{\delta\phi\,\delta\bar\phi} + Q^\Lambda\Big)^{-1} - C^\Lambda\Big] - \Big(\bar\phi,\dot Q^\Lambda\phi\Big)\,,
\end{aligned}$$

to arrive at the 1PI *flow equation*

$$\boxed{\partial_\Lambda\Gamma^\Lambda = \operatorname{Tr}\dot Q^\Lambda\Big[C^\Lambda - \Big(\frac{\delta^2\Gamma^\Lambda[\phi,\bar\phi]}{\delta\phi\,\delta\bar\phi} + Q^\Lambda\Big)^{-1}\Big]}. \tag{2.28}$$

If we define the abbreviation $\Gamma^{(2)} := \delta^2\Gamma^\Lambda/\delta\phi\,\delta\bar\phi$, the flow equation can be written in a more compact form as

$$\partial_\Lambda\Gamma^\Lambda = \partial_\Lambda\operatorname{Tr}\ln Q^\Lambda - \partial_\Lambda\operatorname{Tr}\ln(Q^\Lambda+\Gamma^{(2)}) = \partial_\Lambda\operatorname{Tr}\ln\frac{Q^\Lambda}{Q^\Lambda+\Gamma^{(2)}}, \tag{2.29}$$

where in equation (2.29), the Λ derivative acts only on the cutoff functions inside Q^Λ.

The inverse of the functional $(Q^\Lambda+\Gamma^{(2)})$ is the inverse full propagator in the presence of the fields ϕ, $\bar\phi$ and can be safely defined via a geometric series, as in the Dyson equation. To see this, split $(Q^\Lambda+\Gamma^{(2)})$ into a part independent of ϕ, $\bar\phi$ which is the usual inverse full cutoff propagator $[G^\Lambda]^{-1} = Q^\Lambda - \Sigma^\Lambda$, and a remaining functional $\tilde\Gamma^\Lambda[\phi,\bar\phi]$,

$$Q^\Lambda + \frac{\delta^2\Gamma^\Lambda[\phi,\bar\phi]}{\delta\phi\,\delta\bar\phi} = (G^\Lambda)^{-1} + \tilde\Gamma^\Lambda[\phi,\bar\phi], \qquad -\Sigma^\Lambda = \gamma_1^\Lambda = \frac{\delta^2\Gamma^\Lambda[\phi,\bar\phi]}{\delta\phi\,\delta\bar\phi}\Big|_{\phi=\bar\phi=0}\,.$$

Thus,

$$\Big(Q^\Lambda + \frac{\delta^2\Gamma^\Lambda[\phi,\bar\phi]}{\delta\phi\,\delta\bar\phi}\Big)^{-1} = \big(1+G^\Lambda\,\tilde\Gamma^\Lambda\big)^{-1}G^\Lambda = \Big(1 - G^\Lambda\,\tilde\Gamma^\Lambda + [G^\Lambda\,\tilde\Gamma^\Lambda]^2 - \cdots\Big)G^\Lambda.$$

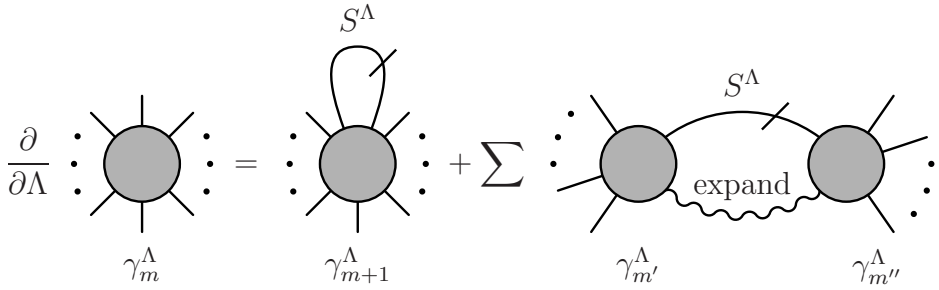
Together with the definition of the single-scale propagator S^Λ in analogy to (2.25),

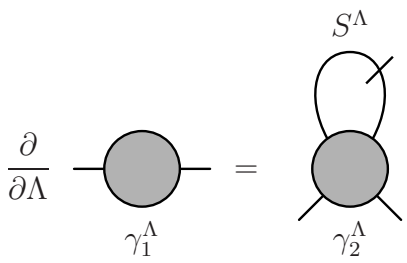
$$S^\Lambda := G^\Lambda \, \dot{Q}^\Lambda \, G^\Lambda \quad (\textit{single-scale propagator}),$$

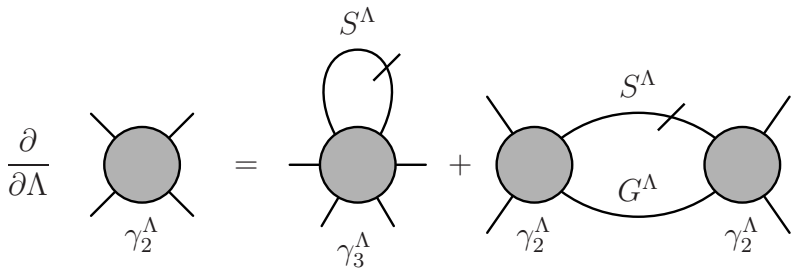
the flow equation becomes

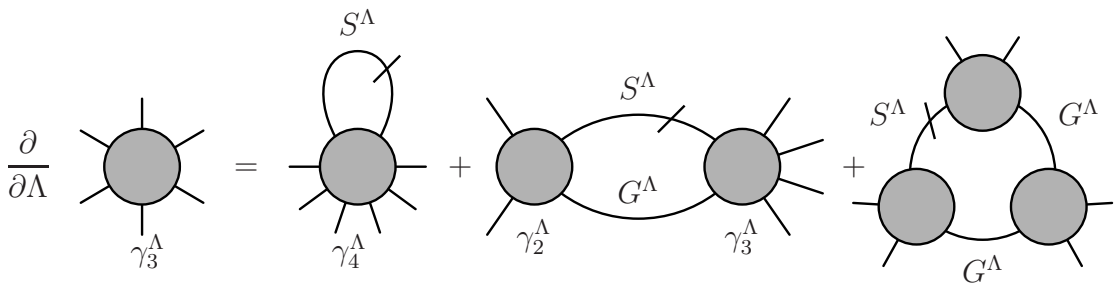
$$\partial_\Lambda \Gamma^\Lambda = \mathrm{Tr}(\dot{Q}^\Lambda [C^\Lambda - G^\Lambda]) + \mathrm{Tr}(S^\Lambda [\tilde{\Gamma}^\Lambda - \tilde{\Gamma}^\Lambda \, G^\Lambda \, \tilde{\Gamma}^\Lambda \, + \cdots]) \tag{2.30}$$

where the last trace consists of a one-loop term with any number of vertices $\tilde{\Gamma}^\Lambda$, which contribute at least two external legs each, connected by one single-scale propagator S^Λ and several full propagators G^Λ. Writing the flow equation in terms of the components γ^Λ_m, we obtain the following diagrams for the general hierarchy of flow equations and for the first few levels of this infinite hierarchy:









In the general form of equation (2.31), the wiggly line in the last diagram denotes that the expansion of the inverse second derivative yields further 1-loop diagrams with an appropriate number of higher vertices insertions, such that the number of external legs on the LHS and RHS matches. This flow scheme is derived in [Weinberg 1976, Nicoll&Chang 1977, Wetterich 1993, BDM 1993, Morris 1994, Salmhofer&Honerkamp 2001].

Sharp-cutoff flow equations

Consider the flow equation (2.29) in a basis where Q is diagonal and the cutoff function χ^Λ is multiplicative so that it can be taken out of Q^Λ,

$$\partial_\Lambda \Gamma^\Lambda = \mathrm{Tr}\left(\partial_\Lambda \chi^\Lambda, \frac{\delta}{\delta \chi^\Lambda}\right) \ln \frac{Q}{Q + \chi^\Lambda \Gamma^{(2)}}. \tag{2.32}$$

Assume that all χ^Λ along the loop have the same value. This is clearly not the general case but is sufficient in our application in Chapter 4 where χ^Λ is a sharp frequency cutoff and all vertices are evaluated at zero frequencies, such that all propagators in the loop have the same frequency and hence the same value of the cutoff function. Then $\partial_\Lambda \chi^\Lambda = -\delta(|\omega| - \Lambda)$ restricts the frequency to the Λ shell but the RHS contains $\Theta(|\omega| - \Lambda)$ which has a step right at the shell. Such expressions are unique if the sharp cutoff is implemented as the limit of increasingly sharp, broadened cutoff functions Θ_ϵ with broadening parameter $\epsilon \to 0$. This is demonstrated by a lemma due to Morris [Morris 1994]: for an arbitrary continuous function $f(t)$,

$$\delta_\epsilon(x - \Lambda)\, f(\Theta_\epsilon(x - \Lambda)) \to \delta_\epsilon(x - \Lambda) \int_0^1 f(t)\, dt \tag{2.33}$$

where $\delta_\epsilon(x) = \Theta'_\epsilon(x)$. Then, equation (2.32) reads

$$\begin{aligned}
\partial_\Lambda \Gamma^\Lambda &= \mathrm{Tr}\, \dot{\chi}^\Lambda \int_0^1 dt\, \frac{d}{dt} \ln \frac{Q}{Q + t\Gamma^{(2)}} \\
&= \mathrm{Tr}\, \dot{\chi}^\Lambda \ln \frac{Q}{Q + \Gamma^{(2)}} \\
&= \mathrm{Tr}\, \dot{\chi}^\Lambda \ln \frac{Q}{Q - \Sigma^\Lambda} \frac{Q - \Sigma^\Lambda}{Q - \Sigma^\Lambda + \tilde{\Gamma}^\Lambda} \\
&= \mathrm{Tr} - \dot{\chi}^\Lambda \left[\ln(1 - C\Sigma^\Lambda) + \ln(1 + \tilde{G}^\Lambda \tilde{\Gamma}^\Lambda)\right] \\
&= \frac{1}{2\pi} \sum_{\omega = \pm\Lambda} \mathrm{tr}\Big[\ln(1 - C\Sigma^\Lambda) - \sum_{k=1}^{\infty} \frac{(-1)^k}{k} (\tilde{G}^\Lambda \tilde{\Gamma}^\Lambda)^k\Big],
\end{aligned} \tag{2.34}$$

where the $T = 0$ Matsubara sum $\frac{1}{2\pi}\int d\omega$ has been performed in the last line such that tr denotes the sum over the remaining spatial indices. The new sharp-cutoff propagator is defined as

$$\tilde{G}^\Lambda := [Q - \Sigma^\Lambda]^{-1}. \tag{2.35}$$

This propagator has no step at $|\omega| = \Lambda$ as opposed to G^Λ, hence the RHS of the flow equation which contains one-loop terms built from powers of $\tilde{G}^\Lambda\tilde{\Gamma}^\Lambda$ is a smooth function of Λ and the vertices $\tilde{\Gamma}^\Lambda$.

However, the sharp frequency cutoff is only possible if the loop integral and hence the vertices $\tilde{\Gamma}^\Lambda$ are continuous: at $T > 0$, an imaginary frequency integral is restricted to discrete Matsubara frequencies $\omega = \omega_n$ at which all vertices have a step as a function of Λ, hence the condition that $f(t)$ be a continuous function in Morris' lemma (2.33) is not satisfied any more.

2.2.4 Connected amputated Green function flow

The Polchinski scheme [Polchinski 1984] has been introduced to prove the renormalizability of the φ^4 theory via the flow of the effective interaction, the generating functional of the connected amputated Green functions (cf. section 2.1.4). In the presence of a cutoff, the effective interaction $\mathcal{V}^\Lambda[\chi, \bar{\chi}]$ is defined as

$$\begin{aligned} e^{-\mathcal{V}^\Lambda[\chi,\bar{\chi}]} &:= \int d\mu_{Q^\Lambda}[\psi,\bar{\psi}]\, e^{-V_0[\psi+\chi,\bar{\psi}+\bar{\chi}]} \\ &= e^{\left(\frac{\delta}{\delta\chi}, C^\Lambda \frac{\delta}{\delta\bar{\chi}}\right)}\, e^{-V_0[\chi,\bar{\chi}]} \\ &= e^{\Delta_{C^\Lambda}}\, e^{-V_0[\chi,\bar{\chi}]}\,. \end{aligned} \tag{2.36}$$

Thus, all Feynman diagrams contain not C but C^Λ on the internal lines. In order to obtain the full $\mathcal{V}$ without cutoff, one has to apply the missing $e^{\Delta_{D^\Lambda}}$ on $e^{-\mathcal{V}^\Lambda}$:

$$\begin{aligned} e^{-\mathcal{V}[\chi,\bar{\chi}]} &= e^{\Delta_C}\, e^{-V_0[\chi,\bar{\chi}]} \\ &= e^{\Delta_{D^\Lambda + C^\Lambda}}\, e^{-V_0[\chi,\bar{\chi}]} \\ &= e^{\Delta_{D^\Lambda}}\, e^{\Delta_{C^\Lambda}}\, e^{-V_0[\chi,\bar{\chi}]} \\ &= e^{\Delta_{D^\Lambda}}\, e^{-\mathcal{V}^\Lambda[\chi,\bar{\chi}]}\,. \end{aligned} \tag{2.37}$$

Equation (2.37) can be interpreted as follows: if all Feynman diagrams (connected and disconnected) with hard internal lines are reconnected again in all possible ways with soft lines, one obtains all diagrams with full lines.

The flow equation for $\mathcal{V}^\Lambda$ is derived by taking the Λ derivative of equation (2.36),

$$\partial_\Lambda \mathcal{V}^\Lambda = -e^{\mathcal{V}^\Lambda}\partial_\Lambda e^{-\mathcal{V}^\Lambda}$$

$$= -e^{\mathcal{V}^\Lambda}\partial_\Lambda(e^{\Delta_{C^\Lambda}}\, e^{-V_0})$$
$$= -e^{\mathcal{V}^\Lambda}\Delta_{\dot{C}^\Lambda}e^{-\mathcal{V}^\Lambda},$$

to arrive at the *Polchinski flow equation*

$$\boxed{\partial_\Lambda \mathcal{V}^\Lambda = \mathrm{Tr}\Big(\dot{C}^\Lambda \frac{\delta^2\mathcal{V}^\Lambda}{\delta\chi\,\delta\bar{\chi}}\Big) - \Big(\frac{\delta\mathcal{V}^\Lambda}{\delta\chi}, \dot{C}^\Lambda\frac{\delta\mathcal{V}^\Lambda}{\delta\bar{\chi}}\Big)}. \tag{2.38}$$

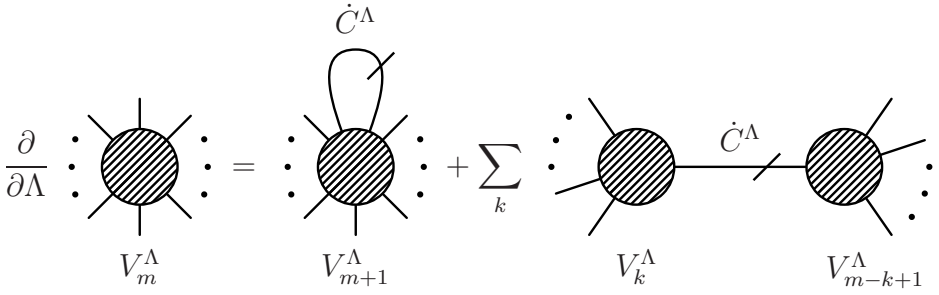
In a more compact notation,

$$\partial_\Lambda \mathcal{V}^\Lambda = \Delta_{\dot{C}^\Lambda}\mathcal{V}^\Lambda - \tfrac{1}{2}\Delta^{12}_{\dot{C}^\Lambda}\mathcal{V}^\Lambda[\chi_1,\bar{\chi}_1]\,\mathcal{V}^\Lambda[\chi_2,\bar{\chi}_2]\Big|_{\chi_1=\chi_2=\chi,\bar{\chi}_1=\bar{\chi}_2=\bar{\chi}} \tag{2.39}$$

where $\Delta^{12}_C = \Big(\frac{\delta}{\delta\chi_1}, C\frac{\delta}{\delta\bar{\chi}_2}\Big) + \Big(\frac{\delta}{\delta\chi_2}, C\frac{\delta}{\delta\bar{\chi}_1}\Big)$ connects two *different* vertices. The initial condition is the bare interaction:

$\mathcal{V}^{\Lambda_0}[\chi,\bar{\chi}] = V_0[\chi,\bar{\chi}] =$  (for a two-particle interaction).

The graphical representation of the Polchinski equation for the connected amputated Green functions V^Λ_m features both tadpole and tree diagrams:



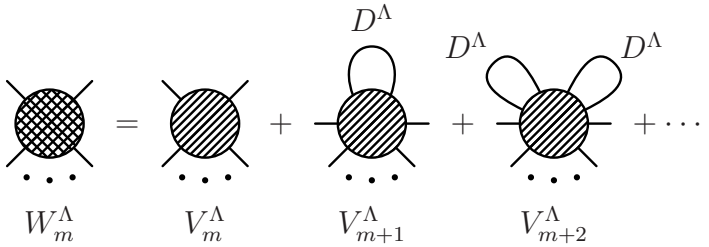
2.2.5 Wick-ordered Green function flow

The connected amputated Green functions are the expansion coefficients of the generating functional $\mathcal{V}$ in terms of *monomials* of the source fields χ, $\bar{\chi}$, whereas the *Wick-ordered* Green functions are the expansion coefficients in terms of Wick-ordered *polynomials* of the source fields, $e^{\Delta_{D^\Lambda}}(\bar{\chi}\chi)^m$. The construction is completely analogous to the use of Hermite polynomials $e^{\partial_x^2}x^m$ as compared to the monomials x^m: any analytical function $f(x)$ can be expanded uniquely in terms of x^m (Taylor expansion) or in terms of Hermite polynomials, which provide another complete orthogonal basis. In appendix A I solve the heat equation in real space using Hermite polynomials; while this is different from the usual textbook solution, it provides

a low-dimensional and intuitive example of the functional formalism. The Wick-ordered generating functional is defined as [Wieczerkowski 1988, Salmhofer 1998, Salmhofer 1999, Salmhofer&Honerkamp 2001]

$$\mathcal{W}^\Lambda[\chi,\bar\chi] = e^{\Delta_{D^\Lambda}}\,\mathcal{V}^\Lambda[\chi,\bar\chi]. \tag{2.40}$$

Diagrammatically, the effect of Wick ordering is that the coefficients W_m^Λ of $\mathcal{W}^\Lambda$ contain all possible D^Λ loops (tadpoles) on the connected amputated Green functions V_m^Λ:



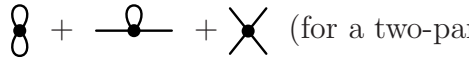
The flow equation for $\mathcal{W}^\Lambda$ can be derived from the Polchinski flow equation (2.39) with the replacement $\Delta_{\dot C^\Lambda} = -\Delta_{\dot D^\Lambda}$ (since $C^\Lambda + D^\Lambda = C$ is independent of Λ),

$$\begin{aligned}
\partial_\Lambda \mathcal{W}^\Lambda &= (\partial_\Lambda e^{\Delta_{D^\Lambda}})\,\mathcal{V}^\Lambda + e^{\Delta_{D^\Lambda}}\,\partial_\Lambda \mathcal{V}^\Lambda \\
&= \Delta_{\dot D^\Lambda} e^{\Delta_{D^\Lambda}} \mathcal{V}^\Lambda + e^{\Delta_{D^\Lambda}}(-\Delta_{\dot D^\Lambda}\mathcal{V}^\Lambda) + e^{\Delta_{D^\Lambda}}(\tfrac12 \Delta^{12}_{\dot D^\Lambda}\mathcal{V}_1^\Lambda \mathcal{V}_2^\Lambda) \\
&= \exp\{\Delta_{D^\Lambda}^{11+12+22}\}\ \tfrac12 \Delta^{12}_{\dot D^\Lambda}\ \mathcal{V}_1^\Lambda\,\mathcal{V}_2^\Lambda \\
&= \tfrac12 (\Delta^{12}_{\dot D^\Lambda} e^{\Delta^{12}_{D^\Lambda}})\,(e^{\Delta^{11}_{D^\Lambda}}\mathcal{V}_1^\Lambda)\,(e^{\Delta^{22}_{D^\Lambda}}\mathcal{V}_2^\Lambda).
\end{aligned}$$

The first two terms in the second line cancel each other, and $\Delta_{D^\Lambda}^{11+12+22} = \Delta_{D^\Lambda}^{11} + \Delta_{D^\Lambda}^{12} + \Delta_{D^\Lambda}^{22}$ contains derivatives with respect to the fields labeled 1 and 2, respectively. Finally, we obtain the *Wick-ordered flow equation*

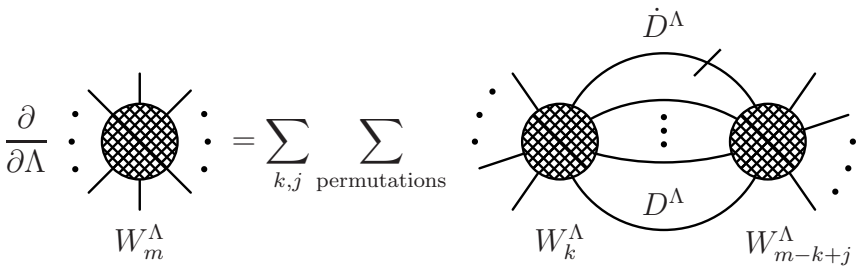
$$\boxed{\partial_\Lambda \mathcal{W}^\Lambda = \tfrac12 \partial_\Lambda (e^{\Delta^{12}_{D^\Lambda}})\,\mathcal{W}_1^\Lambda\,\mathcal{W}_2^\Lambda}. \tag{2.41}$$

The initial condition is

$$\mathcal{W}^{\Lambda_0}[\chi,\bar\chi] = e^{\Delta_C}\,V_0[\chi,\bar\chi] =$$  (for a two-particle interaction).

The Wick-ordered functional $\mathcal{W}^\Lambda$ differs from $\mathcal{V}^\Lambda$ only for $\Lambda > 0$: as $\Lambda \to 0$, $\mathcal{W}^\Lambda \to \mathcal{W} = \mathcal{V}$, i.e., $\mathcal{W}^{\Lambda_0}$ has a different starting point (initial condition) from $\mathcal{V}^{\Lambda_0}$ but flows via a different route to the same final functional (cf. figure 2.1). The diagrammatic

representation of the flow equation for the components W_m^Λ of $\mathcal{W}^\Lambda$ is



Note that all terms on the RHS of the flow equation are bilinear in the vertices and are either tree or higher loop diagrams. In the exact hierarchy without truncation, the flow equation of each vertex has infinitely many terms on the RHS with higher vertices connected by many loops. One internal line is the single-scale propagator $\dot{D}^\Lambda$, while all others are *soft*-mode propagators D^Λ. As the cutoff scale is lowered, only momenta in a small neighborhood of the Fermi surface appear on the internal lines. This justifies a particularly efficient parametrization of the coupling functions which depend on momenta anywhere in the Brillouin zone: at a low cutoff scale, all internal momenta are close to the Fermi surface, so it is sufficient to parametrize the couplings by their values with all momenta projected onto the Fermi surface. This parametrization is employed in computations of the 2D Hubbard model [Halboth&Metzner 2000, Rohe&Metzner 2005].

2.3 Summary

In this chapter I have derived the functional renormalization-group flow equations in the 1PI, Polchinski and Wick-ordered schemes. While this is not new, I believe that the derivations are formally simpler and more straightforward than in much of the literature. Furthermore, the treatment of the sharp cutoff on the functional level (cf. section 2.2.3) has not yet been published to my knowledge.

Figure 2.1 provides an overview over the different fRG schemes: in the center is the *Polchinski scheme* of connected amputated Green functions $\mathcal{V}^\Lambda$ which have essentially the same structure and flow equations as the connected Green functions $\mathcal{G}^\Lambda$. By Legendre transformation to Γ^Λ we have obtained the 1PI *scheme* which starts from the same initial condition but parametrizes the physical properties in a different way particularly suited for symmetry breaking. It has the advantage that the internal lines are full propagators taking into account all self-energy effects already known at scale Λ, while it has the disadvantage that one has to integrate the internal loop over the whole Brillouin zone.

On the other side, the Polchinski scheme leads to the *Wick-ordered* scheme $\mathcal{W}^\Lambda$ which starts from the first-order Hartree-Fock solution as the initial value of the self

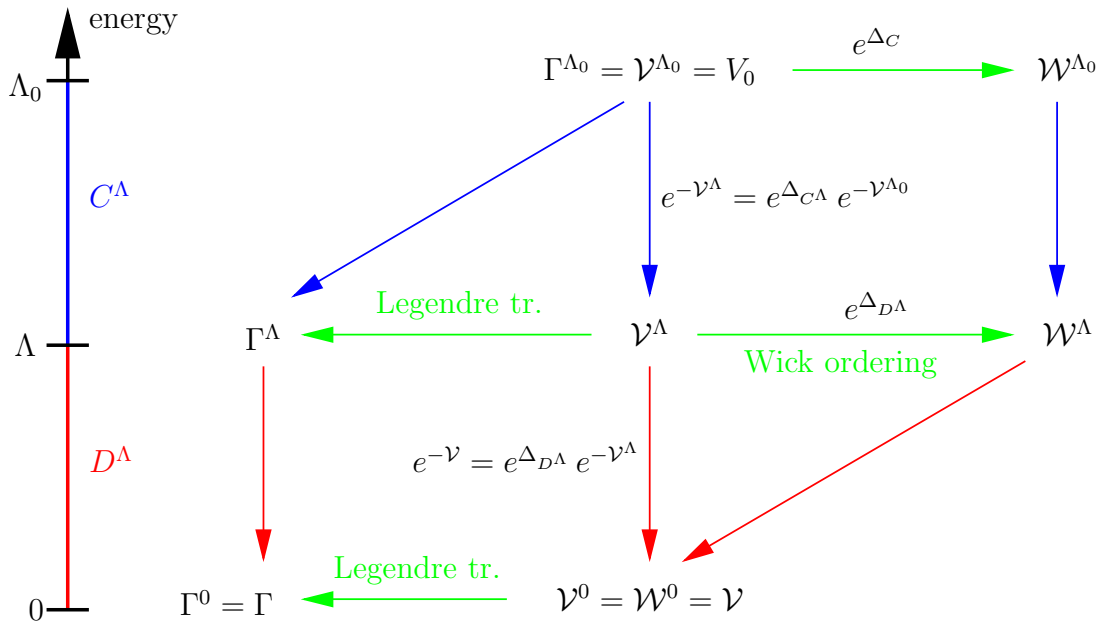


Figure 2.1: *Overview over the relation between the different flow-equation schemes.*

energy but converges towards the same connected amputated Green functions $\mathcal{V}^\Lambda$ at the end of the flow. Its main advantages are that internal lines are restricted to a small neighborhood of the Fermi surface, and that its simple power counting allows rigorous proofs of renormalizability to all orders in perturbation theory.

The next difference arises with truncations. While the full hierarchy of flow equations in any scheme leads to the correct solution to all orders in perturbation theory, the lowest orders in different basis sets of correlation functions capture different aspects of the the solution. As an illustration, imagine a complicated real analytical function $f(x)$, expand it in different sets of orthogonal polynomials and retain only the first few coefficients: the approximate result will look different for each basis set. A third question is whether the basis functions allow for efficient parametrizations in terms of a small set of coefficients, for instance by projecting onto the Fermi surface.

Hence there is not one single flow scheme superior for all applications, but the method of choice depends on the particularities of the model studied.

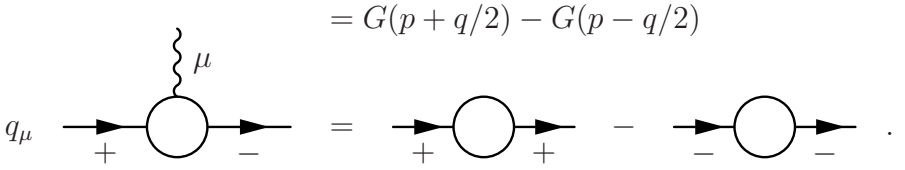
3 Ward identities in the functional RG

In constructing our microscopic model we demand that it satisfies certain physical properties, such as charge conservation. This particular property is guaranteed by the requirement of $U(1)$ *gauge invariance*: by the Noether theorem every continuous symmetry has a conserved quantity associated with it, in this case the electrical charge. In a classical calculation, the conservation of charge is expressed by the continuity equation

$$\partial_t \rho(x) + \boldsymbol{\nabla} \cdot \boldsymbol{j}(x) \equiv \partial_\mu j^\mu(x) = 0$$

where $\rho(x)$ and $\boldsymbol{j}(x)$ are the charge and current densities, respectively. In quantum theory the current $j^\mu(x)$ becomes an operator $\hat{j}^\mu(x)$, and the continuity equation is evaluated inside an expectation value together with insertions of other operators. If the time derivative acts not only on the current operator but also on the time ordering in the expectation value, it generates differences of Green functions [Itzykson&Zuber 1980]. In momentum space with momentum transfer q to the external field, and in units such that the electron charge $e = 1$,

$$\begin{aligned} q_\mu \langle \hat{j}^\mu \, \psi_{p-q/2} \, \bar{\psi}_{p+q/2} \rangle &= \langle \psi_{p-q/2} \, \bar{\psi}_{p-q/2} \rangle - \langle \psi_{p+q/2} \, \bar{\psi}_{p+q/2} \rangle \\ &= G(p+q/2) - G(p-q/2) \end{aligned} \tag{3.1}$$



This is an example of a *Ward identity* (WI): these are constraints on Green functions expressing the underlying symmetry [Ward 1950]. For the one-particle Green functions equation (3.1) can be easily derived by hand, but it will become more tedious as more external legs are added, each corresponding to an operator insertion in the expectation value. Instead, we shall employ the formalism introduced in Chapter 2 to derive a functional Ward identity applicable to *all* m-particle Green functions simultaneously. This will allow us to investigate general properties of Ward identities to all orders in the fields and in the interaction.

Let me mention one important point already now in order to avoid confusion (the issue will be explained in more detail below): there are two versions of the Ward identities in the literature, one relating the difference of Green functions to

the current as above (*response-function Ward identity*), the other relating it to the two-particle interaction with a loop closed (*self-consistent Ward identity*). Both are equivalent in the exact solution and in conserving approximations but generally differ in other approximations such as truncated fRG flows. I will show that in truncated flows the response-function Ward identities can still be satisfied in the absence of a momentum cutoff, for instance in the temperature-flow scheme, while self-consistency and thereby the self-consistent Ward identities are in general violated.

We proceed as follows: after the functional derivation of Ward identities in section 3.1 we shall see how a momentum cutoff breaks response-function Ward identities and how this can be fixed in flow schemes without momentum cutoffs (section 3.2). To answer the related question of self-consistency (section 3.3) we first review the construction of self-consistent conserving approximations of Baym and Kadanoff. We then show that the self-consistent Ward identities are generally violated by truncated flow equations. The results are summarized in section 3.4.

3.1 Gauge invariance and Ward identities

We couple the fermionic action to an external field for two reasons: it allows us to compute linear response by derivatives with respect to the external field, and it is necessary to make the action satisfy the desired symmetry.

In order to compute electrical transport properties, we need to study the response of the system to the external electromagnetic potential. This is done by including in the action a term coupling a current operator $j^\mu(x)$ to the external field $A_\mu(x)$,

$$S[\psi, \bar{\psi}, A] := S[\psi, \bar{\psi}] - (j^\mu, A_\mu) \tag{3.2}$$

where the summation over μ is understood. Then, the response functions are derivatives of the Green functions with respect to $A_\mu(x)$. The current operator $j^\mu[\psi, \bar{\psi}, A]$ is a composite operator of the fields ψ, $\bar{\psi}$ and generally depends also on the external field A. We shall now demand a symmetry and construct the current such that this symmetry holds.

3.1.1 Gauge transformation

The local $U(1)$ gauge transformation is [Zinn-Justin 2002, chapter 12]

$$\begin{cases} \psi'(x) := e^{-i\alpha(x)}\psi(x) & \delta_\alpha\psi(x) = -i\alpha(x)\psi(x) \\ \bar{\psi}'(x) := e^{i\alpha(x)}\bar{\psi}(x) & \delta_\alpha\bar{\psi}(x) = i\alpha(x)\bar{\psi}(x) \\ A'_\mu(x) := A_\mu(x) + \partial_\mu\alpha(x) & \delta_\alpha A_\mu(x) = \partial_\mu\alpha(x), \end{cases} \tag{3.3}$$

where $\alpha(x)$ is a real function, and δ_α an operator which acts on fields and functionals by performing an infinitesimal gauge transformation. The condition of gauge invariance of our model is

$$\delta_\alpha \left([d\psi\bar{\psi}]\ e^{S[\psi,\bar{\psi},A]} \right) \stackrel{!}{=} 0$$

without the integral, i.e., the path integral measure times the weight should stay invariant. In the case of the $U(1)$ gauge transformation (3.3) the measure remains invariant, therefore the gauge invariance reduces to a condition on the action,

$$\delta_\alpha S[\psi, \bar{\psi}, A] \stackrel{!}{=} 0.$$

Consider first the gauge variation of the fermionic action, $\delta_\alpha S[\psi, \bar{\psi}]$. If $\alpha(x) = const$ this transformation probes *global* charge conservation: this is satisfied as long as each term in the action has the same number of fermion annihilation and creation operators. But if we admit an $\alpha(x)$ varying in space-time, the action will in general change proportionally to $\partial_\mu \alpha(x)$,

$$\delta_\alpha S[\psi, \bar{\psi}] = (j^\mu, \partial_\mu \alpha) + \mathcal{O}(\alpha^2), \tag{3.4}$$

where we have called the coefficient of the $\partial_\mu \alpha$ term j^μ. This is the motivation to introduce the gauge field A_μ: if it is coupled to j^μ by (j^μ, A_μ), the gauge variation of the A_μ term will cancel the gauge variation of the fermionic action (3.4) to first order in α.

This raises the question how to construct the current operator j^μ in the action (3.2). In the continuum this is achieved by the procedure of minimal coupling. On the lattice, one has to use lattice gauge theory which is technically quite different (for an introduction, see for instance [Zinn-Justin 2002, chapter 34]). Note that (*i*) the general arguments about symmetries and Ward identities can be seen already in the technically simpler continuum model, and (*ii*) the lattice formalism will be used in this work only in the special case of a 1D lattice where the field-strength tensor vanishes. Therefore, I derive the Ward identities pedagogically only for the continuum case but give the final results also specifically for the 1D lattice (in section 4.4) after the lattice formulation has been introduced in Chapter 4.

3.1.2 Minimal coupling in the continuum

One way to construct a gauge-invariant continuum action is by minimally coupling the gauge field to the fermions: in the quadratic part of the action we replace the partial derivative ∂_μ by the covariant derivative

$$D_\mu := \partial_\mu + iA_\mu(x),$$

such that

$$D'_\mu = e^{-i\alpha} D_\mu e^{i\alpha}, \qquad \delta_\alpha D_\mu = i\partial_\mu \alpha.$$

Likewise, the inverse bare propagator $Q(\partial_\mu)$ is replaced by $Q[A] \equiv Q(D_\mu)$ which is also gauge covariant,

$$Q(D'_\mu) = e^{-i\alpha} Q(D_\mu) e^{i\alpha}, \tag{3.5}$$

such that the kinetic term is gauge invariant,

$$\left(\bar\psi', Q(D'_\mu)\psi'\right) = \left(\bar\psi, Q(D_\mu)\psi\right), \qquad \delta_\alpha \left(\bar\psi, Q(D_\mu)\psi\right) = 0.$$

Then, the current defined as the A dependence of the kinetic term,

$$\left(\bar\psi, Q(D_\mu)\psi\right) =: \left(\bar\psi, Q(\partial_\mu)\psi\right) - (j_0^\mu, A_\mu)$$

makes the quadratic part of the action gauge invariant. Expanding both sides of equation (3.5) to first order in α,

$$\left(\delta_\alpha A_\mu, \frac{\delta Q[A]}{\delta i A_\mu}\right) = \left(\alpha, \partial_\mu \frac{\delta Q[A]}{\delta i A_\mu}\right) = \big[\alpha, Q[A]\big] \tag{3.6}$$

where the commutator $\alpha(x)Q(x,y) - Q(x,y)\alpha(y) = [\alpha(x) - \alpha(y)]Q(x,y)$, and we have integrated by parts.[1]

Consider now the interaction term. The density-density interaction is explicitly gauge invariant,

$$\begin{aligned}
\delta_\alpha V_0[\psi,\bar\psi] &= \delta_\alpha \int dx\, dy\, V(x-y)\bar\psi(x)\bar\psi(y)\psi(y)\psi(x) \\
&= i \int dx\, dy\, V(x-y)\bar\psi(x)\bar\psi(y)\psi(y)\psi(x)\,[\alpha(x) + \alpha(y) - \alpha(y) - \alpha(x)] \\
&= 0.
\end{aligned}$$

On the other hand, for a bare interaction which itself is not gauge invariant ($\delta_\alpha V_0 \neq 0$) some further counter term $(j_V^\mu, A_\mu) := -\delta_\alpha V_0$ is needed to make the action gauge invariant. Combining both the kinetic and the interaction parts of the current operator,

$$j^\mu(x) := j_0^\mu(x) + j_V^\mu(x),$$

the action (3.2) will be gauge invariant.

[1] In this chapter we assume boundary conditions such that the integration by parts yields no boundary term.

Example for quadratic dispersion

Let us give a specific example: for nonrelativistic fermions of mass m in the continuum, the dispersion relation is linear in time and quadratic in space, $Q(\partial_\mu) = -\partial_t + \boldsymbol{\nabla}^2/2m$. We assume a gauge-invariant interaction V_0. Minimal coupling to the external electromagnetic potential $A_\mu(x) = (\varphi, -\boldsymbol{A})$ is given in real space by $\partial_t \mapsto \partial_t + \varphi(x)$, $-i\boldsymbol{\nabla} \mapsto -i\boldsymbol{\nabla} - \boldsymbol{A}(x)$, hence the current which makes the action gauge invariant is constructed as

$$\begin{aligned} S[\psi,\bar\psi,A] &= \int dx\, \bar\psi(x)\left[-\partial_t - \varphi - \tfrac{1}{2m}(-i\boldsymbol{\nabla} - \boldsymbol{A})^2\right]\psi(x) - V_0[\psi,\bar\psi] \\ &\stackrel{!}{=} \big(\bar\psi, Q\psi\big) - (j^\mu, A_\mu) - V_0[\psi,\bar\psi] \\ &\Rightarrow\ j^0 = n, \quad \boldsymbol{j} = \underbrace{\tfrac{1}{2mi}\left[\bar\psi(\boldsymbol{\nabla}\psi) - (\boldsymbol{\nabla}\bar\psi)\psi\right]}_{\text{paramagnetic}} - \underbrace{\tfrac{1}{2m} n\boldsymbol{A}}_{\text{diamagn.}} \end{aligned} \tag{3.7}$$

with the density operator $n(x) := \bar\psi(x)\psi(x)$. The current $\boldsymbol{j}$ has a part independent of A which is called the paramagnetic current and a part proportional to A which is called the diamagnetic current.

3.1.3 Functional derivation of Ward identities

The current operator $j^\mu[\psi,\bar\psi,A]$ constructed in this way is coupled to an external field $A_\mu(x)$. Thereby, all generating functionals depend on A as a parameter,

$$\mathcal{Z}[\eta,\bar\eta,A] := \int d\mu_Q[\psi,\bar\psi]\, e^{-(j^\mu, A_\mu) - V_0[\psi,\bar\psi] - \left(\bar\psi,\eta\right) - (\bar\eta,\psi)}$$

with measure (2.9). The source fields η, $\bar\eta$ transform under gauge transformations as

$$\delta_\alpha\eta(x) := -i\alpha(x)\eta(x), \qquad \delta_\alpha\bar\eta(x) := i\alpha(x)\bar\eta(x). \tag{3.8}$$

Then, the gauge variation of $\mathcal{Z}$ to first order in α,

$$\begin{aligned} \delta_\alpha\mathcal{Z}[\eta,\bar\eta,A] &= \left\{\left(\delta_\alpha\eta, \frac{\delta}{\delta\eta}\right) + \left(\delta_\alpha\bar\eta, \frac{\delta}{\delta\bar\eta}\right) + \left(\delta_\alpha A_\mu, \frac{\delta}{\delta A_\mu}\right)\right\}\mathcal{Z}[\eta,\bar\eta,A] \\ &= \left\{\left(-i\alpha\eta, \frac{\delta}{\delta\eta}\right) + \left(i\alpha\bar\eta, \frac{\delta}{\delta\bar\eta}\right) + \left(\partial_\mu\alpha, \frac{\delta}{\delta A_\mu}\right)\right\}\mathcal{Z}[\eta,\bar\eta,A] \\ &= 0, \end{aligned} \tag{3.9}$$

vanishes because $\mathcal{Z}$ is gauge invariant by construction. Substituting $\mathcal{Z} = e^{-\mathcal{G}}$ we obtain the functional *Ward identity for the connected Green functions*,

$$\boxed{\left(\alpha, \partial_\mu\frac{\delta\mathcal{G}}{\delta iA_\mu}\right) = \left(\frac{\delta\mathcal{G}}{\delta\eta}, \alpha\eta\right) + \left(\bar\eta, \alpha\frac{\delta\mathcal{G}}{\delta\bar\eta}\right)}. \tag{3.10}$$

By the Legendre transformation (2.11) in the presence of the external field,

$$\Gamma[\phi,\bar{\phi},A]+\left(\bar{\phi},Q[A]\phi\right):=\mathcal{G}[\eta,\bar{\eta},A]+\left(\bar{\phi},\eta\right)-\left(\bar{\eta},\phi\right), \tag{3.11}$$

we rewrite equation (3.10) in terms of the 1PI functional $\Gamma[\phi,\bar{\phi},A]$,

$$\begin{aligned}\left(\alpha,\partial_\mu\frac{\delta}{\delta iA_\mu}\{\Gamma+\left(\bar{\phi},Q[A]\phi\right)\}\right)&=\left(\bar{\phi},\alpha\Big\{\frac{\delta\Gamma}{\delta\bar{\phi}}+Q[A]\phi\Big\}\right)+\left(\Big\{\frac{\delta\Gamma}{\delta\phi}-Q^t[A]\bar{\phi}\Big\},\alpha\phi\right)\\&=\left(\frac{\delta\Gamma}{\delta\phi},\alpha\phi\right)+\left(\bar{\phi},\alpha\frac{\delta\Gamma}{\delta\bar{\phi}}\right)+\left(\bar{\phi},\left[\alpha,Q[A]\right]\phi\right).\end{aligned}$$

By equation (3.6) we obtain the 1PI *Ward identity*

$$\boxed{\left(\alpha,\partial_\mu\frac{\delta\Gamma}{\delta iA_\mu}\right)=\left(\frac{\delta\Gamma}{\delta\phi},\alpha\phi\right)+\left(\bar{\phi},\alpha\frac{\delta\Gamma}{\delta\bar{\phi}}\right)}. \tag{3.12}$$

By amputating bare propagators C (without external field) from the external legs of equation (3.10) using (2.14) we obtain

$$\left(\alpha,\partial_\mu\frac{\delta\mathcal{V}}{\delta iA_\mu}\right)=\left(\left[C^t\frac{\delta\mathcal{V}}{\delta\chi}-\bar{\chi}\right],\alpha Q\chi\right)+\left(Q^t\bar{\chi},\alpha\left[C\frac{\delta\mathcal{V}}{\delta\bar{\chi}}+\chi\right]\right)$$

and by rearranging terms the *Polchinski Ward identity*

$$\boxed{\left(\alpha,\partial_\mu\frac{\delta\mathcal{V}}{\delta iA_\mu}\right)=\left(\frac{\delta\mathcal{V}}{\delta\chi},C\alpha Q\chi\right)+\left(\bar{\chi},Q\alpha C\frac{\delta\mathcal{V}}{\delta\bar{\chi}}\right)-\left(\bar{\chi},[\alpha,Q]\chi\right)}. \tag{3.13}$$

On the RHS of equation (3.13) the non-amputated external legs are shifted.

3.1.4 Momentum- and real-space formulation

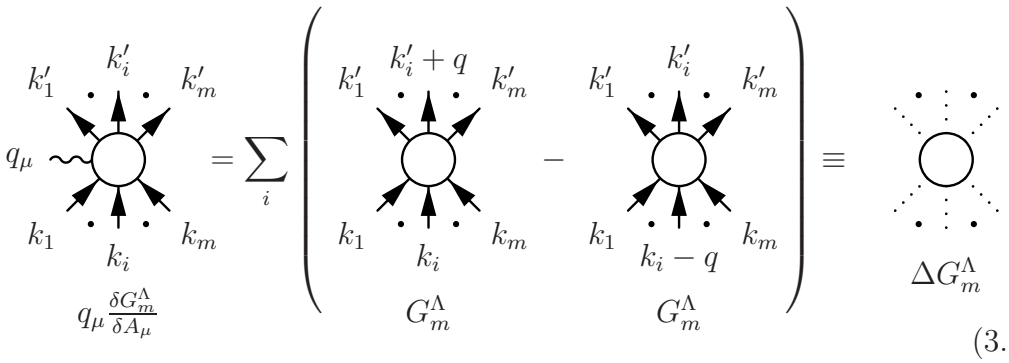
All of the above Ward identities still contain an inner product with the arbitrary gauge-transformation parameter α_{-q}. In Fourier space the transformation (3.8) reads

$$\begin{aligned}\eta'_k&=\eta_k-i\sum_q\alpha_{-q}\eta_{k+q}+\mathcal{O}(\alpha^2)\\\bar{\eta}'_k&=\bar{\eta}_k+i\sum_q\alpha_{-q}\bar{\eta}_{k-q}+\mathcal{O}(\alpha^2)\end{aligned} \tag{3.14}$$

where the mode α_{-q} subtracts momentum q from the fermion. The coefficient of α_{-q} in the Ward identity for the connected Green functions, equation (3.10), is for example

$$q_\mu\frac{\delta\mathcal{G}}{\delta A_\mu(-q)}=\sum_k\left(\frac{\delta\mathcal{G}}{\delta\eta_{k_-}}\eta_{k_+}+\bar{\eta}_{k_-}\frac{\delta\mathcal{G}}{\delta\bar{\eta}_{k_+}}\right)$$

where the indices $k_\pm$ denote $k \pm q/2$. The Ward identities for the other functionals has an analogous form. Taking only the one-particle component of this functional Ward identity by applying $\frac{\delta^2}{\delta\eta_{k_+}\delta\bar{\eta}_{k_-}}|_{\eta=\bar{\eta}=0}$ we obtain the Ward identity given as an example in equation (3.1). Generally, the Ward identities can be represented diagrammatically as



(3.15)

where the wiggly line on the LHS denotes the response function of which the divergence is taken. As momentum q is transferred to the external field, momentum conservation implies $k_1 + \cdots + k_m = q + k_1' + \cdots + k_m'$. The Green functions in the large parentheses are without external field, so any one of the external legs has to be momentum-shifted to satisfy momentum conservation. The rightmost diagram with the dotted external legs shall abbreviate all the combinations of momentum-shifted external lines in the middle.

Generally, for the case of *global* gauge invariance there is only the $q = 0$ mode of α_{-q} and the Ward identity

$$\left(\eta, \frac{\delta\mathcal{G}}{\delta\eta}\right) = \left(\bar{\eta}, \frac{\delta\mathcal{G}}{\delta\bar{\eta}}\right) \tag{3.16}$$

implies only that there are as many creation as annihilation operators in every monomial in the action, independent of their momenta or positions.

In real space, the coefficient of $\alpha(x)$ in equation (3.10) fulfills the Ward identity

$$\partial_\mu \frac{\delta\mathcal{G}}{\delta i A_\mu(x)} = \frac{\delta\mathcal{G}}{\delta\eta(x)}\eta(x) + \bar{\eta}(x)\frac{\delta\mathcal{G}}{\delta\bar{\eta}(x)}.$$

3.2 Cutoff Ward identities

Generally, a momentum cutoff breaks local gauge invariance. The cutoff divides the fields ψ into high and low modes. However, a local gauge transformation $\alpha(x)$ which is multiplicative in real space, $\delta_\alpha\psi(x) \sim \alpha(x)\psi(x)$ from equation (3.3), becomes a convolution in momentum space, $\delta_\alpha\psi_k \sim \sum_q \alpha_{-q}\psi_{k+q}$ from equation (3.14). This

shift of the momenta spoils the division of modes and poses a problem when treating gauge theories using flow equations. These problems would be solved if we could somehow define a gauge-invariant cutoff propagator $Q^\Lambda[A]$. However, in gauge theories, where one integrates over fluctuations of the gauge field A in the path integral, this is difficult except for pure gauge theories [D'Attanasio&Morris 1996]. Note that these problems are absent for global gauge invariance (no momentum shift) and for the temperature and interaction flow schemes which have no momentum cutoff.

There are two ways in the high-energy physics literature to deal with this problem: (*i*) One can give up gauge invariance at intermediate cutoff scales but try to ensure that the full Ward identities are recovered as the cutoff is finally removed ($\Lambda \to 0$); this approach of modified Ward identities is explained in section 3.2.1. (*ii*) One can manifestly satisfy Ward identities in the presence of a cutoff with the help of an auxiliary field, the external background gauge field $\bar{A}$ (section 3.2.2). Both approaches become cumbersome if one has to truncate the flow-equation hierarchy. However, if one uses a manifestly gauge-invariant formulation (section 3.2.3) such as the temperature-flow scheme, we show that the Ward identities can be satisfied exactly even in truncated flows (section 3.2.4).

3.2.1 Modified Ward identities

The Ward identities (3.10) which hold without cutoff are broken at intermediate cutoff scales ($\Lambda > 0$) by modification terms, leading to *modified Ward identities* (mWI). These modification terms vanish in the limit $\Lambda \to 0$. Compatibility of flow and mWI ensures that the full hierarchy of flow equations satisfies the mWI at all scales Λ. This is sufficient for proving perturbative renormalizability of QED; the mWI for the connected amputated Green functions were derived in [Keller&Kopper 1991, Keller&Kopper 1996] and used to prove bounds for the full hierarchy of Green functions (see also [BDM 1994], and [Ellwanger 1994] for mWI in the 1PI scheme). For practical computations, however, the flow equations need to be truncated, and the mWI (and ultimately the original Ward identities at $\Lambda = 0$) are satisfied only to truncation order. Alternatively, if there are only a few relevant components of the flowing vertices, one can determine some of them not by the flow but by the mWI at every scale Λ, thus satisfying the mWI exactly [EHW 1996].

Modified Ward identities for connected Green functions

The definition of the cutoff connected Green functions (2.23) with the addition of the external field can be split into a gauge-invariant part (without cutoff) and a part

containing the cutoff function,

$$e^{-\mathcal{G}^\Lambda[\eta,\bar\eta,A]} = \int \frac{[d\psi\bar\psi]}{\det Q}\, e^{\left(\bar\psi,Q[A]\psi\right)-V_0[\psi,\bar\psi]-\left(\bar\psi,\eta\right)-(\bar\eta,\psi)} \times \frac{\det Q}{\det Q^\Lambda}\, e^{\left(\bar\psi,[Q^\Lambda-Q]\psi\right)}. \quad (3.17)$$

Performing the gauge transformation (3.3), (3.8) on all fields, the first part remains invariant while the latter gives to first order in α a term involving $[Q^\Lambda - Q]$ which breaks gauge invariance at $\Lambda > 0$,

$$\begin{aligned}\delta_\alpha e^{-\mathcal{G}^\Lambda[\eta',\bar\eta',A']} &= \int \frac{[d\psi\bar\psi]}{\det Q^\Lambda}\, e^{\left(\bar\psi,Q[A]\psi\right)-V_0[\psi,\bar\psi]-\left(\bar\psi,\eta\right)-(\bar\eta,\psi)} \qquad (3.18)\\ &\quad \times \left(\bar\psi, i[\alpha, Q^\Lambda - Q]\psi\right)\, e^{\left(\bar\psi,[Q^\Lambda-Q]\psi\right)}\\ &= -\left(\frac{\delta}{\delta\eta}, iX^\Lambda\frac{\delta}{\delta\bar\eta}\right) e^{-\mathcal{G}^\Lambda[\eta,\bar\eta,A]}\,. \qquad (3.19)\end{aligned}$$

The η, $\bar\eta$ derivatives connect two legs of $e^{-\mathcal{G}^\Lambda}$ with a propagator

$$X^\Lambda := [\alpha, Q^\Lambda - Q]$$

which vanishes as $\Lambda \to 0$ or for homogeneous $\alpha(x) \equiv \alpha$. On the other hand, expanding $\mathcal{G}^\Lambda[\eta', \bar\eta', A']$ in the arguments to first order in α as in equation (3.9) yields

$$\delta_\alpha \mathcal{G}^\Lambda[\eta', \bar\eta', A'] = \left\{\left(-i\alpha\eta, \frac{\delta}{\delta\eta}\right) + \left(i\alpha\bar\eta, \frac{\delta}{\delta\bar\eta}\right) + \left(\partial_\mu\alpha, \frac{\delta}{\delta A_\mu}\right)\right\} \mathcal{G}^\Lambda[\eta, \bar\eta, A]. \quad (3.20)$$

We combine (3.19) and (3.20) into the *modified Ward identity*

$$\boxed{\left(\alpha, \partial_\mu\frac{\delta\mathcal{G}^\Lambda}{\delta i A_\mu}\right) - \mathrm{Tr}\left(X^\Lambda\frac{\delta^2\mathcal{G}^\Lambda}{\delta\eta\,\delta\bar\eta}\right) + \left(\frac{\delta\mathcal{G}^\Lambda}{\delta\eta}, X^\Lambda\frac{\delta\mathcal{G}^\Lambda}{\delta\bar\eta}\right) = \left(\frac{\delta\mathcal{G}^\Lambda}{\delta\eta}, \alpha\eta\right) + \left(\bar\eta, \alpha\frac{\delta\mathcal{G}^\Lambda}{\delta\bar\eta}\right)} \quad (3.21)$$

which agrees with the usual Ward identity (3.10) in the limit $\Lambda \to 0$ ($X^\Lambda \to 0$). The modification terms have the same structure as the RHS of the flow equation (2.24) with the replacement $\dot Q^\Lambda \mapsto X^\Lambda$.

Modified Ward identities for 1PI vertex functions

Using the Legendre transformation with cutoff (2.27) we can rewrite equation (3.21) as

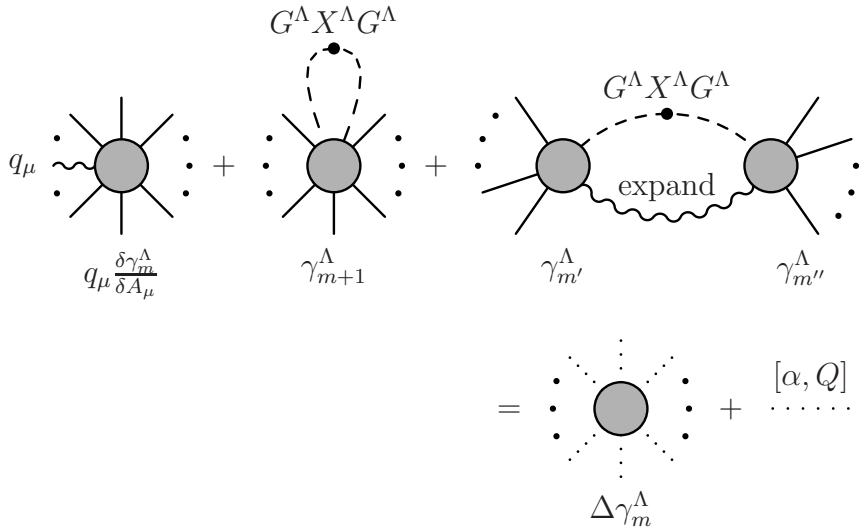
$$\left(\alpha, \partial_\mu\frac{\delta\Gamma^\Lambda}{\delta i A_\mu}\right) - \mathrm{Tr}\big(X^\Lambda\big[Q^\Lambda + \Gamma^{(2)}\big]^{-1}\big) + \big(\bar\phi, X^\Lambda\phi\big)$$

$$= \left(\frac{\delta\Gamma^\Lambda}{\delta\phi}, \alpha\phi\right) + \left(\bar\phi, \alpha\frac{\delta\Gamma^\Lambda}{\delta\bar\phi}\right) + \left(\bar\phi, [\alpha, Q^\Lambda]\phi\right)$$

and finally obtain the 1PI *modified Ward identity*

$$\boxed{\left(\alpha, \partial_\mu \frac{\delta\Gamma^\Lambda}{\delta i A_\mu}\right) - \mathrm{Tr}\left(X^\Lambda\left[Q^\Lambda + \Gamma^{(2)}\right]^{-1}\right) = \left(\frac{\delta\Gamma^\Lambda}{\delta\phi}, \alpha\phi\right) + \left(\bar\phi, \alpha\frac{\delta\Gamma^\Lambda}{\delta\bar\phi}\right) + \left(\bar\phi, [\alpha, Q]\phi\right)}.$$

The modification term is due to the inverse bare propagator $Q^\Lambda - Q + Q[A]$ in equation (3.17), where the cutoff acts only on the A-independent part, while the A dependence is treated as part of the interaction (self energy), $Q^\Lambda - \Sigma^\Lambda[A]$. The modified Ward identities for the 1PI vertex functions Γ^Λ may be written diagrammatically as



where the dashed lines denote the propagator $G^\Lambda X^\Lambda G^\Lambda$ and the dotted lines denote a momentum shift on any external leg as in equation (3.15). The wiggly line in the third diagram means that the expansion of the inverse second derivative yields further one-loop diagrams with an appropriate number of vertices.

The complete LHS, i.e., the response function together with the modification terms, will be interpreted in section 3.2.3 as the divergence of the effective response on scale Λ. In terms of this new response function the Ward identities will be satisfied *without* modification even after truncations (section 3.2.4).

Modified Ward identities for connected amputated Green functions

By amputating C^Λ from the external legs of $\mathcal{G}^\Lambda$ in equation (3.21) we obtain the *Polchinski modified Ward identity*

$$\left(\alpha, \partial_\mu \frac{\delta\mathcal{V}^\Lambda}{\delta i A_\mu}\right) - \mathrm{Tr}\left(C^\Lambda X^\Lambda C^\Lambda \frac{\delta^2\mathcal{V}^\Lambda}{\delta\chi\,\delta\bar\chi}\right) + \left(\frac{\delta\mathcal{V}^\Lambda}{\delta\chi}, C^\Lambda X^\Lambda C^\Lambda \frac{\delta\mathcal{V}^\Lambda}{\delta\bar\chi}\right)$$

$$= \left(\frac{\delta\mathcal{V}^\Lambda}{\delta\chi}, [C^\Lambda \alpha Q + D^\Lambda Q\alpha]\chi\right) + \left(\bar{\chi}, [Q\alpha C^\Lambda + \alpha Q D^\Lambda]\frac{\delta\mathcal{V}^\Lambda}{\delta\bar{\chi}}\right) - (\bar{\chi}, [\alpha, Q]\chi)\,.$$

3.2.2 Background-field method

The background-field method for QED was developed in [Reuter&Wetterich 1994] and summarized in [Freire&Wetterich 1996]: the primary goal is manifest gauge invariance of the 1PI vertex functions at every scale Λ such that one only has to consider the relevant gauge-invariant couplings and not the much more numerous counter terms breaking gauge invariance. This comes, however, at the price of introducing an auxiliary external background gauge field $\bar{A}$ in addition to the internal fluctuating gauge field A. The gauge transformation of $\bar{A}$ is designed to cancel the modification terms in the mWI, such that $\Gamma^\Lambda[\phi, \bar{\phi}, A, \bar{A}]$ is gauge invariant under simultaneous gauge transformations of all fields.

Still, gauge invariance in all fields is not sufficient to guarantee gauge invariance in the physically relevant ψ, $\bar{\psi}$, A fields: this has to be required separately by the background-field identity constraining the $\bar{A}$ dependence of the vertex functions. Moreover, the gauge-fixing term acquires a complicated scale dependence. If there is no fluctuating A field, however, there is no gauge-fixing term, and in special cases a simple gauge-invariant construction is possible.

3.2.3 Manifest gauge invariance

The discussion of the background-field method (cf. section 3.2.2) raises the question whether we can construct a gauge-invariant cutoff kinetic term $Q^\Lambda[A]$ in the presence of an external field A. For a Lorentz-invariant model, $-iD_\mu$ is a hermitean operator and so is $Q[A] = Q(D_\mu)$, with real energy eigenvalues $\epsilon(A)$ depending on the particular configuration of A. This allows to define a cutoff $\chi^\Lambda(|\epsilon(A)|)$ in terms of this energy, instead of frequency or momentum, by

$$Q^\Lambda[A] := \frac{Q[A]}{\chi^\Lambda\big(\sqrt{Q^\dagger[A]Q[A]}\big)} \tag{3.22}$$

for normal operators $Q[A]$. For finite matrices and discrete spectra, $Q[A]$ can be diagonalized and the cutoff applied separately for each eigenvalue ϵ_k, $Q^\Lambda(\epsilon_k) := Q(\epsilon_k)/\chi^\Lambda(\epsilon_k)$.

Because $Q^\Lambda[A]$ is gauge invariant by construction, equation (3.6) now holds also with cutoff,

$$\left(\alpha, \partial_\mu \frac{\delta Q^\Lambda[A]}{\delta i A_\mu}\right) = \big[\alpha, Q^\Lambda[A]\big]. \tag{3.23}$$

In the background-field method the background field $\bar{A}$ is coupled via the term $(Q^\Lambda[\bar{A}] - Q[\bar{A}])$ in the action. Using equation (3.23), the gauge transformation of this term,

$$\left(\delta_\alpha \bar{A}_\mu, \frac{\delta}{\delta \bar{A}_\mu}\{Q^\Lambda[\bar{A}] - Q[\bar{A}]\}\right)\Big|_{\bar{A}=0} = -iX^\Lambda,$$

indeed cancels the modification term X^Λ in equation (3.19). Hence, the $\bar{A}$-dependent cutoff propagator restores the Ward identities without modification.

However, in this work we concentrate on non-relativistic applications with a dispersion relation as in equation (3.7), which contains a *real* time derivative or imaginary frequency. Then the situation is different: $Q[A]$ is not a hermitean operator any more, and it is not even a normal operator if the commutator

$$\big[Q^\dagger[A], Q[A]\big] = -2\partial_t\Big(\varphi + \frac{1}{2m}(i\boldsymbol{\nabla}\cdot\boldsymbol{A} + i\boldsymbol{A}\cdot\boldsymbol{\nabla} + \boldsymbol{A}^2)\Big)$$

does not vanish, i.e., if the electromagnetic potential A depends on time. Then $Q[A]$ and $Q^\dagger[A]$ are not diagonal in the same basis, and the above definition (3.22) of $Q^\Lambda[A]$ is not applicable. Unfortunately, this condition excludes the important case of a finite frequency transfer ω to the external field, even in the limit $\omega \to 0$, which is essential for transport. Thus, energy-momentum cutoffs appear not to be useful in constructing a gauge-invariant $Q^\Lambda[A]$ for non-relativistic models at finite temperature. If Q couples only to the homogeneous $q = 0$ mode of A, the momentum transfer is zero and $Q[A]$ remains diagonal in momentum space, such that one can use a momentum cutoff, $Q^\Lambda[A](K) := Q[A](K)/\chi^\Lambda(K)$, for all frequency shifts ω.

Consider, therefore, alternative flow schemes without an energy-momentum cutoff. If the model is regularized by finite temperature, the temperature- and interaction-flow schemes (cf. section 2.2.1) allow a trivial definition of $Q^\Lambda[A]$. For example, in the interaction-flow scheme with $g = 0 \ldots 1$ we can define $Q^g[A] := Q[A]/g$ for any momentum transfer to the external field. It is essential that the current coupling to the external field is rescaled by the temperature or interaction strength just like the A-independent quadratic part.

In those cases where a gauge-invariant construction of $Q^\Lambda[A]$ is possible we can define a new *gauge-invariant generating functional*[2] as

$$e^{-\mathcal{G}^{\mathrm{gi},\Lambda}[\eta,\bar{\eta},A]} := \int \frac{[d\psi\bar{\psi}]}{\det Q^\Lambda}\, e^{\left(\bar{\psi},Q^\Lambda[A]\psi\right) - V_0[\psi,\bar{\psi}] - \left(j_V^\mu, A_\mu\right) - \left(\bar{\psi},\eta\right) - (\bar{\eta},\psi)} \tag{3.24}$$

[2]Equations (3.24) and (3.26) are equivalent to equation (4.10) in [Reuter&Wetterich 1994] without fluctuations of the gauge field, $a \equiv 0$.

which differs from the previous definition (3.17) in that the cutoff acts also on the A-dependent quadratic part. This yields the Ward identity

$$\boxed{\left(\alpha, \partial_\mu \frac{\delta \mathcal{G}^{\mathrm{gi},\Lambda}}{\delta i A_\mu}\right) = \left(\frac{\delta \mathcal{G}^{\mathrm{gi},\Lambda}}{\delta \eta}, \alpha\eta\right) + \left(\bar{\eta}, \alpha \frac{\delta \mathcal{G}^{\mathrm{gi},\Lambda}}{\delta \bar{\eta}}\right)} \tag{3.25}$$

on any scale Λ. Instead of the Legendre transformation (2.27) we can now define

$$\Gamma^{\mathrm{gi},\Lambda}[\phi, \bar{\phi}, A] + \left(\bar{\phi}, Q^\Lambda[A]\phi\right) = \mathcal{G}^{\mathrm{gi},\Lambda}[\eta, \bar{\eta}, A] + \left(\bar{\phi}, \eta\right) - (\bar{\eta}, \phi)\,. \tag{3.26}$$

Then $\Gamma^{\mathrm{gi},\Lambda}$ evolves under the flow equation

$$\boxed{\partial_\Lambda \Gamma^{\mathrm{gi},\Lambda} = \mathrm{Tr}\, \dot{Q}^\Lambda C^\Lambda - \mathrm{Tr}\, \dot{Q}^\Lambda[A] \Big(Q^\Lambda[A] + \frac{\delta^2 \Gamma^{\mathrm{gi},\Lambda}}{\delta\phi\, \delta\bar{\phi}}\Big)^{-1}} \tag{3.27}$$

and satisfies the Ward identity

$$\boxed{\left(\alpha, \partial_\mu \frac{\delta \Gamma^{\mathrm{gi},\Lambda}}{\delta i A_\mu}\right) = \left(\frac{\delta \Gamma^{\mathrm{gi},\Lambda}}{\delta \phi}, \alpha\phi\right) + \left(\bar{\phi}, \alpha \frac{\delta \Gamma^{\mathrm{gi},\Lambda}}{\delta \bar{\phi}}\right)}. \tag{3.28}$$

This new functional converges to the original one, $\Gamma^{\mathrm{gi},\Lambda} \to \Gamma$ in the limit $\Lambda \to 0$, and $\Gamma^{\mathrm{gi},\Lambda} = \Gamma^\Lambda$ for $A = 0$. However, it has the advantage that its vertex functions are manifestly gauge invariant during the whole flow, i.e., the Ward identities are not modified. Even for a truncated flow-equation hierarchy this remains true as I will show in section 3.2.4: while the flowing response vertex at $\Lambda = 0$ approximates the exact response vertex only to truncation order, it still satisfies the Ward identities exactly to all orders.

Gauge-invariant response vertex

Let us give an explicit example of the current-response operator with cutoff. We diagonalize $Q[A]$, apply the cutoff on the eigenvalues and take the A derivative to obtain the current. To leading order in A, all modes $A(q)$ couple independently, and it is sufficient to consider a single q mode. We therefore capture the generic situation by considering a two-state system with momenta $k \pm q/2 \equiv \pm$ and an inverse propagator

$$Q[A] = \begin{pmatrix} Q_+ & -JA \\ -(JA)^* & Q_- \end{pmatrix} + \mathcal{O}(A^2),$$

which is diagonal for $A = 0$, and where the coupling to A transfers momentum q between the two states, $JA = J^\mu(q;+;-)A_\mu(q)$, $(JA)^* = J^\mu(-q;-;+)A_\mu(-q)$, and the current

$$J^\mu = \begin{pmatrix} 0 & J^\mu(q;+;-) \\ J^\mu(-q;-;+) & 0 \end{pmatrix}.$$

Generally, $Q[A]$ does not need to be a hermitean matrix but only a normal matrix; then the general formula (3.22) has to be used. For a pedagogical derivation, however, we assume that $Q[A]$ is hermitean, as for instance with a purely quadratic dispersion $Q(k_\mu) = |k|^2/2m$. Then $Q[A]$ is diagonalized,

$$Q[A] = \begin{pmatrix} 1 & \frac{JA}{Q_+ - Q_-} \\ -\frac{(JA)^*}{Q_+ - Q_-} & 1 \end{pmatrix} \begin{pmatrix} Q_+ & 0 \\ 0 & Q_- \end{pmatrix} \begin{pmatrix} 1 & -\frac{JA}{Q_+ - Q_-} \\ \frac{(JA)^*}{Q_+ - Q_-} & 1 \end{pmatrix} + \mathcal{O}(A^2),$$

where notably, the eigenvalues depend only quadratically on A. Replacing the diagonal Q by $Q^\Lambda = \begin{pmatrix} Q_+^\Lambda & 0 \\ 0 & Q_-^\Lambda \end{pmatrix}$, we obtain

$$Q^\Lambda[A] = \begin{pmatrix} Q_+^\Lambda & -\frac{Q_+^\Lambda - Q_-^\Lambda}{Q_+ - Q_-} JA \\ -\frac{Q_+^\Lambda - Q_-^\Lambda}{Q_+ - Q_-} (JA)^* & Q_-^\Lambda \end{pmatrix} + \mathcal{O}(A^2),$$

and the cutoff current operator reads

$$J^{\mu,\Lambda} = \frac{Q_+^\Lambda - Q_-^\Lambda}{Q_+ - Q_-} J^\mu ,$$

i.e., the original current rescaled by a number. As a check, the current operator thus constructed has the right limit, $J^{\mu,\Lambda} \to J^\mu$ as $\Lambda \to 0$, and satisfies $q^\mu J^{\mu,\Lambda} = Q_+^\Lambda - Q_-^\Lambda$ as a consequence of the gauge invariance of $Q^\Lambda[A]$, equation (3.23).

3.2.4 Ward identities in truncated flows

If the model and flow scheme permit the construction of a gauge-invariant cutoff bare action as in section 3.2.3, i.e., if $Q^\Lambda[A]$ and the bare interaction are manifestly gauge invariant at any scale, then the full flow-equation hierarchy satisfies the *unmodified* Ward identities on all scales. We shall see that in this case even truncated flows can satisfy the Ward identities exactly.

The most commonly used truncation of the flow-equation hierarchy *without* external field is to set the flow of higher Green functions to zero,

$$\partial_\Lambda G_m^\Lambda(A = 0) := 0 \quad \forall m \geq m_0, \tag{3.29}$$

for some $m_0 > 0$ usually determined by practical considerations and justified perturbatively in the renormalized interaction. I will now show that the Ward identities are satisfied if we demand the same truncation (3.29) also *with* external field,

$$\boxed{\partial_\Lambda G_m^\Lambda(A) := 0 \quad \forall m \geq m_0 \text{ and } \forall A} \tag{3.30}$$

and take derivatives with respect to A_μ in order to obtain the truncated flow equations of the response functions $G^{\mu,\Lambda}_{m;1}(A) := \delta_{A_\mu} G^\Lambda_m(A)$. In particular, also the response functions with $m \geq m_0$ do not flow,

$$\partial_\Lambda G^{\mu,\Lambda}_{m;1}(A) := 0 \quad \forall m \geq m_0. \tag{3.31}$$

The response-function Ward identities (3.25) are of the form

$$\partial_\mu G^{\mu,\Lambda}_{m;1}(A) = i\,\mathsf{S}\, G^\Lambda_m(A) \quad \forall m \tag{3.32}$$

homogeneous in the number of fermion lines, where S represents the momentum shift on the external legs. By the truncation, neither side of equation (3.32) flows for $m \geq m_0$, so the higher Green functions remain at their initial condition—given by the bare action—which by construction is gauge invariant and satisfies the Ward identities.

For $m < m_0$, the RHS of the truncated flow equation is built up completely from bare propagators $Q^\Lambda[A]$ and single-scale propagators $\dot{Q}^\Lambda[A]$ which by construction are manifestly gauge covariant on any scale Λ, as well as from Green functions $G^\Lambda_m(A)$ which we assume to be gauge covariant on a particular scale Λ. Under a gauge transformation, all Green functions and propagators acquire phase factors which cancel on all internal lines, leaving only the phase factors on the external legs which, in turn, imply gauge covariance of the RHS. Then, by infinitesimal induction the Green functions $G^{\Lambda-d\Lambda}_m(A)$ at an infinitesimally lower scale $\Lambda - d\Lambda$ will also be gauge covariant, and hence the Ward identities are satisfied during the complete fRG flow.

This argument is valid in any fRG scheme where the Ward identities are homogenous in the number of fermion lines, which holds in the Polchinski, 1PI and Wick-ordered schemes presented in this work.

3.3 The role of self-consistency

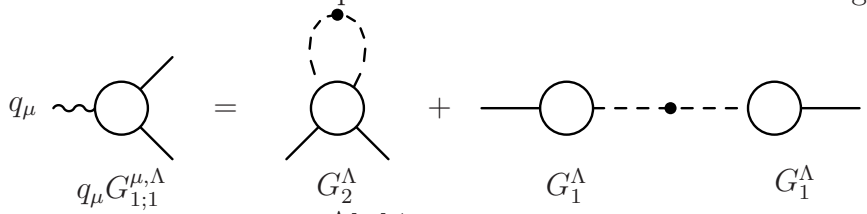
The generating functional $\mathcal{G}^{\mathrm{gi},\Lambda}[\eta,\bar\eta,A]$ defined in equation (3.24) has a redundant parametrization: there are two different ways to obtain the response functions, either by taking a derivative with respect to A_μ or by inserting $\left(\bar\psi, \frac{\delta Q^\Lambda[A]}{\delta A_\mu}\psi\right)$ into the path integral. Assuming from now on a gauge-invariant interaction V_0 and dropping the label "gi", we have

$$\begin{aligned}\frac{\delta}{\delta A_\mu} e^{-\mathcal{G}^\Lambda[\eta,\bar\eta,A]} &= \int \frac{[d\psi\bar\psi]}{\det Q^\Lambda} \left(\bar\psi, \frac{\delta Q^\Lambda[A]}{\delta A_\mu}\psi\right) e^{\left(\bar\psi, Q^\Lambda[A]\psi\right) - V_0[\psi,\bar\psi] - \left(\bar\psi,\eta\right) - (\bar\eta,\psi)} \\ &= -\left(\frac{\delta}{\delta\eta}, \frac{\delta Q^\Lambda[A]}{\delta A_\mu}\frac{\delta}{\delta\bar\eta}\right) e^{-\mathcal{G}^\Lambda[\eta,\bar\eta,A]}.\end{aligned}$$

The second derivative yields terms linear and quadratic in $\mathcal{G}^\Lambda$,

$$\boxed{\frac{\delta \mathcal{G}^\Lambda}{\delta A_\mu} = -\operatorname{Tr}\Big(\frac{\delta Q^\Lambda[A]}{\delta A_\mu}\,\frac{\delta^2 \mathcal{G}^\Lambda}{\delta\eta\,\delta\bar\eta}\Big) + \Big(\frac{\delta \mathcal{G}^\Lambda}{\delta\eta}, \frac{\delta Q^\Lambda[A]}{\delta A_\mu}\,\frac{\delta \mathcal{G}^\Lambda}{\delta\bar\eta}\Big)}. \tag{3.33}$$

This *self-consistency equation* expresses the response functions in terms of higher Green functions with a loop closed, and tree terms. Equation (3.34) illustrates the relation between one- and two-particle connected Green function diagrammatically,



(3.34)

where the dashed lines are $\delta Q^\Lambda[A]/\delta A_\mu$. This relation is generally broken by truncated flows, as we shall see in section 3.3.1. Using the gauge transformation of the quadratic part (3.23) we can write the divergence of equation (3.33) as

$$\Big(\alpha, \partial_\mu \frac{\delta \mathcal{G}^\Lambda}{\delta i A_\mu}\Big) = -\operatorname{Tr}\Big(\big[\alpha, Q^\Lambda[A]\big]\frac{\delta^2 \mathcal{G}^\Lambda}{\delta\eta\,\delta\bar\eta}\Big) + \Big(\frac{\delta \mathcal{G}^\Lambda}{\delta\eta}, \big[\alpha, Q^\Lambda[A]\big]\frac{\delta \mathcal{G}^\Lambda}{\delta\bar\eta}\Big), \tag{3.35}$$

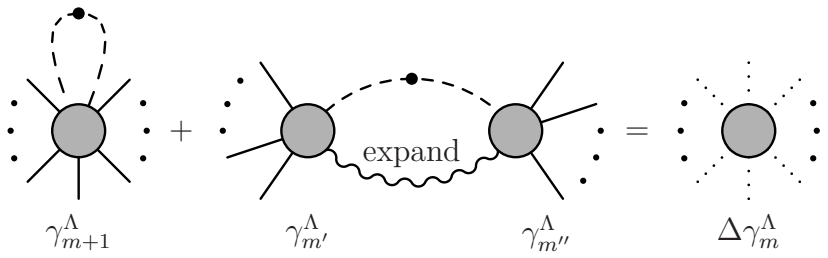
and replace the response function in the Ward identity (3.25) to obtain the *self-consistent Ward identity*

$$\boxed{-\operatorname{Tr}\Big(\big[\alpha, Q^\Lambda[A]\big]\frac{\delta^2 \mathcal{G}^\Lambda}{\delta\eta\,\delta\bar\eta}\Big) + \Big(\frac{\delta \mathcal{G}^\Lambda}{\delta\eta}, \big[\alpha, Q^\Lambda[A]\big]\frac{\delta \mathcal{G}^\Lambda}{\delta\bar\eta}\Big) = \Big(\frac{\delta \mathcal{G}^\Lambda}{\delta\eta}, \alpha\eta\Big) + \Big(\bar\eta, \alpha\frac{\delta \mathcal{G}^\Lambda}{\delta\bar\eta}\Big)}. \tag{3.36}$$

Note that we would arrive at the same self-consistent Ward identities to leading order in A if we would start with the generating functional (3.17) and the modified Ward identities (3.21). By Legendre transformation (3.26) we obtain the self-consistent Ward identity for the 1PI vertex functions,

$$\boxed{-\operatorname{Tr}\Big(\big[\alpha, Q^\Lambda[A]\big]\,\big(Q^\Lambda[A] + \delta^2\Gamma^\Lambda\big)^{-1}\Big) = \Big(\frac{\delta\Gamma^\Lambda}{\delta\phi}, \alpha\phi\Big) + \Big(\bar\phi, \alpha\frac{\delta\Gamma^\Lambda}{\delta\bar\phi}\Big)}. \tag{3.37}$$

The topological structure of the A derivative on the LHS is the same as that of the Λ derivative in equations (2.24), (2.28). The self-consistent Ward identities for the 1PI vertex functions are represented diagrammatically as



where the dashed lines feature the propagator $G^\Lambda\big[\alpha, Q^\Lambda[A]\big]G^\Lambda$.

By amputating bare propagators $C^\Lambda[A]$ from the external legs in equation (3.36) we obtain the *self-consistent Polchinski Ward identity*

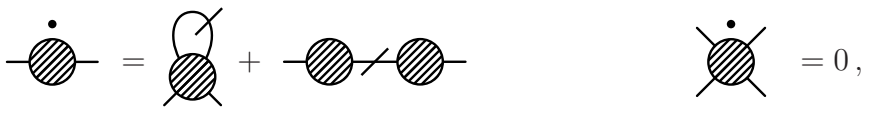
$$\boxed{\mathrm{Tr}\Big(\big[\alpha, C^\Lambda[A]\big]\frac{\delta^2\mathcal{V}^\Lambda}{\delta\chi\,\delta\bar{\chi}}\Big) - \Big(\frac{\delta\mathcal{V}^\Lambda}{\delta\chi}, \big[\alpha, C^\Lambda[A]\big]\frac{\delta\mathcal{V}^\Lambda}{\delta\bar{\chi}}\Big) = \Big(\frac{\delta\mathcal{V}^\Lambda}{\delta\chi}, \alpha\chi\Big) + \Big(\bar{\chi}, \alpha\frac{\delta\mathcal{V}^\Lambda}{\delta\bar{\chi}}\Big)}\,. \tag{3.38}$$

While the previous response-function Ward identities were homogeneous in the number of external electron legs, the self-consistent Ward identities close a loop on higher Green or vertex functions and thereby decrease the number of external legs. This "inhomogeneity" leads to severe problems: when the flow is truncated the lower Green functions are flowing but the higher ones are not, hence self-consistency is violated, and the above self-consistent Ward identities (3.36), (3.37), and (3.38) are only satisfied to truncation order. Despite intensive search a general solution to the problem of self-consistency remains elusive.

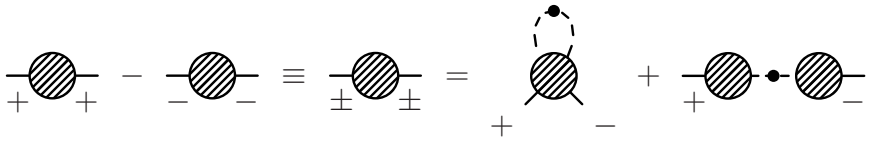
In the upcoming section 3.3.1 I will illustrate how the self-consistent Ward identities are broken by the standard truncation that we have used in section 3.2.4. In section 3.3.2 I review the conserving approximations of Baym and Kadanoff which are self-consistent and satisfy these Ward identities, but turn out to be in general incompatible with truncated flow equations except for special cases (section 3.3.3).

3.3.1 Self-consistent Ward identities in truncated flows

Let us give an example of how a simple truncation breaks the self-consistent Ward identities. This example shows how the problem arises generically. Consider the Polchinski scheme with the truncated flow equations (2.39),



where slashed lines denote $\dot{C}^\Lambda$. The corresponding Ward identities (3.38) are



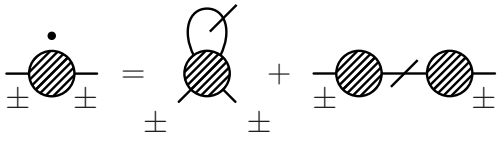
(3.39)

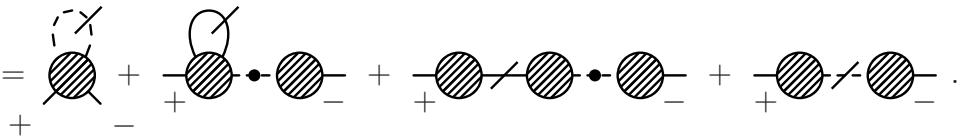


(3.40)

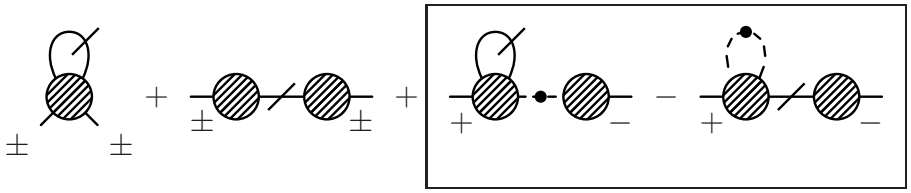
where dots on the external legs denote a momentum shift on any one of the legs as in equation (3.15), and dashed lines denote $[\alpha, C^\Lambda]$. This truncation is simpler than the ones used in practice; however, it is useful pedagogically because it demonstrates the problems already at second order in the renormalized interaction. A truncation at a higher level would display the same type of problem, only further down in the hierarchy where the diagrammatics is more tedious.

If the Ward identity is to be compatible with the truncated flow, the Λ derivatives of the LHS and RHS of the Ward identity (3.39) for the one-particle function should agree:

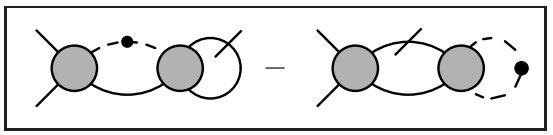
$\partial_\Lambda \mathrm{LHS(WI)} =$ 

$\partial_\Lambda \mathrm{RHS(WI)} =$ 

The second line can be rewritten using both Ward identities above and $\partial_\Lambda[\alpha, C^\Lambda] = [\alpha, \dot{C}^\Lambda]$,

$\partial_\Lambda \mathrm{RHS(WI)} =$ 

The LHS and RHS differ, thus we cannot complete a proof of the Ward identities by induction: even if the Ward identities are satisfied at some scale Λ, the flow violates them by the terms highlighted in the box. There is no reason why these terms should in general vanish, or why the Ward identities should be miraculously satisfied at the end of the flow even though they are violated during the flow. Similarly, in the 1PI scheme with a truncation such that the two-particle vertex function does not flow, the violation is of the form

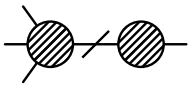
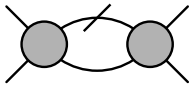


(3.41)

If one had not truncated the flow and Ward identity of the two-particle Green function, they would have generated the missing terms. The difference to the formulation of the Ward identities in terms of response functions can be seen in (3.32) and (3.39): while the one-particle response function follows the same flow equation (3.30) as the

one-particle Green function, only with an additional A derivative, the two-particle Green function follows by truncation a different flow equation and is, therefore, not determined by the same approximation (in the sense explained below) as the one-particle function. Hence, self-consistency and with it the self-consistent Ward identities are violated. This will be illustrated more clearly in the next section 3.3.2 on conserving approximations.

Note, however, that this violation may be not so bad numerically: the violation terms highlighted in the boxes all have the structure of the terms neglected by the truncation,

 (Polchinski),  (1PI) (3.42)

but with another dashed line closed, and vice versa with the slashed and dashed lines interchanged. Therefore, if the truncation is justified because the truncated terms are small, then also the violation will be small.

3.3.2 Conserving approximations of Baym and Kadanoff

Baym and Kadanoff [Baym&Kadanoff 1961, Baym 1962] introduced a formalism to obtain *conserving approximations* which by construction satisfy the self-consistent Ward identities. We shall compare the fRG to these approximations and see whether, under certain conditions, the fRG might also provide conserving approximations.

Proof of number conservation

In order to make the reader familiar with the derivation of conserving approximations, we shall discuss the proof of the number conservation law due to [Baym 1962]. During the proof it will become clear what the requirements are, and we will try to answer the question whether truncated fRG schemes might satisfy these requirements.

Baym and Kadanoff formulate their theory in terms of propagator lines as basic objects, not the source fields η, $\bar{\eta}$ we have used. Therefore, they add an external field to the partition function,

$$Z(U) := \int [d\psi\bar{\psi}]\, e^{S[\psi,\bar{\psi}]-\left(\bar{\psi},U\psi\right)}$$

with $U = U(1,1')$ *bilocal* in space-time:[3] $\left(\bar{\psi},U\psi\right) = \int d1\, d1'\, \bar{\psi}(1)\, U(1,1')\, \psi(1')$. The labels 1, 1′ are abbreviations for x_1, $x_{1'}$ with all space-time components, and the

[3]This should not easily be confused with the two-particle interaction U^Λ in Chapter 4.

integral $\int d1 \equiv \int dr_1 \int_0^{-i\beta} dt_1$. Thereby, all Green functions are functionals of the external field U, such as the bare propagator $G_0(1-1';U)$ and the full propagator $G(1,1';U)$. The linear response of $G(1,1';U)$ to the external field is the two-particle correlation function,

$$L(12,1'2') := -\frac{\delta G(1,1';U)}{\delta U(2',2)}\Big|_{U=0} = [G_2(12,1'2') - G(1-1')G(2-2')]_{U=0}\,.$$

The Dyson equation

$$G^{-1}(1,1';U) = G_0^{-1}(1-1') - U(1,1') - \Sigma(1,1';G(U)) \tag{3.43}$$

shall be satisfied exactly even by an approximate $G(U)$ and self energy Σ.

The first requirement is that Σ be a functional of the full propagator $G(U)$ and the *bare* gauge-invariant density-density interaction V_0. We shall see below that this may be relaxed a little to include any propagator that transforms in the same way as $G(U)$ under change of U.

In order to show that the approximate L satisfies the local number conservation law, we choose an external disturbance U that corresponds to a gauge transformation,

$$\big(\bar\psi, U\psi\big) = \int d1 \left[\frac{\partial\alpha(1)}{\partial t_1}\rho(1) + \boldsymbol{\nabla}\alpha(1)\cdot\big\{\boldsymbol{j}(1) + \frac{1}{2m}\boldsymbol{\nabla}\alpha(1)\rho(1)\big\}\right].$$

The equation for the bare propagator becomes

$$\Big\{i\frac{\partial}{\partial t_1} - \frac{\partial\alpha(1)}{\partial t_1} + \frac{1}{2m}\big[\boldsymbol{\nabla}_1 + i\boldsymbol{\nabla}\alpha(1)\big]^2\Big\}G_0(1,1';\alpha) = \delta(1-1') \tag{3.44}$$

with the solution

$$G_0(1,1';\alpha) = e^{-i\alpha(1)}\,G_0(1-1')\,e^{i\alpha(1')} \tag{3.45}$$

where $G_0(1-1')$ satisfies (3.44) with $\alpha\equiv 0$. If we assume the boundary condition of the external disturbance to be

$$\alpha(r,\tau=0) = \alpha(r,\tau=-i\beta) \tag{3.46}$$

then also the solution $G_0(\alpha)$ satisfies this boundary condition. The full propagator is the solution of the Dyson equation (3.43),

$$\Big\{i\frac{\partial}{\partial t_1} - \frac{\partial\alpha(1)}{\partial t_1} + \frac{1}{2m}\big[\boldsymbol{\nabla}_1 + i\boldsymbol{\nabla}\alpha(1)\big]^2\Big\}G(1,1';\alpha) - \int d\bar1\,\Sigma(1,\bar1;G(\alpha))\,G(\bar1,1';\alpha)$$
$$= \delta(1-1'). \tag{3.47}$$

We will now show that if Σ is a functional of $G(\alpha)$ (as we have assumed), also $G(\alpha)$ will transform analogously to equation (3.45). To this end, substitute

$$G(1,1';\alpha) \mapsto e^{-i\alpha(1)}\,\bar{G}(1,1';\alpha)\,e^{i\alpha(1')} \tag{3.48}$$

in equation (3.47) and in the functional $\Sigma(G(\alpha))$. If and only if all propagators in Σ depend on U in the same way, at each vertex V_0 there will be four phase factors. Because particles are assumed to be conserved at each vertex (by the gauge invariance $\delta_\alpha V_0 = 0$), these factors cancel exactly at each interaction vertex and remain only at the external legs, such that Σ transforms as

$$\Sigma(1,1';G(\alpha)) = e^{-i\alpha(1)}\,\Sigma(1,1';\bar{G})\,e^{i\alpha(1')}.$$

Then, equation (3.47) becomes

$$\begin{aligned}
&\Big\{i\frac{\partial}{\partial t_1} - \frac{\partial\alpha(1)}{\partial t_1} + \frac{1}{2m}\big[\boldsymbol{\nabla}_1 + i\boldsymbol{\nabla}\alpha(1)\big]^2\Big\}e^{-i\alpha(1)}\,\bar{G}(1,1';\alpha)\,e^{i\alpha(1')} \\
&\quad - \int d\bar{1}\,e^{-i\alpha(1)}\,\Sigma(1,\bar{1};\bar{G})\,\bar{G}(\bar{1},1';\alpha)\,e^{i\alpha(1')} \\
&= e^{-i\alpha(1)}\,\left[\Big\{i\frac{\partial}{\partial t_1} + \frac{1}{2m}\boldsymbol{\nabla}_1^2\Big\}\bar{G} - \int \Sigma\,\bar{G}\right] e^{i\alpha(1')} = \delta(1-1').
\end{aligned}$$

Because of the δ function on the RHS the two phase factors cancel, and we obtain

$$\Big\{i\frac{\partial}{\partial t_1} + \frac{1}{2m}\boldsymbol{\nabla}_1^2\Big\}\bar{G} - \int \Sigma\,\bar{G} = \delta(1-1'),$$

which is the Dyson equation (3.47) defining $G(1-1';\alpha=0)$. Because the solution to this equation is unique,

$$\bar{G}(1,1';\alpha) = G(1-1';\alpha=0)\,,$$

and using equation (3.48),

$$G(1,1';\alpha) = e^{-i\alpha(1)}\,G(1-1';\alpha=0)\,e^{i\alpha(1')}\,, \tag{3.49}$$

which is the same transformation law as for the bare propagator, equation (3.45). Now we expand both sides of equation (3.49) to first order in α:

$$\begin{aligned}
&\int d2\left\{\frac{\partial\alpha(2)}{\partial t_2}L(12,1'2) + \boldsymbol{\nabla}\alpha(2)\cdot\left[\frac{\boldsymbol{\nabla}_2 - \boldsymbol{\nabla}'_2}{2im}L(12,1'2')\right]_{2'=2}\right\} \\
&= i[\alpha(1)-\alpha(1')]G(1-1').
\end{aligned}$$

Integrating by parts on the LHS using the boundary condition (3.46) and comparing the coefficient of $\alpha(2)$ yields the number conservation law for L, which is equivalent to the self-consistent Ward identity (3.36):

$$\frac{\partial}{\partial t_2} L(12,1'2) + \boldsymbol{\nabla}_2 \cdot \left[\frac{\boldsymbol{\nabla}_2 - \boldsymbol{\nabla}_2'}{2im} L(12,1'2') \right]_{2'=2} = -i[\delta(1-2) - \delta(1'-2)] G(1-1').$$

The conservation law in the $1,1'$ variables of L follows if we demand in addition that L be symmetric in $1,1' \leftrightarrow 2,2'$:

$$\frac{\delta G(1,1')}{\delta U(2',2)} = \frac{\delta G(2,2')}{\delta U(1',1)}.$$

This requirement of vanishing "curl" implies, except for pathological cases, that there exists a functional $W(U)$ such that

$$G(1,1') = \frac{\delta W}{\delta U(1',1)}.$$

The Φ functional

For completeness, let us mention that Baym and Kadanoff express the $1,1'$ conservation of L also as a condition on Σ. Σ is assumed there—in contrast to this work—to be a functional only of $G(U)$ and V_0 but not of other propagators like $G_0(U)$, or U directly. Then they derive that a similar vanishing-"curl" condition must be required of Σ,

$$\frac{\delta \Sigma(1,1')}{\delta G(2',2)} = \frac{\delta \Sigma(2,2')}{\delta G(1',1)},$$

and hence, there exists a functional $\Phi[G(U), V_0]$, such that

$$\Sigma(1,1') = \frac{\delta \Phi}{\delta G(1',1)},$$

and $\delta\Sigma/\delta G$ is the *effective particle-hole interaction*. In equilibrium when $U(1,1') = \delta(t_1 - t_1')\,\bar{U}(r_1, r_1')$, W and Φ are related by $W = \Phi - \mathrm{tr}(\Sigma G) - \mathrm{tr}\ln(-G)$. An approximation for $\Sigma[G]$ that can be written as $\delta\Phi/\delta G$ is called Φ-*derivable*.

Diagrammatic interpretation of conserving approximations

Let us give a diagrammatic illustration of the Baym-Kadanoff formalism. In the exact theory $W(U)$ contains every vacuum diagram of perturbation theory with bare vertices V_0 and propagators $G_0(U)$. A derivative with respect to U acts on the $G_0(U)$

lines in each diagram by plucking out one line. The full propagator $G(U) = \delta W/\delta U$ is, therefore, made up of all connected vacuum diagrams with two external legs. A second derivative with respect to U plucks out a second line from each diagram, generating $L = -\delta G/\delta U$, which consists of all diagrams with four external legs.

Consider approximations defined by choosing a possibly infinite subset of all Feynman diagrams for $W(U)$, $G(U)$, and L. In principle, one could choose completely different sets of diagrams for each correlation function. But an approximation is conserving if and only if $L = -\delta G/\delta U$ is satisfied *exactly*, i.e., the diagrams contributing to L are obtained by plucking out one line in each diagram of G, or equivalently, the G diagrams are obtained by closing one loop on each diagram of L. Such an approximation for L is conserving in the $2, 2'$ variables; it can be made conserving also in the $1, 1'$ variables if we demand further that the diagrams of G are derived from those of W by plucking out one line.

Obviously this leaves no room for truncations only on a certain level of the hierarchy of Green functions: the flow equation for the zero-particle component $W(U)$ must completely determine all higher flow equations in order that the classes of diagrams contributing to each Green function are compatible.

3.3.3 How important is self-consistency?

It has become clear that at the core of the problem are not the response-function Ward identities but self-consistency: the relation $L = -\delta G/\delta U$ is not satisfied in the above example where the one-particle function flows but the flow of the two-particle function is truncated. This incompatibility of the truncated flow with conserving approximations raises the question under which circumstances it is a problem not to have a conserving approximation. The answer depends on the physical problem at hand: there are problems which work surprisingly well in the truncated fRG, while others fail miserably.

A favorable example are the 1D impurity problems presented in Chapters 4 and 5. Already for simple truncations the fRG results are very close to the exact asymptotic solution known from Bethe ansatz. This suggests that the terms neglected by the truncation are small. Following the discussion surrounding equation (3.42), also self-consistency is then fulfilled to a high degree of accuracy. Moreover, in the model of Chapter 4 the self-consistent Hartree-Fock approximation, a simple conserving approximation, is known to produce the wrong physical phase (charge-density wave). This is due to the fact that an approximation, while being conserving, can miss important contributions. Generally, if the truncated flow does not diverge, one can even determine some components of $G(U)$ and L self-consistently: one can use any truncated flow to obtain an approximate $W^\Lambda(U)$ in the presence of U and take

numerical derivatives with respect to U to obtain approximate values for $G(U)$ and L which are conserving by construction (cf. section 4.3).

An example of the opposite situation where the violation of the self-consistent Ward identities is disastrous is the reduced BCS model [SHML 2004]. This model is solved exactly by the self-consistent Hartree-Fock approximation. In the presence of a tiny symmetry-breaking term (gap) of magnitude ϵ in the action, the interaction grows very large to $1/\epsilon$ but does not diverge. In the truncated flow equation, this result is only reproduced if one has exactly the correct value of the gap (a component of the one-particle function) in the flow equation for the two-particle interaction. This would be guaranteed by the self-consistent Ward identity relating the one- and two-particle functions; however, even if the truncated flow violates the Ward identity only slightly the interaction may diverge prematurely at $\Lambda > 0$. This problem can be solved by a modification of the flow-equation hierarchy [Katanin 2004]: if the single-scale propagator S^Λ in the 1PI scheme is replaced by the Λ derivative of the full propagator $-\partial_\Lambda G^\Lambda = G^\Lambda(\partial_\Lambda Q^\Lambda - \partial_\Lambda \Sigma^\Lambda)G^\Lambda$ in the truncated flow equation for the two-particle vertex, then the fRG flow reproduces exactly the self-consistent Hartree-Fock solution for models where the two-particle interaction has a reduced momentum dependence. This modification leads to significant improvements also in the single-impurity Anderson model [HMPS 2004].

There are promising approaches to self-consistency by writing the fRG flow equations in terms of both fermionic and bosonic degrees of freedom. For instance, (*i*) [Wetterich 2002] thereby obtains the flow of 2PI vertex functions. (*ii*) The Luttinger model without backscattering is treated in [SBK 2004]; using the separate conservation of the number of left and right movers the flow-equation hierarchy can be closed and solved exactly.

3.4 Summary

In this chapter I have shown how Ward identities, which express the symmetry of the Hamiltonian in terms of Green or vertex functions, are derived in the functional formalism. There are two common formulations of Ward identities. In the field-theoretical and high-energy physics literature, Ward identities are written in terms of response functions. This form of the Ward identities relates for example the self energy to the current response but assumes no particular relation between the self energy and the interaction. A momentum cutoff breaks these response-function Ward identities. This is a problem for the treatment of gauge theories, leading either to modified Ward identities or the introduction of a background gauge field $\bar{A}$. Alternatively, one can use a manifestly gauge-invariant flow scheme such as the temperature flow. It is shown that in this case even truncated flows satisfy the

unmodified Ward identities exactly on all scales.

In the condensed-matter literature, a different form of Ward identity is more common which assumes self-consistency: the response functions in the Ward identities can be expressed as higher Green functions with a loop closed by a special propagator. An example of approximations which satisfy these self-consistent Ward identities without cutoff are the conserving approximations of Baym and Kadanoff. However, I have shown that self-consistency is violated by common truncations, which neglect the flow of Green functions beyond a certain level in the flow-equation hierarchy. For special models with exact mean-field solutions, modified truncated flow equations are known which reproduce these solutions.

4 Functional RG technique in one dimension

In this chapter I introduce the one-dimensional lattice model of a Luttinger liquid (cf. Chapter 5) and explain in detail how the fRG is used to compute observables such as the effective impurity potential, the density-response vertex and the conductance. This chapter is organized as follows: in the first section 4.1 the microscopic lattice model is defined. In section 4.2 I show how the flow equations are set up and solved, with an emphasis on the finite-temperature flow and a new efficient algorithm in 1D. I proceed to explain how to compute the conductance in the fRG framework in section 4.4, giving an argument why vertex corrections play no role in our approximation.

4.1 Microscopic model

Consider a model of spinless fermions on a 1D lattice with nearest-neighbor interaction and various types of impurity potentials. Following [AEMMSS 2004], the Hamiltonian has the form

$$H = H_0 + H_{\text{int}} + H_{\text{imp}}$$

with the kinetic term given by nearest-neighbor hopping with an amplitude $-t$ and chemical potential μ (I will henceforth choose units such that $t = 1$, and the lattice spacing $a = 1$),

$$H_0 = -t \sum_j \left(c_{j+1}^\dagger c_j + c_j^\dagger c_{j+1} \right) - \mu \sum_j n_j,$$

where $n_j = c_j^\dagger c_j$ is the local density operator. The nearest-neighbor interaction of strength $U_{j,j+1} = U_{j+1,j}$ on the bond between sites j and $j+1$ enters as

$$H_{\text{int}} = \sum_j U_{j,j+1} n_j n_{j+1} \tag{4.1}$$

while the static impurity potential $V_{jj'}$ is represented by a term

$$H_{\text{imp}} = \sum_{j,j'} V_{jj'}\, c_j^\dagger c_{j'}.$$

For the conductance calculations, we will couple an interacting system on lattice sites $1, \ldots, N$ on both sides to semi-infinite, non-interacting leads which are described

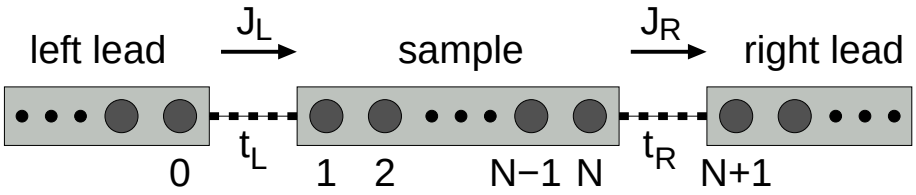


Figure 4.1: *The microscopic setup of the system with leads. The current operators $J_{L,R}$ will only be needed for the conductance calculations.*

completely by H_0 (figure 4.1). In order that electrons do not scatter off the beginning of the interacting region, the interaction has to be switched on smoothly. Explicitly, we choose a spatial profile

$$U_{j,j+1} := U \frac{\arctan\left[(j-j_s)/w\right] - \arctan\left[(1-j_s)/w\right]}{\arctan\left[(N/2-j_s)/w\right] - \arctan\left[(1-j_s)/w\right]} \qquad (j = 1, \ldots, N/2)$$

for the left side of the system, and likewise for the right, where U is the bulk interaction. We have chosen the parameters $w = 4$ and $j_s = 56$ such that the interaction falls to 10% of its value over a typical distance 22 lattice sites.[1]

4.1.1 Projection method applied to the wire

In order to treat this infinite system with leads numerically, we express it (exactly) by an effective Hamiltonian on the N-site interacting region via the projection technique. Consider splitting the Hilbert space of the Hamiltonian H into disjoint subspaces with projection operators $P + Q = \mathbf{1}$:

$$H = \begin{pmatrix} H_{PP} & H_{PQ} \\ H_{QP} & H_{QQ} \end{pmatrix}.$$

The one-particle Green function is the resolvent

$$G(z) := \frac{1}{z - H} = \begin{pmatrix} G_{PP}(z) & G_{PQ}(z) \\ G_{QP}(z) & G_{QQ}(z) \end{pmatrix}$$

with components [PTVF 1986, equation (2.7.23)]

$$G_{PP}(z) = P \frac{1}{z-H} P = \frac{1}{zP - H_{PP} - \underbrace{H_{PQ} \frac{1}{zQ - H_{QQ}} H_{QP}}_{=:\Sigma_{PP}(z)}} \tag{4.2}$$

[1] Although the difference $|U_{j_s-1,j_s} - U_{j_s,j_s+1}| \approx 0.08\,U$ is rather large, the corresponding backscattering component of the effective potential Σ is typically below 10^{-4}, and the conductance at $T = 0$ deviates from the unitary limit by less than 10^{-8}.

$$
\begin{aligned}
G_{PQ}(z) &= P\frac{1}{z-H}Q = -G_{PP}(z)H_{PQ}\frac{1}{zQ-H_{QQ}} \\
G_{QP}(z) &= Q\frac{1}{z-H}P = -\frac{1}{zQ-H_{QQ}}H_{QP}G_{PP}(z) \\
G_{QQ}(z) &= Q\frac{1}{z-H}Q = \frac{1}{zQ-H_{QQ}} + \frac{1}{zQ-H_{QQ}}H_{QP}G_{PP}(z)H_{PQ}\frac{1}{zQ-H_{QQ}}.
\end{aligned}
$$

For the wire, P shall project onto the Hilbert space of the states in the interacting sample with site indices $1, \ldots, N$, while Q shall denote the remaining non-interacting leads on sites $\ldots, 0$ and $N+1, \ldots$. Thus,

$$
\begin{aligned}
H_{PP} &= -t\sum_{n=1}^{N-1}\big(|n+1\rangle\langle n| + |n\rangle\langle n+1|\big) - \mu\sum_{n=1}^{N}|n\rangle\langle n| + H_{\text{int}} + H_{\text{imp}} \\
H_{PQ} &= -t_L|1\rangle\langle 0| - t_R|N\rangle\langle N+1| \\
H_{QP} &= -t_L|0\rangle\langle 1| - t_R|N+1\rangle\langle N| \\
H_{QQ} &= -t\sum_{\substack{n<0,\\ n\geq N+1}}\big(|n+1\rangle\langle n| + |n\rangle\langle n+1|\big) - \mu\sum_{\substack{n\leq 0,\\ n\geq N+1}}|n\rangle\langle n|.
\end{aligned}
$$

The left and right leads in H_{QQ} do not couple directly but only through the sample. In order to compute Σ_{PP} in equation (4.2) we need to know the Green function of the (left) lead at the interface site 0, $\langle 0|(zQ - H_{QQ})^{-1}|0\rangle$. To this end, consider a semi-infinite lead ranging from $-\infty$ up to some site j, and denote the Green function at the rightmost site j as $g_L(z) := (z - H_0)^{-1}_{j,j}$. Consider adding one more site $j+1$ to the right, with the same hopping amplitude $-t$. Because the lead is semi-infinite and homogeneous, the Green function $g'_L(z)$ at the new site $j+1$ should be the same as $g_L(z)$. Again using the same formula (4.2) with Q now denoting the states on sites $-\infty, \ldots, j$ and P for $j+1$,

$$
\begin{aligned}
[g'_L(z)]^{-1} &= (z-H_0)_{j+1,j+1} - (H_0)_{j+1,j}\,(z-H_0)^{-1}_{j,j}\,(H_0)_{j,j+1} \\
&= (z+\mu) - t\,g_L(z)\,t \stackrel{!}{=} [g_L(z)]^{-1}.
\end{aligned}
$$

This leads to a quadratic equation for $g_L(z)$,

$$
t^2 g_L^2(z) - (z+\mu)\,g_L(z) + 1 = 0
$$

with solution ($t = 1$)

$$
g_L(z) = \frac{1}{2}\left(z + \mu \mp i\sqrt{4 - (z+\mu)^2}\right) \tag{4.3}
$$

and $g_R(z) = g_L(z)$ because the right lead has the same structure as the left lead. $g_L(z)$ has a branch cut at the real axis $\operatorname{Im} z = 0$. The sign $\pm$ is chosen such that the

imaginary part of $g_L(z)$ changes sign across the branch cut. For the local density of states of the leads we obtain

$$\rho_L(\omega) := -\frac{1}{\pi}\mathrm{Im}\, g_L(\omega + i0) = \frac{1}{2\pi}\sqrt{4-(\omega+\mu)^2},$$

for $|\omega + \mu| \leq 2$. Now we have all ingredients for the lead contributions to the propagator of the sample, equation (4.2):

$$\begin{aligned}
\Sigma_{PP}(z) &:= H_{PQ}\frac{1}{zQ - H_{QQ}}H_{QP} \\
&= t_L|1\rangle\langle 0|(zQ - H_{QQ})^{-1}|0\rangle\langle 1|t_L \\
&\quad + t_R|N\rangle\langle N+1|(zQ - H_{QQ})^{-1}|N+1\rangle\langle N|t_R \\
&= t_L^2\, g_L(z)\,|1\rangle\langle 1| + t_R^2\, g_R(z)\,|N\rangle\langle N| \qquad (4.4)
\end{aligned}$$

$$\begin{aligned}
G_{j0}(z) &= \langle j|G_{PQ}(z)|0\rangle \\
&= -\langle j|G_{PP}(z)|1\rangle\, t_L\, \langle 0|(zQ - H_{QQ})^{-1}|0\rangle \\
&= -G_{j1}(z)\, t_L\, g_L(z) \qquad (j = 1, \ldots, N) \qquad (4.5)
\end{aligned}$$

$$\begin{aligned}
G_{N+1,j}(z) &= \langle N+1|G_{QP}(z)|j\rangle \\
&= -\langle N+1|(zQ - H_{QQ})^{-1}|N+1\rangle\, t_R\, \langle N|G_{PP}(z)|j\rangle \\
&= -g_R(z)\, t_R\, G_{Nj}(z) \qquad (j = 1, \ldots, N) \qquad (4.6)
\end{aligned}$$

$$\begin{aligned}
G_{N+1,0}(z) &= \langle N+1|G_{QQ}(z)|0\rangle \\
&= \langle N+1|(zQ - H_{QQ})^{-1}|0\rangle \;\; (= 0 \text{ as left and right leads do not couple directly}) \\
&+ \langle N+1|(zQ - H_{QQ})^{-1}|N+1\rangle\, t_R\, \langle N|G_{PP}(z)|1\rangle\, t_L\, \langle 0|(zQ - H_{QQ})^{-1}|0\rangle \\
&= g_R(z)\, t_R\, G_{N1}(z)\, t_L\, g_L(z). \qquad (4.7)
\end{aligned}$$

In the non-interacting leads, $H_{QQ} = H_0$. In the sample, the quadratic (non-interacting) part of H_{PP} shall include the impurity:

$$\xi_{jj'} := (H_0 + H_{\mathrm{imp}})_{jj'} = -t(\delta_{j,j'+1} + \delta_{j,j'-1}) - \mu\delta_{jj'} + V_{jj'}.$$

The lead contribution is also independent of the interaction,

$$\Sigma^{\mathrm{leads}}(z) := \Sigma_{PP}(z) = t_L^2\, g_L(z)\,|1\rangle\langle 1| + t_R^2\, g_R(z)\,|N\rangle\langle N|, \qquad (4.8)$$

and all non-interacting contributions are combined into the inverse *bare* propagator in the sample,

$$Q_{jj'}(z) \equiv [G_0^{-1}(z)]_{jj'} := z\delta_{jj'} - \xi_{jj'} - \Sigma^{\mathrm{leads}}_{jj'}(z). \qquad (4.9)$$

The interaction H_{int} creates an effective one-particle potential $\Sigma(z, T)$ at temperature T. The *full* sample propagator is determined by the Dyson equation,

$$[G^{-1}(z, T)]_{jj'} = Q_{jj'}(z) - \Sigma_{jj'}(z, T). \qquad (4.10)$$

4.1.2 Bare vertices

The fRG is formulated in terms of a path integral weighted by the action, so the bare and interaction parts of the Hamiltonian have to be translated into the Lagrangian language: the inverse bare propagator $Q(z)$ defined in equation (4.9) becomes the quadratic part of the Lagrangian, and the bare interaction H_{int} becomes the interaction part:

$$S[\psi,\bar{\psi}] = T\sum_{n,j,j'} Q_{jj'}(i\omega_n)\,\bar{\psi}_j(i\omega_n)\psi_{j'}(i\omega_n) + \sum_{1,1',2,2'} I_{1',2';1,2}\,\bar{\psi}(1')\bar{\psi}(2')\psi(2)\psi(1)$$

where $I_{1',2';1,2}$ is the bare antisymmetrized interaction vertex equivalent to H_{int}, and the sum over $1, 1', \ldots$ includes Matsubara frequencies and lattice indices. The nearest-neighbor interaction conserves frequency but has no further frequency dependence. The remaining spatial dependence has the real-space form

$$I_{j_1',j_2';j_1,j_2} = U_{j_1,j_2}[\delta_{j_1,j_2-1} + \delta_{j_1,j_2+1}](\delta_{j_1,j_1'}\delta_{j_2,j_2'} - \delta_{j_1,j_2'}\delta_{j_2,j_1'}). \tag{4.11}$$

In the bulk $U_{j,j+1} \equiv U$ is homogeneous, hence the bare interaction is translationally invariant and can be expressed in a momentum basis:

$$I_{k_1',k_2';k_1,k_2} = 2U[\cos(k_1'-k_1) - \cos(k_2'-k_1)]\delta^{(2\pi)}_{k_1+k_2,k_1'+k_2'} \tag{4.12}$$

where the Kronecker δ implements momentum conservation (modulo 2π).

4.2 Functional RG flow equations

For computing the properties of the 1D fermion system, we use the 1PI version of the fRG, cf. section 2.2.3. We cut off the infrared part of the free propagator on a scale Λ and differentiate the generating functional for the vertex functions with respect to this scale. Thereby we obtain an exact hierarchy of flow equations for the irreducible vertex functions.

4.2.1 Truncated 1PI flow equations

As in [AEMMSS 2004], we choose a cutoff in Matsubara frequency. The cutoff bare propagator $G_0^\Lambda(i\omega)$ (with the notation $G_0 \equiv C$) is defined by

$$G_0^\Lambda(i\omega) := \chi^\Lambda(\omega)\,G_0(i\omega), \tag{4.13}$$

where the characteristic function $\chi^\Lambda(\omega)$ is unity on the high-energy modes and vanishes on the low-energy modes. The exact form of χ^Λ depends on whether $T = 0$ or $T > 0$, as explained below.

Second, we truncate the infinite hierarchy of flow equations by neglecting the flow of the three-particle and higher vertex functions. This closes the hierarchy of flow equations for the one- and two-particle vertex functions and is justified by a small renormalized interaction. The results agree remarkably well quantitatively with known exact results (DMRG, Bethe ansatz) not only for weak but also for moderate interaction strength [AEMMSS 2004, Andergassen 2005].

The truncated 1PI flow equations are written in terms of the one-particle vertex Σ^Λ at scale Λ (self energy) and the two-particle interaction vertex[2] Γ^Λ [AEMMSS 2004],

$$\partial_\Lambda \Sigma^\Lambda(1',1) = -T \sum_{2,2'} e^{i\omega_2 0^+} S^\Lambda(2,2')\, \Gamma^\Lambda(1',2';1,2) \tag{4.14}$$

$$\begin{aligned}\partial_\Lambda \Gamma^\Lambda(1',2';1,2) = T \sum_{3,3'} \sum_{4,4'} & G^\Lambda(3',3)\, S^\Lambda(4,4') \\ & \times \Big[\Gamma^\Lambda(1',2';3,4)\, \Gamma^\Lambda(3',4';1,2) \\ & \quad - \Gamma^\Lambda(1',4';1,3)\, \Gamma^\Lambda(3',2';4,2) - (3 \leftrightarrow 4, 3' \leftrightarrow 4') \\ & \quad + \Gamma^\Lambda(2',4';1,3)\, \Gamma^\Lambda(3',1';4,2) + (3 \leftrightarrow 4, 3' \leftrightarrow 4') \Big].\end{aligned} \tag{4.15}$$

The indices $1, 2, \ldots$ label both frequency and spatial indices. The full propagator is determined from the self energy by the Dyson equation

$$G^\Lambda = [Q^\Lambda - \Sigma^\Lambda]^{-1}, \tag{4.16}$$

where $Q^\Lambda \equiv [G_0^\Lambda]^{-1} = Q/\chi^\Lambda$ is the inverse bare cutoff propagator. S^Λ denotes the *single-scale propagator* which will select only modes with frequency near Λ for the frequency cutoff,

$$S^\Lambda := G^\Lambda \dot{Q}^\Lambda G^\Lambda = -\dot{\chi}^\Lambda \frac{1}{Q - \chi^\Lambda \Sigma^\Lambda} Q \frac{1}{Q - \chi^\Lambda \Sigma^\Lambda}, \tag{4.17}$$

where the dot denotes ∂_Λ. The convergence factor $e^{i\omega_2 0^+}$ in the Σ^Λ flow equation is only necessary to define the initial condition of the flow at $\Lambda = \Lambda_0 \to \infty$ (see below).

Parametrization of the interaction

The two-particle interaction vertex $\Gamma^\Lambda(1',2';1,2)$ is in general a very complicated function. However, in the low-energy limit the flow of Σ^Λ and Γ^Λ is dominated by very few channels of the interaction [Andergassen 2005, AEMMSS 2004]. At any Λ, perturbation theory in the renormalized interaction strength provides a guide for a simple parametrization of Γ^Λ. For a model of spinless fermions with nearest-neighbor

[2] Not to be confused with the full functional $\Gamma^\Lambda[\phi, \bar{\phi}]$!

interaction and only few impurities (i.e., not disordered), the following parametrization captures the qualitative as well as the quantitative features of Luttinger liquids very well. The renormalized interaction vertex Γ^Λ is assumed to be frequency independent beyond the conservation of frequency, and the RHS of the flow equation is evaluated with all external frequencies set to zero. Likewise, its spatial dependence is approximated by a renormalized nearest-neighbor interaction U^Λ, and in the flow all external momenta are projected to $\pm k_\mathrm{F}$. The internal lines carry propagators without the self energy or the impurity potential, which would lead to corrections only at higher order in the interaction.

In the bulk $U_{j,j+1} \equiv U$ is homogeneous, and Γ^Λ has the momentum-space form (independent of frequency)

$$\Gamma^\Lambda_{k_1',k_2';k_1,k_2} = 2U^\Lambda[\cos(k_1'-k_1)-\cos(k_2'-k_1)]\delta^{(2\pi)}_{k_1+k_2,k_1'+k_2'}$$

which is just the bulk bare interaction (4.12),

$$I_{k_1',k_2';k_1,k_2} = 2U[\cos(k_1'-k_1)-\cos(k_2'-k_1)]\delta^{(2\pi)}_{k_1+k_2,k_1'+k_2'}$$

rescaled by U^Λ/U. The particular flow equation for U^Λ depends on the cutoff chosen and will be given below for several types of cutoff. However, the general form is a consequence of the above parametrization,

$$\partial_\Lambda U^\Lambda = -(U^\Lambda)^2\, T\sum_\omega \dot\chi^\Lambda(\omega) \oint \frac{dp}{2\pi} f(p,\omega) \tag{4.18}$$

where $f(p,\omega)$ is the sum of the three different channels (PP, PH, PH') in equation (4.15) [AEMMSS 2004]. For instance at half filling where $\mu = 0$ and $\xi_p = -2\cos(p) = \xi_{-p}$,

$$f(p,\omega) = \frac{2\sin^2(p)}{(i\omega-\xi_p)(-i\omega-\xi_{-p})} - \frac{\cos^2(p)}{(i\omega-\xi_p)^2} - \frac{[1+\sin(p)]^2}{(i\omega-\xi_p)(-i\omega-\xi_p)} \tag{4.19}$$

$$= -\cos^2(p)\left[\frac{1}{(i\omega-\xi_p)(-i\omega-\xi_p)} + \frac{1}{(i\omega-\xi_p)^2}\right]. \tag{4.20}$$

Going from the bulk $U_{j,j+1} \equiv U$ back to the lattice, we apply the U^Λ flow equation for each $U^\Lambda_{j,j+1}$ locally.

Parametrizing Γ^Λ by a renormalized nearest-neighbor interaction $U^\Lambda_{j,j+1}$ has the great advantage that the self energy is a tridiagonal matrix in real space: only the matrix elements $\Sigma^\Lambda_{j,j(\pm1)}$ are non-zero. The tridiagonal flow equations for a general cutoff are

$$\begin{aligned}\partial_\Lambda \Sigma^\Lambda_{j,j} &= T\sum_\omega \dot\chi^\Lambda \sum_{r=\pm1} U^\Lambda_{j,j+r}\, S^\Lambda_{j+r,j+r}(i\omega)\\ \partial_\Lambda \Sigma^\Lambda_{j,j\pm1} &= -T\sum_\omega \dot\chi^\Lambda U^\Lambda_{j,j\pm1}\, S^\Lambda_{j,j\pm1}(i\omega).\end{aligned} \tag{4.21}$$

Note that the self energy remains independent of frequency and real because the interaction does not depend on frequency in our parametrization.

4.2.2 Frequency cutoff at zero temperature

At zero temperature we choose the sharp cutoff

$$\chi^\Lambda(\omega) := \Theta(|\omega| - \Lambda), \qquad \dot{\chi}^\Lambda(\omega) = -\delta(|\omega| - \Lambda) \tag{4.22}$$

which cuts off all modes with frequency smaller than Λ. As explained in section 2.2.3, a sharp cutoff at $T = 0$ allows to integrate over the Θ step functions analytically which leaves only *smooth* propagators $\tilde{G}$ in each loop diagram (2.34),

$$\tilde{G}^\Lambda(i\omega) := [Q(i\omega) - \Sigma^\Lambda]^{-1}, \tag{4.23}$$

as opposed to $G^\Lambda(i\omega)$ from equation (4.16) which has a step at $|\omega| = \Lambda$. The flow equations (4.21) at $T = 0$ for a sharp frequency cutoff then read (with $T\sum_\omega \mapsto \frac{1}{2\pi}\int d\omega$)

$$\partial_\Lambda \Sigma^\Lambda_{j,j} = -\frac{1}{2\pi} \sum_{\omega=\pm\Lambda} \sum_{r=\pm 1} U^\Lambda_{j,j+r} \tilde{G}^\Lambda_{j+r,j+r}(i\omega) \tag{4.24}$$

$$\partial_\Lambda \Sigma^\Lambda_{j,j\pm 1} = \frac{1}{2\pi} \sum_{\omega=\pm\Lambda} U^\Lambda_{j,j\pm 1} \tilde{G}^\Lambda_{j,j\pm 1}(i\omega)\,. \tag{4.25}$$

Flow of the interaction

Inserting equation (4.22) into (4.18), the flow equation for U^Λ is

$$\partial_\Lambda U^\Lambda = (U^\Lambda)^2 \frac{1}{2\pi} \sum_{\omega=\pm\Lambda} \oint \frac{dp}{2\pi} f(p,\omega). \tag{4.26}$$

For instance at half filling, the momentum integral over the bubble $f(p,\omega)$ is

$$\begin{aligned}
\oint \frac{dp}{2\pi} \sum_{\omega=\pm\Lambda} f(p,\omega) &= -\oint \frac{dp}{2\pi} \cos^2(p)\, 2\mathrm{Re}\Big[\frac{1}{(i\Lambda - \xi_p)(-i\Lambda - \xi_p)} + \frac{1}{(i\Lambda - \xi_p)^2}\Big] \\
&= -\oint \frac{dp}{2\pi} \frac{[2\cos(p)]^4}{(\Lambda^2 + [2\cos(p)]^2)^2} \\
&= -\left(1 - \Lambda \frac{\Lambda^2 + 6}{(\Lambda^2+4)^{3/2}}\right).
\end{aligned}$$

The differential equation (4.26) separates,

$$\partial_\Lambda \left(\frac{1}{U^\Lambda}\right) = \frac{1}{2\pi}\left(1 - \Lambda \frac{\Lambda^2 + 6}{(\Lambda^2+4)^{3/2}}\right).$$

Integrating each side separately from $\Lambda = \infty$ down to Λ with initial condition $U^{\Lambda=\infty} = U$,

$$\frac{1}{U^\Lambda} - \frac{1}{U} = \frac{1}{2\pi}\left(\Lambda - \frac{2+\Lambda^2}{\sqrt{4+\Lambda^2}}\right)$$

and finally

$$U^\Lambda = \frac{U}{1 + \left(\Lambda - \frac{2+\Lambda^2}{\sqrt{4+\Lambda^2}}\right) U/(2\pi)} \xrightarrow{\Lambda\to 0} \frac{U}{1 - U/(2\pi)}\,. \tag{4.27}$$

Even away from half filling, the flow equation can be integrated analytically using contour integration [Andergassen 2005].

At $T = 0$, the simple expression (4.27) yields the correct low-energy asymptotics to second order in the renormalized vertex and moreover contains the second-order corrections from the lattice dispersion to the vertex (with all external lines at the Fermi surface) at any scale Λ.

Initial conditions

The flow, being given by the solution of an ODE in Λ, is determined uniquely by the flow equation and the initial condition. At the initial upper cutoff scale $\Lambda = \Lambda_0$, the initial condition has contributions from the bare interaction and from the bare impurity potential [AEMMSS 2004]. At $T = 0$, only the combination $\tilde{G}^{-1} = Q - \Sigma^\Lambda$ appears in the flow, such that there is no difference whether one treats the impurity potential as the initial condition for Σ^Λ at the beginning of the flow or, alternatively, as part of the bare propagator Q as in this work. The contribution of the interaction as $\Lambda = \Lambda_0 \to \infty$ is

$$\Sigma^{\Lambda_0}_{1,1'} := \frac{1}{2}\sum_2 I_{1',2;1,2} \tag{4.28}$$

$$\Gamma^{\Lambda_0}_{1',2';1,2} := I_{1',2';1,2}\,, \tag{4.29}$$

where $I_{1',2';1,2}$ is the bare antisymmetrized interaction (4.11). The initial condition for the self energy is usually compensated by a local potential to avoid that the filling changes (see section 4.2.6 below). Only if the interaction extends to an open boundary without lead, a boundary term $\Sigma^{\Lambda_0}_{\text{boundary}} := -U/2$ remains.

4.2.3 Frequency cutoff at finite temperature

At $T > 0$, a sharp cutoff $\chi^\Lambda(\omega_n) = \Theta(|\omega_n| - \Lambda)$ analogous to the $T = 0$ case would lead to a δ peak on the RHS of the flow equation of Σ^Λ at every fermionic Matsubara

frequency $\Lambda = |\omega_n|$. This creates finite jumps in the integrated Σ^Λ, therefore, the Θ integration formula (2.33) cannot be applied as it is only valid for continuous functions. For the ODE integration, a smooth right-hand side is best, but this has to be balanced against the number of Matsubara frequencies ω_n on which $\dot{\chi}^\Lambda(\omega_n) > 0$ for every particular value of Λ.

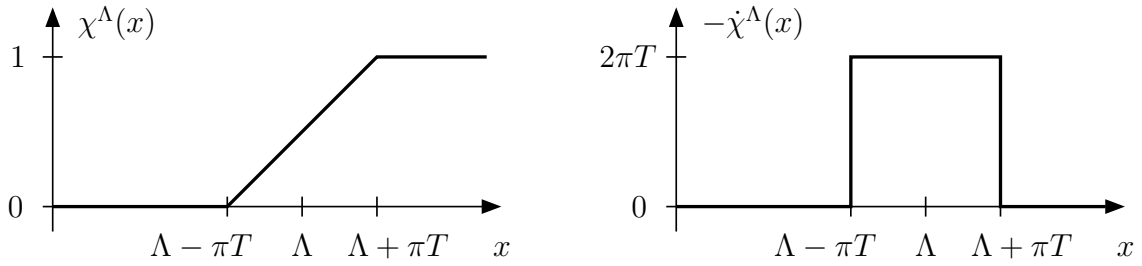


Figure 4.2: *The cutoff function used at finite temperature.*

As a compromise, we use a cutoff function (cf. figure 4.2)

$$\chi^\Lambda(\omega_n) := \begin{cases} 0 & |\omega_n| \leq \Lambda - \pi T \\ \frac{1}{2} + \frac{|\omega_n| - \Lambda}{2\pi T} & \Lambda - \pi T \leq |\omega_n| \leq \Lambda + \pi T \\ 1 & \Lambda + \pi T \leq |\omega_n| \end{cases}$$

with the accompanying Λ derivative

$$-\dot{\chi}^\Lambda(\omega_n) = \begin{cases} \frac{1}{2\pi T} & \Lambda - \pi T < |\omega_n| < \Lambda + \pi T \\ 0 & \text{otherwise.} \end{cases}$$

A Matsubara sum over the single-scale propagator (4.17) with this cutoff contains exactly one term $\pm\omega_n$ in the Matsubara sum,

$$T \sum_n S^\Lambda(i\omega_n) = T \sum_n -\dot{\chi}^\Lambda(\omega_n) \cdots = \frac{1}{2\pi} \sum_{\omega_n \approx \pm\Lambda} \cdots$$

The flow equation for the self energy Σ^Λ has the same general form as for $T = 0$, but for $T > 0$, the single-scale propagator S^Λ cannot be further simplified to $\tilde{G}$:

$$\begin{aligned} \partial_\Lambda \Sigma^\Lambda_{j,j} &= -\frac{1}{2\pi} \sum_{\omega_n \approx \pm\Lambda} \sum_{r=\pm 1} U^\Lambda_{j,j+r} \\ &\quad \times \left[\frac{1}{Q(i\omega_n) - \chi^\Lambda(\omega_n)\Sigma^\Lambda} Q(i\omega_n) \frac{1}{Q(i\omega_n) - \chi^\Lambda(\omega_n)\Sigma^\Lambda} \right]_{j+r,j+r} \\ \partial_\Lambda \Sigma^\Lambda_{j,j\pm 1} &= \frac{1}{2\pi} \sum_{\omega_n \approx \pm\Lambda} U^\Lambda_{j,j\pm 1} \end{aligned} \tag{4.30}$$

$$\times \left[\frac{1}{Q(i\omega_n) - \chi^\Lambda(\omega_n)\Sigma^\Lambda} Q(i\omega) \frac{1}{Q(i\omega_n) - \chi^\Lambda(\omega_n)\Sigma^\Lambda} \right]_{j,j\pm1} .$$

At every $\Lambda = \omega_n - \pi T$, a switch from ω_n to ω_{n-1} occurs and the integrated flow has a kink, instead of a jump for a sharp cutoff. At large frequencies, the self energy is still so small that an adaptive step-size integration algorithm efficiently takes steps of many Matsubara frequencies at once, while at small frequencies it inefficiently takes many small steps to resolve the kink accurately. But since the positions of the kinks are known, we can instead integrate only in the interval between each pair of kinks. Empirically, the switch between continuous integration and integration only between kinks is best done around $\omega_n \approx t$. As there are $\mathcal{O}(1/T)$ such intervals, the runtime for the complete flow scales as $\mathcal{O}(N/T)$.

Flow of the interaction

The flow of the interaction is simpler: as self-energy corrections on the internal lines of the interaction flow equation would be of $\mathcal{O}((\Gamma^\Lambda)^3)$, we take only bare propagators on the internal lines, such that the bare single-scale propagator is (setting $\Sigma^\Lambda = 0$)

$$S_0^\Lambda(i\omega_n) = \frac{-\dot{\chi}^\Lambda(\omega_n)}{Q(i\omega_n)}$$

which is the same as for $T = 0$, except that for each Λ one has to insert instead the nearest discrete ω_n into the propagator. At half filling,

$$\partial_\Lambda \left(\frac{1}{U^\Lambda} \right) = \frac{1}{2\pi} \left(1 - \omega_n \frac{\omega_n^2 + 6}{(\omega_n^2 + 4)^{3/2}} \right) \Big|_{\omega_n \approx \Lambda} .$$

At $T = 0$, Σ^Λ and Γ^Λ flow substantially only in the range $0.1t \lesssim \omega \lesssim t$. At $T > 0$, since the lowest fermionic Matsubara frequency is $\omega_0 = \pi T$, Σ^Λ and Γ^Λ are renormalized substantially only for $T < 1$. The interaction is still correct to second order in U if all external legs lie on the Fermi surface, but the frequency dependence at second order becomes important with inelastic scattering.

Initial conditions

At $T > 0$, the combination $Q - \chi^\Lambda\Sigma^\Lambda$ appears in the single-scale propagator in equation (4.30), i.e., Q and Σ^Λ do not enter on an equal footing. For the exact theory and full hierarchy of flow equations, the final result should be independent of the specific form of the cutoff, but in the truncated flow it does make a difference. Both the bare impurity potential and the lead contribution are contained in the bare propagator (4.9), such that the self energy receives only contributions from the interaction, and the same initial conditions (4.28) and (4.29) as for $T = 0$ apply.

4.2.4 Temperature flow

In the temperature flow (see section 2.2.1 and [Honerkamp&Salmhofer 2001]), the kinetic term in the action,

$$\left(\bar{\psi}, Q\psi\right) = T \sum_n \sum_{\boldsymbol{k}} \bar{\psi}_{\omega_n,\boldsymbol{k}} (i\omega_n - \xi_{\boldsymbol{k}}) \psi_{\omega_n,\boldsymbol{k}} \,,$$

is replaced after a rescaling of the fields, $\psi \mapsto T^{-3/4}\psi$, by

$$\left(\bar{\psi}, Q\psi\right) = \sum_n \sum_{\boldsymbol{k}} \bar{\psi}_{\omega_n,\boldsymbol{k}} \frac{i\omega_n - \xi_{\boldsymbol{k}}}{\sqrt{T}} \psi_{\omega_n,\boldsymbol{k}} \,.$$

We shall postpone the leads for a moment but include the impurity potential in ξ as usual. With the new convention that the scalar product shall contain no further factor of T, we define the *rescaled* inverse bare propagator (indicated by the superscript T) as

$$Q^T = \frac{i\omega_n - \xi}{\sqrt{T}}$$

which yields the rescaled full propagator (with rescaled self energy Σ^T)

$$G^T = \frac{1}{Q^T - \Sigma^T} = \frac{\sqrt{T}}{i\omega_n - \xi - \sqrt{T}\Sigma^T} \,.$$

The T derivatives of these quantities are

$$\begin{aligned}
&\frac{d}{dT}(i\omega_n) = \frac{i\omega_n}{T} \\
&\frac{d}{dT} Q^T = \frac{i\omega_n}{T^{3/2}} - \frac{i\omega_n - \xi}{2T^{3/2}} = \frac{i\omega_n + \xi}{2T^{3/2}} \qquad \text{(note the + sign!)} \\
\Rightarrow \quad & S^T = \frac{1}{2\sqrt{T}} \frac{1}{i\omega_n - \xi - \sqrt{T}\Sigma^T} \left(i\omega_n + \xi\right) \frac{1}{i\omega_n - \xi - \sqrt{T}\Sigma^T} \,.
\end{aligned}$$

Note the unusual + sign in dQ^T/dT which is due to the fact that one does not just have a multiplicative cutoff function $\chi^T = \sqrt{T}$ but the temperature also enters in the Matsubara frequency ω_n.

To understand the structure of the flow equation, consider first the RG flow of the self energy without leads, feedback of the self energy or vertex renormalization, i.e., first-order perturbation theory:

$$-S^T = \frac{d}{dT} C^T = \frac{d}{dT} \left(\frac{\sqrt{T}}{i\omega_n - \xi} \right)$$

$$-\sum_n S^T = \sum_n \frac{d}{dT} C^T = \frac{d}{dT}\left(\frac{1}{\sqrt{T}}\, T \sum_n \frac{e^{i\omega_n 0^+}}{i\omega_n - \xi}\right) = \frac{d}{dT}\left(\frac{f(\xi)}{\sqrt{T}}\right).$$

The flow equation of the rescaled self energy Σ^T is thus

$$\frac{d}{dT}\Sigma^T = -\sum_n \mathrm{tr}(US^T) = \frac{d}{dT}\left[\frac{1}{\sqrt{T}}\,\mathrm{tr}\big(Uf(\xi)\big)\right].$$

With the initial condition $\sqrt{T_0}\,\Sigma^{T_0}\Big|_{T_0\to\infty} = \mathrm{tr}\big(Uf(\xi)\big)\Big|_{T_0\to\infty} \to \frac{1}{2}\,\mathrm{tr}(U)$ as in equation (4.28) we can integrate from $T = T_0$ down to T and obtain

$$\sqrt{T}\,\Sigma^T = \mathrm{tr}(Uf(\xi))$$

as expected from the relation between rescaled and original Green functions, equation (2.19).

Notice one peculiarity of the temperature flow: since the Green functions of the leads depend on the frequency $i\omega_n$, they also depend on temperature and have to be differentiated appropriately in dQ^T/dT. At half filling the expressions are particularly simple,

$$\begin{aligned}
Q^T(i\omega_n) &= \frac{i\omega_n - \Sigma^{\mathrm{leads}}(i\omega_n) - \xi}{\sqrt{T}} \\
g_L(i\omega_n) &= \frac{1}{2}\left(i\omega_n - i\,\mathrm{sgn}(\omega_n)\sqrt{4+\omega_n^2}\right) \\
\frac{d}{dT} g_L(i\omega_n) &= \frac{1}{T}\left(g_L(i\omega_n) + 2i\frac{\mathrm{sgn}(\omega_n)}{\sqrt{4+\omega_n^2}}\right) \\
\frac{d}{dT} Q^T(i\omega_n) &= \frac{1}{2T^{3/2}}\left[i\omega_n - \Sigma^{\mathrm{leads}}(i\omega_n) + \xi - 4i\frac{\mathrm{sgn}(\omega_n)}{\sqrt{4+\omega_n^2}}\big(t_L^2|1\rangle\langle 1| + t_R^2|N\rangle\langle N|\big)\right].
\end{aligned}$$

Temperature flow of the interaction

The temperature flow of the interaction U^T has the structure of the usual one-loop diagrams of the perturbation expansion in the original ψ fields, but with a temperature derivative of the particle-hole and particle-particle bubbles [Honerkamp&Salmhofer 2001]. In our 1D case,

$$\frac{dU^T}{dT} = (U^T)^2\,\frac{d}{dT} B^T \tag{4.31}$$

where

$$B^T := \oint \frac{dp}{2\pi}\, T \sum_n f(p,\omega) \tag{4.32}$$

is the sum of the three bubble contributions. For instance at half filling,

$$B^T = -\oint \frac{dp}{2\pi}\,\cos^2(p)\Big[\frac{f(\xi_p)-\frac{1}{2}}{\xi_p} - \frac{f'(\xi_p)}{T}\Big]$$
$$= \oint \frac{dp}{2\pi}\Big[\frac{\cos(p)}{4}\tanh\left(\frac{\cos(p)}{T}\right) + \frac{\cos^2(p)}{4T}\left(\tanh^2\left(\frac{\cos(p)}{T}\right)-1\right)\Big].$$

In the limit $T\to 0$, $B^T \to \frac{1}{2\pi}$, while for $T\to\infty$, $B^T\to 0$ vanishes. Equation (4.31) can be written as

$$d\left(\frac{1}{U^T}\right) = -dB^T.$$

Integrating from $T=\infty$ (with $U^{T=\infty}=U$) down to T, we obtain

$$U^T = \frac{U}{1-UB^T}.$$

For $T=0$, the result $U^{T=0} = U/\big(1-U/(2\pi)\big)$ agrees with the frequency-cutoff result (4.27) at $\Lambda=0$.

Initial conditions

The initial conditions for $\Sigma=\sqrt{T}\,\Sigma^T$ and $U=U^T$ in the limit $T=T_0\to=\infty$ are the same as for the frequency cutoff, equations (4.28) and (4.29).

4.2.5 Interaction flow

In the interaction flow scheme (cf. section 2.2.1 or [HRAE 2004]) the propagators are slowly switched on by a global scale factor $\chi^\Lambda = g$, $g=0\ldots 1$, irrespective of frequency or momentum. We define the inverse bare propagator

$$Q^g(i\omega) := \frac{Q(i\omega)}{g} = \frac{i\omega - \Sigma^{\text{leads}}(i\omega)-\xi}{g}$$

and the full propagator

$$G^g(i\omega) := \frac{1}{Q^g-\Sigma^g} = \frac{g}{i\omega-\Sigma^{\text{leads}}(i\omega)-\xi-g\Sigma^g}$$

where ξ shall include the impurity potential V. Then the "single-scale" propagator (which is not at all single-scale) is

$$S^g := G^g\dot{Q}^gG^g = -\frac{1}{Q(i\omega)-g\Sigma^g}Q(i\omega)\frac{1}{Q(i\omega)-g\Sigma^g}.$$

Furthermore, because the bare $G_0^g = gG_0$ contains one g factor and $S_0^g = G_0$ contains none, the flow equation for the interaction vertex contains the combination $G_0^g S_0^g + S_0^g G_0^g = 2gG_0G_0$ in the bubble,

$$\frac{d}{dg}U^g = (U^g)^2\, 2gB^T$$

with the bubble integral B^T at temperature T, equation (4.32). Integrating from $g = 0$ (with $U^{g=0} = U$) up to g,

$$\begin{aligned} U^g &= \frac{U}{1 - g^2 U B^T} \\ &= \frac{U}{1 - g^2 U/(2\pi)} \quad (T = 0). \end{aligned}$$

At the end of the flow,

$$U^{g=1} = \frac{U}{1 - UB^T} = U^T.$$

The initial condition for the self energy is $\Sigma^{g=0} = 0$ because all propagators vanish, but $\Gamma^{g=0}$ is the same as for the frequency cutoff, equation (4.29).

4.2.6 Initial conditions for general filling

At any filling n, we wish to fulfill two conditions for the model without impurities: (i) at the end of the flow, the density profile should be uniformly $n_j \equiv n$, both in the interacting region and in the leads, such that power-law exponents depending on the density can be read off reliably; (ii) no backscattering should occur at the ends of the wire where the interaction is switched on, i.e., the transmission without impurity should be perfect. In order to achieve this, we allow the freedom to add to our microscopic model a local potential in the wire that depends only on the interaction strength but not on the temperature, while with changing temperature only the global chemical potential $\mu(T)$ may be adjusted.

At half filling, these conditions are met without a local potential and by setting $\mu = 0$. Away from half filling, we use the following procedure:

1. At zero temperature, the global chemical potential is defined as $\mu := -2t\cos(k_\mathrm{F}) \neq 0$ such that $\xi_{k_\mathrm{F}} = 0$, where the Fermi wave vector $k_\mathrm{F} \equiv n\pi$ at filling n. Second, finding the local potential at all N lattice sites such that at the end of the flow $n_j \equiv n$ (without impurities) is a complicated N-parameter optimization problem, but we obtain a very good guess in the following way: the problem is first solved in the bulk where the global potential, implemented as the initial

condition of the self energy $\Sigma^{\Lambda_0}_{\text{bulk}}$, is tuned self-consistently until $\Sigma^{\Lambda=0}_{k_\text{F}} = 0$. Then the initial condition of the self energy on the lattice (the local potential) is defined as

$$\Sigma^{\Lambda_0}_{jj} := \frac{U_{j-1,j} + U_{j,j+1}}{2U} \Sigma^{\Lambda_0}_{\text{bulk}}$$

such that in the middle of the system where $U_{j,j+1} \equiv U$ is homogeneous, the bulk initial condition holds, while towards the ends when the system becomes non-interacting $U_{j,j+1} \to 0$, no local potential is necessary. Equivalently, the local potential may also be written as part of the interaction term (4.1),

$$H_\text{int} = \sum_j U_{j,j+1}(n_j - \nu)(n_{j+1} - \nu)$$

where $\nu = (1 - \Sigma^{\Lambda_0}_{\text{bulk}}/U)/2$.

2. Now the temperature $T > 0$ is switched on and μ is tuned self-consistently until the bulk density $n(\mu) \equiv \frac{1}{2\pi} \int dk\, f(\epsilon_k - \mu) = n$ at the end of the flow, with the non-interacting bulk dispersion ϵ_k of the leads. By the above construction also the density in the interacting region, obtained using the dispersion $\epsilon_k + \Sigma_k$ with renormalized hopping and potential, has the same value to a high accuracy, and the density computed using a flowing density vertex (see below) deviates by less than 1% for $|U| \leq 1$.

Only at this stage, impurities are inserted into the lattice and change the homogeneous density profile.

4.2.7 Algorithm for tridiagonal matrices

With the parametrization of the interaction by one single bulk parameter U^Λ, the most time-consuming part of the ODE flow is the flow of the self energy. On the RHS of the Σ^Λ flow equation, both Q and Σ^Λ are tridiagonal matrices, hence it involves the inversion of tridiagonal matrices. I have developed an efficient inversion algorithm to compute the RHS in $\mathcal{O}(N)$ time at any temperature. Therefore, the runtime scales only linearly with the system size N, and the self energy of systems as large as $N = 10^7$ sites (at $T = 0$) can be computed. At $T = 0$, only the tridiagonal part of the inverse tridiagonal matrix $\tilde{G}^\Lambda$ is needed in (4.24), and an algorithm by the author was presented already in [AEMMSS 2004] and is reprinted in appendix B.1. For $T > 0$, the RHS of the flow equation (4.30) is more complicated: a matrix product of an inverse tridiagonal matrix (which is a full matrix), a tridiagonal matrix Q, and another inverse tridiagonal matrix. In a forthcoming article and in appendix B.2, I

present an algorithm to compute even this product of full $N \times N$ matrices in $\mathcal{O}(N)$ time [Enss 2005]. However, the RHS, which has jumps in Λ at every Matsubara frequency (see section 4.2.3), makes the integration at finite temperature scale as $\mathcal{O}(N/T)$, such that only systems up to $N = 10^4$ have been computed so far for low temperatures $T = 10^{-4}$.

The flow equation (4.35) of the density-response vertex used below for the Friedel oscillations at $T = 0$ is of the same computational complexity as the self-energy flow at $T > 0$: the RHS involves the matrix product of an inverse tridiagonal, a tridiagonal, and another inverse tridiagonal matrix. This can also be done in $\mathcal{O}(N)$ time by the same algorithm in appendix B.2, and at $T = 0$ the density profile n_j of a system of size $N = 10^7$ can be computed in a few hours for each j.

4.3 Flow of the density-response vertex

The expectation value of the local density n_j could be computed from the local one-particle propagator G_{jj} if G was known exactly. However, the approximate flow equations for Σ can be expected to describe the asymptotic behavior of G correctly only at long distances between creation and annihilation operators in time and/or space, while in the local density operator time and space variables coincide. In the standard RG terminology n_j is a *composite* operator, which has to be renormalized separately.

To derive a flow equation for n_j, we follow the usual procedure for the renormalization of correlation functions involving composite operators: one adds a term $\phi_j n_j$ with a small field ϕ_j to the Hamiltonian and takes derivatives with respect to ϕ_j in the flow equations. The local density is given by

$$n_j = \left.\frac{\partial \Omega(\phi_j)}{\partial \phi_j}\right|_{\phi_j=0},$$

where $\Omega(\phi_j)$ is the grand canonical potential of the system in the presence of the field ϕ_j. Note that I use the same symbol n_j for the density operator and its expectation value. In the presence of a cutoff Λ the grand canonical potential obeys the exact flow equation

$$\partial_\Lambda \Omega^\Lambda = T \sum_\omega \operatorname{tr}\left\{ e^{i\omega 0^+} \left[\partial_\Lambda Q^\Lambda(i\omega)\right] \left[G^\Lambda(i\omega) - G_0^\Lambda(i\omega)\right] \right\},$$

which follows from the flow equations for the vertex functions, equation (2.30), and the relation between the grand canonical potential and the zero-particle vertex, $\Omega^\Lambda = -\gamma_0^\Lambda$. At zero temperature (which is the only case I consider here) the Matsubara

frequency sum becomes an integral which, for the sharp frequency cutoff (4.22), can be carried out analytically. This yields

$$\partial_\Lambda \Omega^\Lambda = \frac{1}{2\pi} \sum_{\omega=\pm\Lambda} \mathrm{tr} \left\{ e^{i\omega 0^+} \ln[1 - G_0(i\omega)\, \Sigma^\Lambda(i\omega)] \right\} , \tag{4.33}$$

which is the first term of equation (2.34). Because at $T = 0$ any perturbation of the Hamiltonian can be shifted between the bare propagator and the self energy, in this section I choose to attribute ϕ_j to the interaction part of the Hamiltonian, not to H_0, such that G_0 remains independent of ϕ_j. The self energy is modified via the additional local and frequency-independent contribution $\phi_j\, \delta_{jj'}$ to its initial value $\Sigma^{\Lambda_0}_{jj'}$ at scale Λ_0.

The density profile can be obtained from the above equations and the flow equation for Σ^Λ by computing the shift of Ω^Λ generated by a small finite perturbation ϕ_j, i.e., by numerical differentiation (cf. section 3.3.3). Alternatively, one may carry out the ϕ_j derivative analytically in the flow equations, which yields a flow equation for the density in terms of the density response vertex. Taking the ϕ_j derivative in equation (4.33) yields

$$\partial_\Lambda n^\Lambda_j = -\frac{1}{2\pi} \sum_{\omega=\pm\Lambda} \mathrm{tr} \left[e^{i\omega 0^+} \tilde{G}^\Lambda(i\omega)\, R^\Lambda_j(i\omega) \right] \tag{4.34}$$

with the density-response vertex

$$R^\Lambda_j(i\omega) = \left. \frac{\partial \Sigma^\Lambda(i\omega)}{\partial \phi_j} \right|_{\phi_j = 0}$$

and the propagator $\tilde{G}^\Lambda$ as defined in equation (4.23), i.e., in the absence of ϕ_j. We compute the self energy Σ^Λ in the presence of ϕ_j within the same approximation as previously. It is thus determined from the flow equation (4.24) with a frequency-independent two-particle vertex Γ^Λ. Taking a derivative of that equation with respect to ϕ_j at $\phi_j = 0$ yields the flow equation for the response vertex

$$\partial_\Lambda R^\Lambda_{j;1',1} = -\frac{1}{2\pi} \sum_{\omega=\pm\Lambda} \sum_{2,2'} \sum_{3,3'} \tilde{G}^\Lambda_{2,3'}(i\omega)\, R^\Lambda_{j;3',3}\, \tilde{G}^\Lambda_{3,2'}(i\omega)\, \Gamma^\Lambda_{1',2';1,2} .$$

Note that R^Λ_j is frequency independent in our approximation and that there is no contribution from the ϕ_j derivative of Γ^Λ since we neglect self-energy contributions in the flow of the two-particle vertex.

For spinless fermions with a (renormalized) nearest-neighbor interaction, the matrix R^Λ_j is tridiagonal, i.e., only the components $R^\Lambda_{j;l,l}$ and $R^\Lambda_{j;l,l\pm1}$ are non-zero, and their flow is given by

$$\partial_\Lambda R^\Lambda_{j;l,l} = -\frac{1}{2\pi} \sum_{\omega=\pm\Lambda} \sum_{l'} \sum_{r=\pm1} \sum_{r'=0,\pm1} U^\Lambda_{l,l+r} \tilde{G}^\Lambda_{l+r,l'}(i\omega)\, R^\Lambda_{j;l',l'+r'}\, \tilde{G}^\Lambda_{l'+r',l+r}(i\omega)$$

$$\partial_\Lambda R^\Lambda_{j;l,l\pm1} = \frac{1}{2\pi} \sum_{\omega=\pm\Lambda} \sum_{l'} \sum_{r'=0,\pm1} U^\Lambda_{l,l\pm1} \tilde{G}^\Lambda_{l,l'}(i\omega)\, R^\Lambda_{j;l',l'+r'}\, \tilde{G}^\Lambda_{l'+r',l\pm1}(i\omega)\,. \tag{4.35}$$

Then, the flow of n^Λ_j is

$$\partial_\Lambda n^\Lambda_j = -\frac{1}{2\pi} \sum_{\omega=\pm\Lambda} \sum_{l'} \sum_{r'=0,\pm1} \tilde{G}^\Lambda_{l'+r',l'}(i\omega)\, R^\Lambda_{j;l',l'+r'}\,.$$

Although naively the flow of R^Λ scales as $\mathcal{O}(N^2)$ in time because of the unrestricted loops over l, l', it can be performed in $\mathcal{O}(N)$ by the method described in the appendix B.2. The initial condition for the response vertex is $R^{\Lambda_0}_{j;l,l'} = \delta_{jl}\delta_{ll'}$. The initial condition for the density is $n^{\Lambda_0}_j = \frac{1}{2}$, for any filling, due to the slow convergence of the flow equation (4.34) at large frequencies, which yields a finite contribution to the integrated flow from $\Lambda = \infty$ to Λ_0 for arbitrarily large finite Λ_0, as in the case of the self energy Σ^{Λ_0}.

To avoid the interference of Friedel oscillations emerging from the impurity or one boundary with those coming from the (other) boundaries of the system one suppresses the influence of the latter by coupling the finite chain to semi-infinite non-interacting leads, with a smooth decay of the interaction at the contacts (cf. section 4.1.1).

4.4 Computation of the conductance

The linear-response conductance is defined via the infinitesimal current induced by an infinitesimal voltage drop at zero bias voltage, $G = dI/dV$. It is a global quantity defined over the whole wire, from one lead through the interacting (scattering) region to the other lead. Even for a perfectly clean wire (interacting or not), the conductance is limited to e^2/h per channel. For a 1D system of spinless fermions there is exactly one channel, while for spin-$\frac{1}{2}$ fermions there are two channels.

I choose the conductance as the appropriate observable for transport, as opposed to the local quantity conductivity, because I am interested not in bulk properties but the effect of a specific spatial setup of impurities at defined positions, the double barrier, for which there are experimental data available [PTYGD 2001].

4.4.1 Kubo formula

The conductance is computed, just as the linear-response conductivity, via the Kubo formula from the current-current correlation function, see for instance [Mahan 2000, chapters 3 and 7]. This correlation function at finite frequency and temperature is

defined as

$$\pi(i\omega) := \int_0^\beta d\tau\, e^{i\omega\tau} \langle T_\tau J_R(\tau) J_L(0)\rangle$$

with $J_{L,R}$ the current operators at the left and right ends of the system. The retarded correlation function $\pi_{\mathrm{ret}}(\omega)$ is obtained by analytical continuation $i\omega \mapsto \omega + i0$, and the dc conductance is given by finally taking the limit $\omega \to 0$,

$$G := \frac{e^2}{\hbar} \lim_{\omega\to 0} \frac{\pi_{\mathrm{ret}}(\omega) - \pi_{\mathrm{ret}}(0)}{i\omega}\,. \tag{4.36}$$

It is important that one does not set $\omega = 0$ from the beginning because the limits $\omega \to 0$ and $q \to 0$ (macroscopic transport from one end of the system to the other) do not commute [Luttinger 1964]. Another way to compute the conductance at zero temperature via persistent currents is explained in [Meden&Schollwöck 2003a, Meden&Schollwöck 2003b].

Consider the following microscopic setup (cf. figure 4.1 on page 54). The scattering region on the lattice sites $1, \ldots, N$ ("sample") is interacting; it is connected to semi-infinite, non-interacting leads at the interfaces at sites 1 and N. The current and total number operators are

$$\begin{aligned} J_L &:= it_L(c_1^\dagger c_0 - c_0^\dagger c_1) \\ J_R &:= it_R(c_{N+1}^\dagger c_N - c_N^\dagger c_{N+1}) \\ n_C &:= \sum_{j=1}^N n_j \end{aligned} \tag{4.37}$$

with J_L the current flowing from the left lead into the sample, J_R the current flowing out from the sample into the right lead, and n_C the total particle number in the interacting region.[3]

In the exact theory, the current-current correlation function can be expressed in terms of the bare current operators $J_{L,R}$ and the 1PI two-particle interaction vertex Γ, see figure 4.3. The expressions for these two contributions to $\pi(i\omega)$ are

$$\pi^{(a)}(i\omega) = -(it_L)(it_R)T\sum_{i\epsilon}\Big[G_{N,1}(i\epsilon + i\omega)\, G_{0,N+1}(i\epsilon) + G_{N+1,0}(i\epsilon + i\omega)\, G_{1,N}(i\epsilon)$$

[3] The components of the gauge potential $A_\mu = \big(\varphi(t,j), A(t,[j,j+1])\big)$ are the scalar potential φ at time t and on site j, and the vector potential A on the (directed) bond from site j to site $j+1$, respectively, where we have introduced the notation $[j,j+1]$ for the bond. Coupling to the potential A_μ changes the bare dispersion ξ to [Zinn-Justin 2002, chapter 34]

$$\begin{aligned} \xi_{j,j} &= -\mu - e\varphi(t,j) \\ \xi_{j,j+1} &= -te^{ieA(t,[j,j+1])} = \xi_{j+1,j}^*. \end{aligned}$$

Derivatives with respect to a $A([0,1])$, $A([N,N+1])$ and a global φ yield the expressions (4.37).

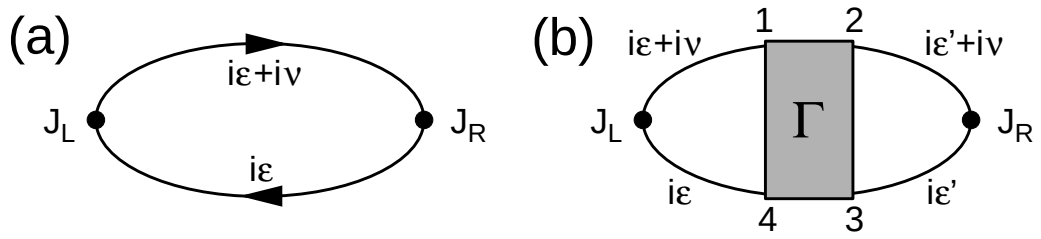


Figure 4.3: *Two contributions to the current-current correlation function $\pi(i\omega)$. The shaded region represents the vertex part $\Gamma_{1,2;3,4}(i\epsilon, i\epsilon'; i\omega)$.*

$$- G_{N+1,1}(i\epsilon + i\omega)\, G_{0,N}(i\epsilon) - G_{N,0}(i\epsilon + i\omega)\, G_{1,N+1}(i\epsilon)\Big],$$

$$\begin{aligned}\pi^{(b)}(i\omega) = -(it_L)(it_R)T^2 \sum_{i\epsilon, i\epsilon'} \sum_{j_1,\ldots,j_4=1}^{N} & \\ \Big[G_{j_1,1}(i\epsilon + i\omega)\, G_{0,j_4}(i\epsilon) - G_{j_1,0}(i\epsilon + i\omega)\, G_{1,j_4}(i\epsilon)\Big] & \\ \times \Gamma_{j_1,j_2;j_3,j_4}(i\epsilon, i\epsilon'; i\omega) & \\ \times \Big[G_{N,j_2}(i\epsilon' + i\omega)\, G_{j_3,N+1}(i\epsilon') - G_{N+1,j_2}(i\epsilon' + i\omega)\, G_{j_3,N}(i\epsilon')\Big]. &\end{aligned}$$

Kubo formula projected into the interacting region

Using equations (4.5), (4.6), and (4.7), we can express $\pi^{(a,b)}(i\omega)$ in terms of Green functions with indices in the interacting region $1, \ldots, N$,

$$\pi^{(a)}(i\omega) = T \sum_{i\epsilon} \lambda_L(i\epsilon, i\epsilon + i\omega)\, G_{1,N}(i\epsilon)\, \lambda_R(i\epsilon, i\epsilon + i\omega)\, G_{N,1}(i\epsilon + i\omega) \tag{4.38}$$

$$\pi^{(b)}(i\omega) = T \sum_{i\epsilon} \sum_{j_1,j_4=1}^{N} \lambda_L(i\epsilon, i\epsilon + i\omega)\, G_{1,j_4}(i\epsilon)\, P_{R;j_4,j_1}(i\epsilon, i\epsilon + i\omega)\, G_{j_1,1}(i\epsilon + i\omega)$$

with bare current vertices on sites 1 and N, respectively,

$$\begin{aligned}\lambda_L(i\epsilon, i\epsilon + i\omega) &= -it_L^2[g_L(i\epsilon + i\omega) - g_L(i\epsilon)] \\ \lambda_R(i\epsilon, i\epsilon + i\omega) &= +it_R^2[g_R(i\epsilon + i\omega) - g_R(i\epsilon)]\end{aligned}$$

and the current-vertex correction

$$\begin{aligned}P_{R;j_4,j_1}(i\epsilon, i\epsilon + i\omega) := T \sum_{i\epsilon'} \sum_{j_2,j_3=1}^{N} & \Gamma_{j_1,j_2;j_3,j_4}(i\epsilon, i\epsilon'; i\omega) \\ & \times G_{j_3,N}(i\epsilon')\, \lambda_R(i\epsilon'; i\epsilon' + i\omega)\, G_{N,j_2}(i\epsilon' + i\omega)\end{aligned}$$

and likewise for P_L.

Analytical continuation of the Kubo formula

The Green function (4.3) of the lead has a branch cut at the real axis,

$$\begin{aligned} g_{L,R}(\epsilon \pm i\delta) &= \frac{1}{2}\left(\epsilon + \mu \pm i\delta \mp i\sqrt{4-(\epsilon+\mu\pm i\delta)^2}\right) \\ &= \frac{1}{2}\left(\epsilon + \mu \mp i\sqrt{4-(\epsilon+\mu)^2}\right) + \mathcal{O}(\delta). \end{aligned}$$

Thus, for small ω,

$$\begin{aligned} \lambda_{L,R}(\epsilon \pm i\omega, \epsilon \pm i0) &= \mathcal{O}(\omega) \\ \lambda_L(\epsilon + i\omega, \epsilon - i0) &= +t_L^2\sqrt{4-(\epsilon+\mu)^2} + \mathcal{O}(\omega) \\ \lambda_R(\epsilon + i\omega, \epsilon - i0) &= -t_R^2\sqrt{4-(\epsilon+\mu)^2} + \mathcal{O}(\omega), \end{aligned}$$

and only the current vertices with incoming and outgoing legs on opposite sides of the branch cut contribute in the limit $\omega \to 0$. The Matsubara sum in the bubble term (4.38) is evaluated by a contour integral as explained in [Mahan 2000, chapter 7],

$$\begin{aligned} \pi^{(a)}(i\omega) = i\int \frac{d\epsilon}{2\pi} f(\epsilon) \\ \times\big(&+ \lambda_L(\epsilon+i0, \epsilon+i\omega)\, G_{1,N}(\epsilon+i0)\, \lambda_R(\epsilon+i0, \epsilon+i\omega)\, G_{N,1}(\epsilon+i\omega) \\ &- \lambda_L(\epsilon-i0, \epsilon+i\omega)\, G_{1,N}(\epsilon-i0)\, \lambda_R(\epsilon-i0, \epsilon+i\omega)\, G_{N,1}(\epsilon+i\omega) \\ &+ G_{1,N}(\epsilon-i\omega)\, \lambda_R(\epsilon-i\omega, \epsilon+i0)\, G_{1,N}(\epsilon+i0)\, \lambda_L(\epsilon-i\omega, \epsilon+i0) \\ &- G_{1,N}(\epsilon-i\omega)\, \lambda_R(\epsilon-i\omega, \epsilon-i0)\, G_{1,N}(\epsilon-i0)\, \lambda_L(\epsilon-i\omega, \epsilon-i0)\big)\,. \end{aligned}$$

The first and fourth term on the RHS have frequency arguments on the same side of the branch cut and are, therefore, of $\mathcal{O}(\omega^2)$, hence they will vanish in the limit $\omega \to 0$ in equation (4.36). We retain the other two terms and perform the analytical continuation of the external frequency, $i\omega \mapsto \omega + i0$,

$$\begin{aligned} \pi^{(a)}_{\mathrm{ret}}(\omega) = i\int \frac{d\epsilon}{2\pi} f(\epsilon) \\ \times\big(&- \lambda_L(\epsilon-i0, \epsilon+\omega+i0)\, G_{1,N}(\epsilon-i0)\lambda_R(\epsilon-i0, \epsilon+\omega+i0)\, G_{N,1}(\epsilon+\omega+i0) \\ &+ \lambda_L(\epsilon-\omega-i0, \epsilon+i0)\, G_{1,N}(\epsilon-\omega-i0)\lambda_R(\epsilon-\omega-i0, \epsilon+i0)\, G_{N,1}(\epsilon+i0)\big). \end{aligned}$$

We then substitute $\epsilon \mapsto \epsilon + \omega$ in the second term,

$$\begin{aligned} \pi^{(a)}_{\mathrm{ret}}(\omega) = i\int \frac{d\epsilon}{2\pi} [f(\epsilon+\omega) - f(\epsilon)] \\ \times\lambda_L(\epsilon-i0, \epsilon+\omega+i0)\, G_{1,N}(\epsilon-i0)\, \lambda_R(\epsilon-i0, \epsilon+\omega+i0)\, G_{N,1}(\epsilon+\omega+i0)\,. \end{aligned}$$

As the final step we take the limit $\omega \to 0$,

$$\begin{aligned} G^{(a)} &= \frac{e^2}{\hbar} \lim_{\omega\to 0} \frac{\pi^{(a)}_{\rm ret}(\omega)}{i\omega} \\ &= \frac{e^2}{\hbar} \int \frac{d\epsilon}{2\pi} f'(\epsilon) \lambda_L(\epsilon - i0, \epsilon + i0)\, G_{1,N}(\epsilon - i0)\, \lambda_R(\epsilon - i0, \epsilon + i0)\, G_{N,1}(\epsilon + i0) \\ &= \frac{e^2}{h} \int d\epsilon \big(-f'(\epsilon)\big)\, \mathcal{T}^{(a)}(\epsilon, T). \end{aligned} \tag{4.39}$$

$\mathcal{T}^{(a)}(\epsilon, T)$ is the transmission probability at temperature T without vertex corrections,

$$\mathcal{T}^{(a)}(\epsilon, T) := t_L^2\, t_R^2\, [4 - (\epsilon + \mu)^2]\, |G_{N,1}(\epsilon + i0)|^2 \tag{4.40}$$

where we have used $G_{1,N}(\epsilon - i0)\, G_{N,1}(\epsilon + i0) = |G_{N,1}(\epsilon + i0)|^2$: because the Hamiltonian is time-reversal invariant, the amplitude from site 1 to N is the same as from N to 1, and $G_{jj'}$ is symmetric (not hermitean). The energy integration extends over the band of the non-interacting leads, while the factor $[4-(\epsilon+\mu)^2]$ from the density of states of the leads suppresses the transmission towards the edge of the band.

The fRG provides an approximation of the frequency-independent self energy $\Sigma_{jj'}(T)$ at zero or finite temperature. Σ acts as an effective static potential by which non-interacting electrons are scattered. The full propagator is determined via the Dyson equation (4.10).

4.4.2 Vertex corrections

The second contribution $\mathcal{T}^{(b)}(\epsilon, T)$ to the transmission is due to current-vertex corrections. It is obtained from $\pi^{(b)}$ following the same steps as for $\mathcal{T}^{(a)}$. We have approximated the full effective two-particle interaction vertex Γ by a renormalized nearest-neighbor interaction with all external frequencies set to zero, i.e., without branch cuts. Then the vertex corrections are, omitting the lattice indices and denoting the loop summation by the trace,

$$\begin{aligned} P_R(i\omega) &= T \sum_{i\epsilon'} \mathrm{tr}\big(G(i\epsilon')\lambda_R(i\epsilon', i\epsilon' + i\omega)\, G(i\epsilon' + i\omega)\, \Gamma\big) \\ &= i \int \frac{d\epsilon'}{2\pi} f(\epsilon')\, \mathrm{tr}\big(+ G(\epsilon' + i0)\, \lambda_R(\epsilon' + i0, \epsilon' + i\omega)\, G(\epsilon' + i\omega)\, \Gamma \\ &\qquad - G(\epsilon' - i0)\, \lambda_R(\epsilon' - i0, \epsilon' + i\omega)\, G(\epsilon' + i\omega)\, \Gamma \\ &\qquad + G(\epsilon' - i\omega)\, \lambda_R(\epsilon' - i\omega, \epsilon' + i0)\, G(\epsilon' + i0)\, \Gamma \\ &\qquad - G(\epsilon' - i\omega)\, \lambda_R(\epsilon' - i\omega, \epsilon' - i0)\, G(\epsilon' - i0)\, \Gamma\big). \end{aligned}$$

Again, the first and fourth term on the RHS are by an $\mathcal{O}(\omega)$ smaller than the other two, so we retain only the second and third term and perform the analytical continuation $i\omega \mapsto \omega + i0$. Substituting $\epsilon' \mapsto \epsilon' + \omega$ in the second term,

$$P_R(\omega + i0) = i \int \frac{d\epsilon'}{2\pi} \underbrace{[f(\epsilon' + \omega) - f(\epsilon')]}_{\mathcal{O}(\omega)} \times \operatorname{tr}\Big(G(\epsilon' - i0)\, \lambda_R(\epsilon' - i0, \epsilon' + \omega + i0)\, G(\epsilon' + \omega + i0)\, \Gamma \Big) \xrightarrow{\omega \to 0} 0$$

vanishes since there is no division by ω as in equation (4.36). Because Γ is frequency independent, there are no vertex corrections, hence equation (4.40) is the complete transmission probability in our approximation.

Conformance with Ward identities

The approximation that Γ is frequency independent has another consequence: by the flow equation, it follows that $\operatorname{Im}\Sigma = 0$, i.e., we do not capture inelastic processes at second order in the interaction. They could be included in the flow equation by retaining the frequency dependence and imaginary part of Γ.

However, the fact that the vertex corrections and $\operatorname{Im}\Sigma$ vanish simultaneously shows that our approximation is at least consistent with the (non-perturbative) Ward identity associated with global particle number (charge) conservation. The global continuity equation for the interacting region is $\partial n_C/\partial t + J_R - J_L = 0$. Following [Oguri 2001], we define the number and current response functions as the time-ordered expectation values of the current and number operators (4.37) with two extra electron legs ($1 \le j, j' \le N$),

$$\begin{aligned}
\Phi_{C;jj'}(\tau; \tau_1, \tau_2) &= \langle T_\tau [n_C(\tau) - \langle n_C \rangle]\, c_j(\tau_1)\, c_{j'}^\dagger(\tau_2) \rangle \\
\Phi_{L;jj'}(\tau; \tau_1, \tau_2) &= \langle T_\tau J_L(\tau)\, c_j(\tau_1)\, c_{j'}^\dagger(\tau_2) \rangle \\
\Phi_{R;jj'}(\tau; \tau_1, \tau_2) &= \langle T_\tau J_R(\tau)\, c_j(\tau_1)\, c_{j'}^\dagger(\tau_2) \rangle .
\end{aligned}$$

Performing a Fourier transform on each of these ($x = L, R, C$),

$$\Phi_x(\tau; \tau_1, \tau_2) = T^2 \sum_{i\epsilon, i\omega} \Phi_x(i\epsilon, i\epsilon + i\omega)\, e^{-i\epsilon(\tau_1 - \tau)}\, e^{-i(\epsilon+\omega)(\tau - \tau_2)} .$$

The 1PI response vertices are obtained by amputating full propagators,

$$\Lambda_x(i\epsilon, i\epsilon + i\omega) := [G(i\epsilon)]^{-1}\, \Phi_x(i\epsilon, i\epsilon + i\omega)\, [G(i\epsilon + i\omega)]^{-1}$$

which can be written in terms of the bare current and the vertex corrections as

$$\begin{aligned}
\Lambda_{L,jj'}(i\epsilon, i\epsilon + i\omega) &= \lambda_L(i\epsilon, i\epsilon + i\omega)\, \delta_{j',1}\delta_{j,1} + P_{L,jj'}(i\epsilon, i\epsilon + i\omega) \\
\Lambda_{R,jj'}(i\epsilon, i\epsilon + i\omega) &= \lambda_R(i\epsilon, i\epsilon + i\omega)\, \delta_{j',N}\delta_{j,N} + P_{R,jj'}(i\epsilon, i\epsilon + i\omega) \ .
\end{aligned} \tag{4.41}$$

The 1PI Ward identity (3.12) in terms of these response vertices then reads

$$\begin{aligned}&i\omega\Lambda_C(i\epsilon, i\epsilon + i\omega) + i\Lambda_R(i\epsilon, i\epsilon + i\omega) - i\Lambda_L(i\epsilon, i\epsilon + i\omega)\\ &= G^{-1}(i\epsilon + i\omega) - G^{-1}(i\epsilon).\end{aligned}$$

Clearly, the knowledge of the RHS is not sufficient to determine Λ_C, Λ_R, and Λ_L separately but fixes only the difference. We use the Dyson equation (4.10) on the RHS, continue analytically to $i\epsilon + i\omega \mapsto \epsilon + \omega + i0$ and $i\epsilon \mapsto \epsilon - i0$, and take the limit $\omega \to 0$. Thereby, the density-response term is suppressed, and we are left with a relation between current and self energy, using equation (4.8) for the lead contribution,

$$\begin{aligned}&\Lambda_R(\epsilon - i0, \epsilon + i0) - \Lambda_L(\epsilon - i0, \epsilon + i0)\\ &\quad = -\mathrm{Im}\,\Sigma(\epsilon + i0) - \mathrm{Im}\,\Sigma^{\mathrm{leads}}(\epsilon + i0) + \mathrm{Im}\,\Sigma(\epsilon - i0) + \mathrm{Im}\,\Sigma^{\mathrm{leads}}(\epsilon - i0)\\ &\quad = \lambda_R|N\rangle\langle N| - \lambda_L|1\rangle\langle 1| - 2\mathrm{Im}\,\Sigma(\epsilon + i0)\,.\end{aligned}$$

By equation (4.41),

$$P_R(\epsilon - i0, \epsilon + i0) - P_L(\epsilon - i0, \epsilon + i0) = -2\,\mathrm{Im}\,\Sigma(\epsilon + i0)\,. \tag{4.42}$$

Thus, the current-vertex corrections are related to the imaginary part of the self energy. At $T = 0$, both sides vanish exactly because there is no inelastic scattering, while at higher temperatures, neglecting inelastic processes is a consistent approximation we made. If one tried to improve the approximation by computing vertex corrections but keeping a real Σ, it might be no improvement at all because one would violate number conservation, as explained in [Baym&Kadanoff 1961].

4.4.3 Different flow schemes

In order to check the robustness of our fRG results, I have considered also the temperature-flow scheme (cf. section 4.2.4) where the temperature is successively lowered during the fRG flow. Another option is the recently introduced interaction-flow scheme (cf. section 4.2.5) which slowly switches on the interaction strength during the flow (at finite temperature, or even at zero temperature because in the model at hand, the finite size already provides a regularization). Using these schemes, I have obtained the same results as for the Matsubara-frequency cutoff presented in section 4.2.3 for a few test cases (cf. figure 4.4). The frequency cutoff scheme at finite temperature remains numerically the most efficient method.

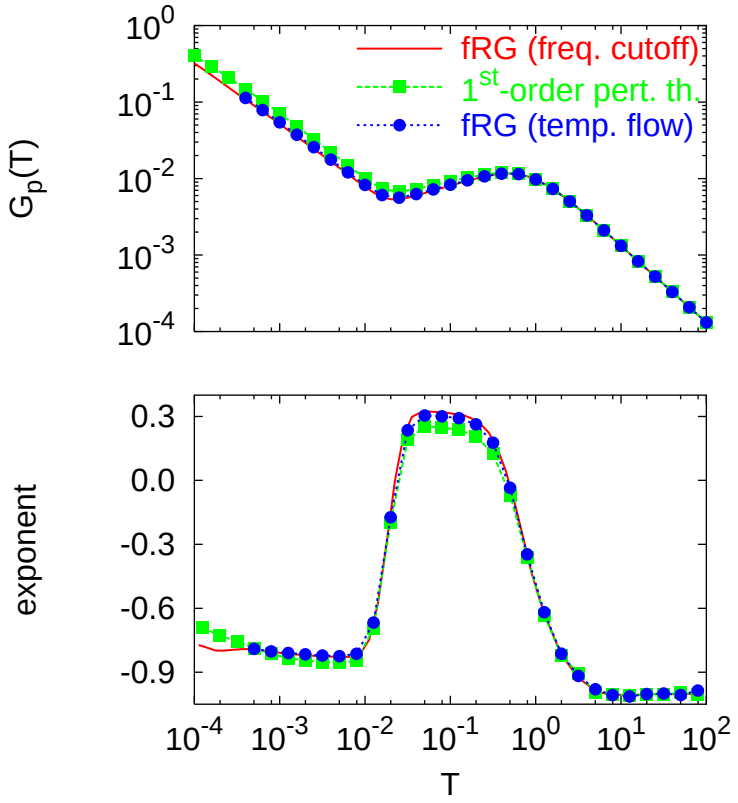


Figure 4.4: *Comparison of frequency cutoff and temperature flow fRG schemes to first-order perturbation theory for the resonant conductance through a double barrier ($N = 10^4$, $U = 0.5$, $V = 10$, $N_{dot} = 100$). This shows that different fRG schemes essentially give the same results, indicating the robustness of the method.*

5 Luttinger liquids with impurities

The behavior of three-dimensional metals can be described by Fermi-liquid theory, where the elementary excitations are fermionic quasi-particles. In one dimension, however, the situation is completely different (for reviews see [Voit 1995, Giamarchi 2003]).

A model for interacting 1D spinless fermions with linear dispersion was introduced by [Tomonaga 1950] and [Luttinger 1963] and has been solved by [Mattis&Lieb 1965]. It is characterized by a gapless spectrum of collective bosonic, density-wave elementary excitations with a linear dispersion, as well as charge and current excitations, and correlation functions decaying at zero temperature algebraically in space and time. [Luther&Peschel 1974a] and [Mattis 1974] introduced the technique of bosonization as a particularly simple method to describe the low-energy properties of this model. Any non-linearity of the fermion dispersion, for instance on the lattice, gives rise to interactions between the collective modes. For spinless fermions, a perturbative expansion of these bosonic couplings is completely regular in the infrared, and the low-energy excitation spectrum is similar to the Luttinger-model spectrum [Haldane 1981]. Therefore, the term *Tomonaga-Luttinger liquid* (TLL) was coined for the generic low-energy phase of interacting 1D fermions. The correlation functions obey power laws with exponents that are functions of a single interaction parameter K with $K = 1$ in the non-interacting case, $0 < K < 1$ for repulsive and $K > 1$ for attractive interaction.

In the presence of impurities or boundaries there are further characteristic power laws. For example, the local density of states $\rho_j(\omega) = -\frac{1}{\pi}\mathrm{Im}\, G_{jj}(\omega + i0)$ near a single impurity or boundary is suppressed for repulsive interaction as [Kane&Fisher 1992c]

$$\rho_j(\omega) \sim |\omega|^{\alpha_B} \quad \text{for } \omega \to 0$$

where

$$\alpha_B = 1/K - 1$$

is the *boundary exponent*. The linear conductance across an impurity of arbitrary strength scales as [Kane&Fisher 1992a]

$$G(T) \sim T^{2\alpha_B} \quad \text{for } T \to 0.$$

For repulsive interaction ($\alpha_B > 0$), a system containing even a very weak impurity is insulating at $T = 0$, effectively cutting the chain into two disconnected parts. Another TLL signature is the decay of Friedel oscillations: an impurity or boundary induces oscillations in the density profile n_j whose amplitude scales with the distance x as [Egger&Grabert 1995]

$$\Delta n_j \sim x^{-K} \quad \text{for } x \to \infty,$$

in contrast to $\Delta n_j \sim x^{-1}$ for a 1D Fermi gas. These power laws are strictly valid only in the low-energy limit. This raises the question at which scales N, T the asymptotic TLL behavior sets in for a specific model, and how the system behaves before reaching the asymptotic limit.

One way to study TLL behavior is to consider the 1D model of spinless fermions on the lattice with nearest-neighbor interaction U, which we have defined already in section 4.1. Without impurity, this model can be solved exactly by the Bethe ansatz [Yang&Yang 1966]; it is a Luttinger liquid at any interaction strength U and any filling, except for $|U| > 2$ at half filling. The TLL interaction parameter K is given for $|U| \leq 2$ at half filling by [Haldane 1980]

$$K^{-1} = \frac{2}{\pi} \arccos\left(-\frac{U}{2}\right).$$

For $U > 2$ at half filling, a phase transition towards a charge-density wave occurs, while for $U < -2$ the system undergoes phase separation. In this work we shall concentrate on TLL physics, so parameters have to be chosen to stay away from these phase transitions.

The local density of states has been studied in depth by [Andergassen 2005]; I will present new results for Friedel oscillations (section 5.1) and transport through double barriers (section 5.2). The FRG turns out to be a versatile tool to study physical effects on energy scales ranging over several orders of magnitude, at weak to intermediate interaction strength.

5.1 Friedel oscillations

In a normal Fermi-liquid metal, impurities induce Friedel oscillations in the density profile [Friedel 1958, Tüttő&Zawadowski 1985] which far away from the impurity have the form

$$\Delta n(x) \sim \cos(2k_{\mathrm{F}}x + \delta)\, x^{-d}$$

where $\Delta n(x) = \langle \hat{n}(x) - n_0 \rangle / n_0$ is the normalized density profile, k_{F} is the Fermi wave vector, x the distance from the impurity, d the dimension of space, and δ a

phase shift. This raises the question which density profile is generated in a Luttinger liquid.

The continuum 1D Luttinger model with a single impurity is integrable, hence Friedel oscillations should be computable exactly for any coupling strength. However, this is technically difficult, and only approximate results have been obtained except for an exact solution at $K = \frac{1}{2}$ [LLS 1996]. The asymptotic behavior for very *weak* and very *strong* impurities was studied by [Kane&Fisher 1992a, Kane&Fisher 1992b] using the RG method described below. On the other hand, the crossover at *intermediate* impurity strength is particularly important for understanding transport in 1D wires and was analyzed for weak interaction by [MYG 1993].

[Egger&Grabert 1995] first studied arbitrary impurities for repulsive interaction using bosonization, which is valid at low temperatures. For a strong scatterer, the amplitude of the Friedel oscillations decays as x^{-K}. For a weak scatterer, there is a crossover from the asymptotic x^{-K} decay for large distances ($x \gg x_0$) to linear-response decay [Voit 1995] as x^{1-2K} for short distances ($x \ll x_0$). The crossover scale diverges as $x_0 \sim V^{-1/(1-K)}$ for $V \to 0$.

Shortly after, [LLS 1996] obtained exact results for the density profile in the continuum for $K = \frac{1}{2}$ at arbitrary temperature. For this particular interaction, the problem can be mapped to a free-fermion model, which simplifies the calculation. At $T = 0$,

$$\Delta n(x) = 4h \cos(2k_\mathrm{F}x + \eta_\mathrm{F})\, e^{8\pi h^2 x} K_0(8\pi h^2 x)$$

with impurity strength $h = \lambda/\sqrt{2}$ (λ is the coefficient of the $\cos[\phi(0)]$ term in the bosonized Hamiltonian), $K_0(x)$ is a modified Bessel function and $\eta_\mathrm{F} = -K\pi\lambda/k_\mathrm{F}$ a phase shift. For large distances, the amplitude decays like $x^{-\frac{1}{2}}$ as expected. At $T > 0$,

$$\Delta n(x) = \cos(2k_\mathrm{F}x + \eta_\mathrm{F}) \sqrt{\frac{4\pi T}{\sinh(2\pi T x)}}\, F\left(\frac{1}{2}, \frac{1}{2}; 1 + 2\frac{h^2}{T}, \frac{1 - \coth(2\pi T x)}{2}\right)$$

with the hypergeometric function $F(a, b; c, d)$. For $x \gg 1/T$ the amplitude of the Friedel oscillations decays exponentially.

Recently, [GYL 2004] used the functional bosonization technique and a self-consistent harmonic approximation at low temperature and weak impurity strength to obtain the Green function at arbitrary interaction K. It shows the full crossover from the impurity-dominated behavior at short distances to the pure TLL behavior at large distances. From the Green function, one can extract the density profile as

$$\Delta n(x) = \cos(2k_\mathrm{F}x + \eta_\mathrm{F})\, |\sinh(2\pi T x K/v_\mathrm{F})|^{-K}.$$

For distances shorter than the thermal coherence length, $x \ll \pi v_F/T$, the amplitude decreases as x^{-K}, while for larger distances it is suppressed exponentially.

In section 4.3 above I have described how to compute the density profile in the fRG framework, illustrating the renormalization of a composite operator and the flow of response functions in a concrete example. In the following section I will present my results for the density profile for a wide range of parameters and compare them with exact DMRG results and the asymptotic formulae from bosonization presented here.

5.1.1 Results

Figure 5.1 shows fRG and DMRG results for the density profile n_j for a spinless-fermion chain with 128 sites and interaction strength $U = 1$ at half filling. The Friedel oscillations emerge from both boundaries and interfere in the center of the chain. The accuracy of the fRG results is excellent for all j.

For incommensurate filling factors the density profile looks more complicated. This can be seen in figure 5.2, where fRG results are shown for the density modulation $|n_j - n|$ near the boundary of a system with an average density $n = 0.393$ and 8192 sites. For long distances from the boundary the oscillation amplitude has a well-defined envelope which fits to a power law as a function of j. In the following I will examine the large-distance behavior of the amplitudes more closely for the half-filled case.

Figure 5.3 shows fRG results for the amplitude of density oscillations emerging from an *open boundary*, for a very long spinless fermion chain with $2^{19} + 1$ sites and various interaction strengths U at half filling. The other end of the chain (opposite to the open boundary) is smoothly connected to a non-interacting lead. In a log-log plot (upper panel of figure 5.3) the amplitude follows a straight line for almost all j, corresponding to a power-law dependence. Deviations from a perfect power law can be seen more clearly by plotting the effective exponent α_j, defined as the negative logarithmic derivative of the amplitude with respect to j (see the lower panel of figure 5.3). The effective exponent is almost constant except at very short distances or when j approaches the opposite end of the interacting chain, which is not surprising. From a comparison with the exact exponent (horizontal lines in the figure) one can assess the quantitative accuracy of the fRG results.

Effective exponents describing the decay of Friedel oscillations generated by *site impurities* of various strengths are shown in figure 5.4, for a half-filled spinless fermion chain with $2^{18} + 1$ sites and interaction $U = 1$. Both ends of the interacting chain are coupled to non-interacting leads to suppress oscillations otherwise induced by the boundaries. For strong impurities the results are close to the boundary result (cf. figure 5.3), as expected. For weaker impurities the oscillations decay

more slowly, i.e., with a smaller exponent, and do not reach the boundary behavior within the range of our chain for $V < 1$. For very weak impurities ($V = 0.01$ in figure 5.4) the oscillation amplitude follows a power law corresponding to the linear-response behavior with exponent $2K - 1$ at intermediate distances.

The same crossover between linear-response behavior for very weak impurities and TLL behavior for strong renormalized impurities is observed in the oscillations of the effective impurity potential Σ_{jj} (cf. figure 5.5). When the density oscillations decay with exponent K, the Σ_{jj} oscillations decay with exponent 1. In the linear-response regime, however, the respective exponents are $2K - 1$ and K. This was explained in [MMSS 2002a, MMSS 2002b]:

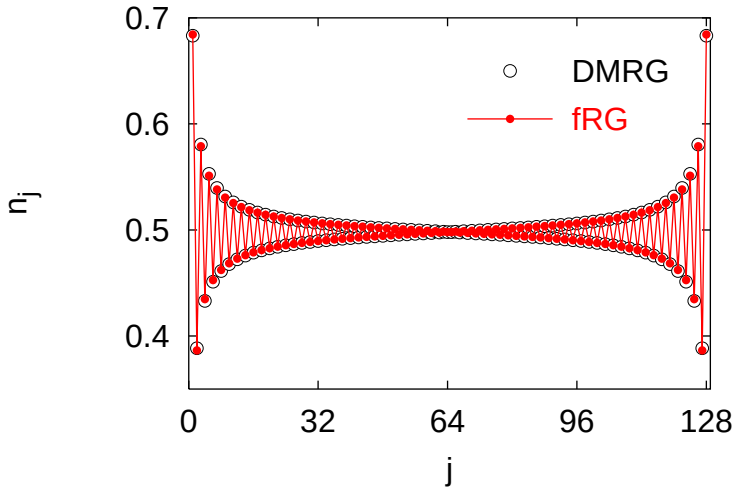


Figure 5.1: *Density profile n_j for a spinless fermion chain with* 128 *sites and interaction strength $U = 1$ at half filling. fRG results show an excellent agreement with numerically exact* DMRG *data.*

since the linear-response backscattering amplitude scales with the cutoff Λ as $V_{k_F,-k_F} \sim (1/\Lambda)^{1-K}$, this provides the generic scaling law in the low-energy regime, and also the self energy scales away from $2k_F$ with the same exponent, $\Sigma_{k,k'} \sim (k - k' - 2k_F)^{1-K}$. Performing a Fourier transform, the real-space decay scales as $|j - j_0|^{-K}$.

Finally, I present results for the effective exponent of the density-oscillation decay in the case of an *attractive* interaction $U = -1$, see figure 5.6. In that case the effective impurity strength should scale to zero at low energies and long distances [Kane&Fisher 1992a]. Indeed, for weak and moderate bare impurity potentials the effective exponent in figure 5.6 approaches the linear-response exponent $2K-1$. Only for very strong impurities the density oscillations decay with the smaller exponent K over several orders of magnitude.

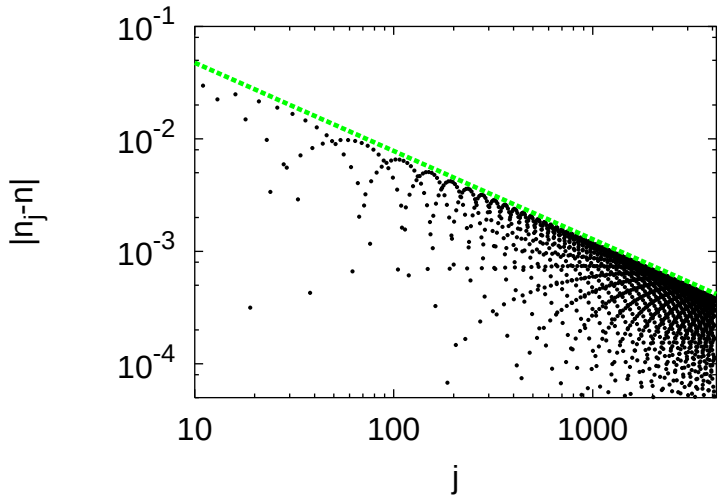


Figure 5.2: *Density modulation* $|n_j - n|$ *as a function of the distance from a boundary, for spinless fermions with interaction strength* $U = 1$ *and average density* $n = 0.393$ *on a chain with* 8192 *sites; the dashed line is a power-law fit to the envelope of the oscillation amplitudes with exponent* $K = 0.785$ *corresponding to* $\alpha_B \approx 0.274$*. It shows that Friedel oscillations display the expected behavior also away from half filling.*

5.2 Transport through double barriers

The motivation to study double barriers using the fRG is twofold: (*i*) the double barrier is physically interesting and experimentally accessible, for example in specifically fabricated quantum wires or double kinks in carbon nanotubes, see for instance [Chamon&Wen 1993, PTYGD 2001], and (*ii*) it is a multi-scale problem; in addition to the temperature T, there are additional scales such as the size of the dot region N_{dot} between the barriers and the strength of the barriers $V_{L,R}$, cf. figure 5.7. The double barrier exhibits universal scaling in certain limits—we observe several different power laws—but also non-universal crossover behavior in between, as different physical processes become relevant. This is particularly important because in experimental setups, the parameters are usually in the intermediate range. Therefore, the double barrier provides a showcase for the power of the fRG to treat all scales on an equal footing. Nevertheless, as a note of caution, several important ingredients for a realistic description are still missing in our model, although they can in principle be handled by our method, such as the spin degree of freedom, higher-dimensional leads, and realistic contacts. We therefore refrain from a detailed comparison of our findings to experiments.

For a weak *single* impurity, the conductance in the limit $T \to 0$ is suppressed for

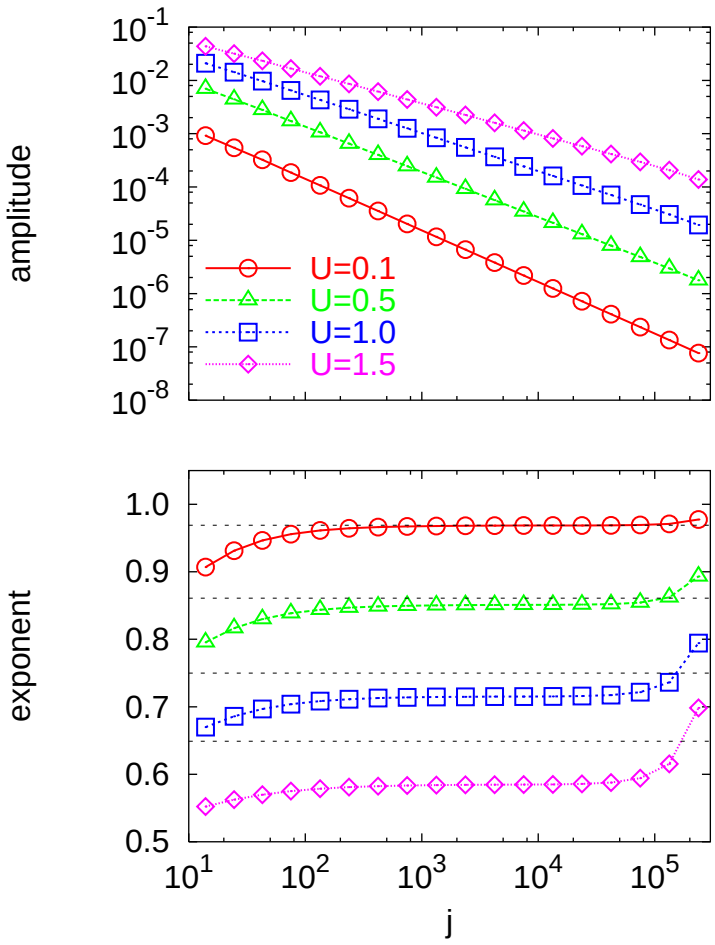


Figure 5.3: *Amplitude (envelope) of oscillations of the density profile n_j induced by a* boundary *as a function of the distance from the boundary, for spinless fermions with various interaction strengths U at half filling; the interacting chain with $2^{19}+1$ sites is coupled to a semi-infinite non-interacting lead at the end opposite to the boundary.* Upper panel: *log-log plot of the amplitude.* Lower panel: *effective exponents for the decay, and the exact asymptotic exponents (Bethe ansatz) as horizontal lines. The plateaux allow to read off the exponents very accurately.*

repulsive interaction and enhanced for attractive interaction as compared to the non-interacting case [Luther&Peschel 1974b, Apel&Rice 1982]. [Kane&Fisher 1992a] showed that this is a universal result independent of the impurity strength: for repulsive interaction, the conductance across the impurity scales as $G(T) \sim T^{2\alpha_B}$, such that asymptotically for $T \to 0$ the wire becomes insulating. This was derived using an RG method: a weak barrier, or rather its backscattering component $V(2k_F)$, is a relevant perturbation of the clean system and grows stronger in the RG flow. On the other

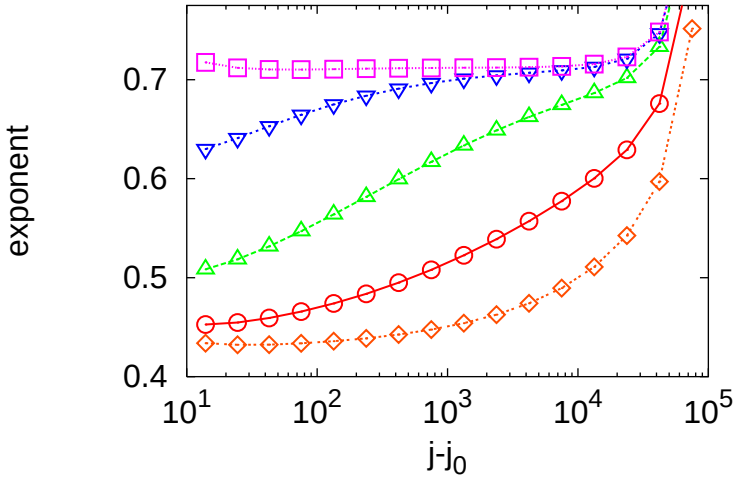


Figure 5.4: *Effective exponent for the decay of density oscillations as a function of the distance from a* site impurity *of strengths* $V = 0.01,\ 0.1,\ 0.3,\ 1,\ 10$ *(from bottom to top); the impurity is situated at the center of a spinless fermion chain with* $2^{18} + 1$ *sites and interaction strength* $U = 1$ *at half filling; the interacting chain is coupled to semi-infinite non-interacting leads at both ends. This shows the crossover from the density response regime* ($V \ll 1$) *to the boundary behavior* ($V \gg 1$).

hand, a weak link between two otherwise separate semi-infinite chains is an irrelevant perturbation which remains weak in the RG flow. Because in the weak-impurity and weak-link limits the direction of the RG flow is compatible towards a strong barrier or weak link, respectively, Kane and Fisher connected both perturbatively accessible limits and concluded that any barrier becomes strong in the asymptotic limit. This is supported by an exact solution at $K = \frac{1}{2}$. Conversely, an *attractive* interaction suppresses an initial backscattering to yield perfect transmission even for a system with an impurity. The fRG has been used successfully to reproduce the one-parameter scaling of the conductance for $1/2 \leq K \leq 1$ [MAMSS 2003].

In the case of a double barrier, there are resonance peaks in the conductance $G(V_G)$ as the gate voltage V_G is varied. Using an RG analysis similar to the one for the single barrier for asymptotically low temperatures, [Kane&Fisher 1992c] derived a phase diagram for the *peak conductance* G_p depending on the barrier strength V and interaction parameter K. For attractive interaction $K > 1$ there is perfect transmission for any V_G, while for repulsive $\frac{1}{2} < K < 1$ there are sharp conductance peaks at which perfect transmission is reached. For $K < \frac{1}{4}$ no transmission is possible for any V_G, and for $\frac{1}{4} < K < \frac{1}{2}$ there is a line (*Kosterlitz-Thouless separatrix*) of critical barrier strengths: for stronger barriers no transmission is possible, while for

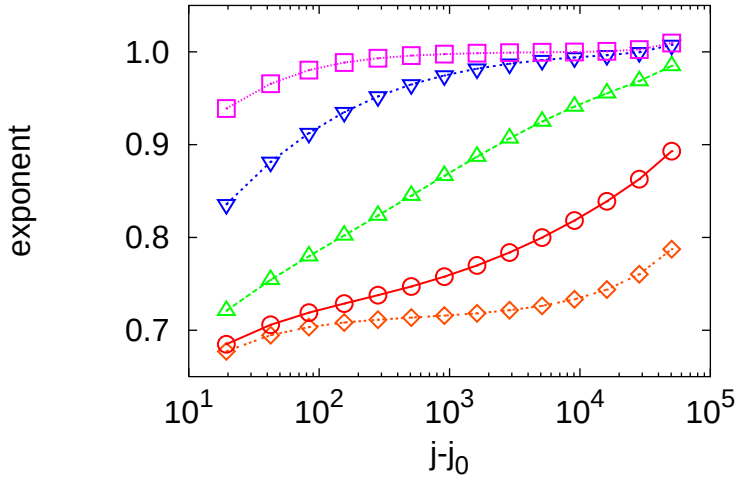


Figure 5.5: *Effective exponent for the decay of oscillations of* $\Sigma_{j,j}$ *as a function of the distance from a site impurity of strengths* $V = 0.01,\ 0.1,\ 0.3,\ 1,\ 10$ *(from bottom to top), for the spinless fermion model at half filling and interaction strength* $U = 1$*; the impurity is situated at the center of a chain with* $L = 2^{18}+1$ *sites.*

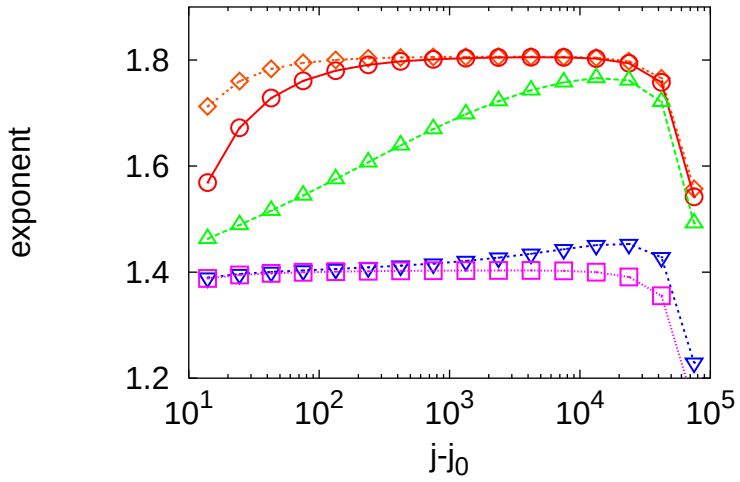


Figure 5.6: *Effective exponent for the decay of density oscillations as a function of the distance from a site impurity of strengths* $V = 0.1,\ 1,\ 10,\ 100,\ 1000$ *(from top to bottom) for the same chain as in figure 5.4 but now with an* attractive *interaction,* $U = -1$*. This demonstrates that our method works well also for negative* U*.*

weaker barriers conductance peaks appear. The line shape of the resonance peaks is

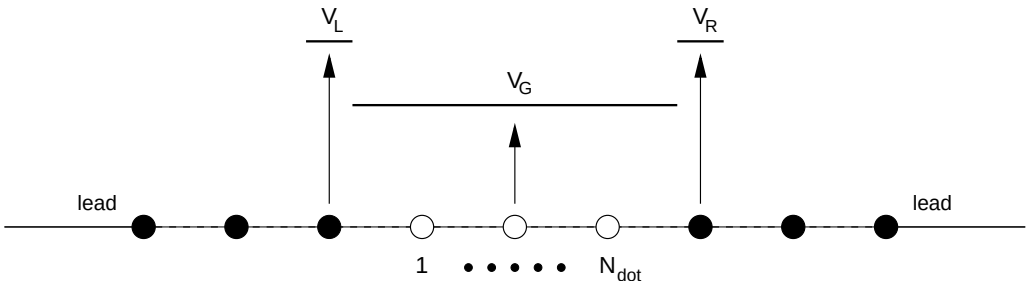


Figure 5.7: *Model of the double barrier.*

non-Lorentzian, the tails falling off as $(\Delta V_G)^{-2/K}$, where ΔV_G is the detuning from resonance.

Shortly afterwards, [Furusaki&Nagaosa 1993] studied the double barrier for arbitrary interaction by second-order perturbation theory in the barrier strength $V \ll 1$. At low temperatures, the deviation of the resonant $G_\mathrm{p}(T)$ from e^2/h scales as T^{2K}. As the temperature is increased, perturbation theory in the inverse barrier strength $1/V \ll 1$ and a Master-equation approach [Furusaki 1998] yield a regime of *uncorrelated sequential tunneling* (UST) characterized by peaks of height $G_\mathrm{p}(T) \sim T^{\alpha_B - 1}$ and width $w(T) \sim T$, for $T \ll \Delta_\mathrm{dot}$, where $\Delta_\mathrm{dot} := \pi v_\mathrm{F}/N_\mathrm{dot}$ is the level spacing of the dot. For $\Delta_\mathrm{dot} \ll T \ll B$, where B is the bandwidth, $G_\mathrm{p}(T)$ increases as $T^{2\alpha_B}$ for increasing T.

However, recent experiments on carbon nanotubes [PTYGD 2001] have reported for the temperature range $\Gamma \ll T \ll \Delta_\mathrm{dot}$ that both the resonant peak height $G_\mathrm{p}(T) \sim T^{0.7}$ and $G(V_G)$ peak width $w(T) \sim T$ decrease with decreasing temperature. Here, Γ is the width of a resonance in the transmission probability $\mathcal{T}(\epsilon)$ given by equation (4.40), which for strong barriers is related to the tunneling rate into and out of the dot. While also [Furusaki&Nagaosa 1993, Furusaki 1998] found power laws with a positive power of T, they were expected to occur only for very strong repulsive interactions, where α_B is at least twice as large as the value $\alpha_B \approx 0.6 \ldots 1.0$ observed in carbon nanotubes. [PTYGD 2001] suggested that *correlated sequential tunneling* (CST) with exponent $2\alpha_B - 1 > 0$ dominates over UST with exponent $\alpha_B - 1 < 0$ in the temperature range $\Gamma \ll T \ll \Delta_\mathrm{dot}$. Subsequently, [TGCPD 2002, TEG 2004] argued that cotunneling processes of second order in the end-tunneling local density of states (each with exponent α_B) are the leading contribution to the peak conductance (hence the $2\alpha_B$), and claimed perfect agreement with the experimental data of [PTYGD 2001]. In contrast, [Furusaki 1998] had found that cotunneling via virtual intermediate states dominated the *tails* of the conductance peak away from the resonance. This led to a renewed interest in transport through double barriers, with several new methods available to advance beyond asymptotically low temperatures.

Shortly after, [Polyakov&Gornyi 2003, Nazarov&Glazman 2003] studied the double barrier at arbitrary temperature and impurity strength but weak interaction using the leading-log resummation of [MYG 1993, YGM 1994]. They considered the RG flow of the energy-dependent scattering amplitudes, based on a resummation of perturbation-theory diagrams with leading logarithmic divergences ${\alpha_B}^n \ln^n(\frac{1}{|k-k_F|d})$, where d is the spatial range of the interaction. Inelastic processes are sub-leading at weak interaction. Their results for a single resonant level agreed with [Furusaki&Nagaosa 1993] for $T < \Delta_{\rm dot}$, finding UST but not CST. [Polyakov&Gornyi 2003] extended the RG study to a multi-level dot and weak barriers (closer to experimental parameters) but again confirmed UST.

Recently, [Komnik&Gogolin 2003] found an exact solution for a special model at interaction strength $K = \frac{1}{2}$. However, in that model the conductance scales as T^{-1} even for $T < \Delta_{\rm dot}$ where one would expect UST, as if the fermions were non-interacting. Because it shows no sign of either UST or CST, this result is probably not generic and cannot help to resolve the puzzle.

[Hügle&Egger 2004] computed the conductance using the Quantum Monte Carlo (QMC) method for interaction $K = 0.6$ and obtained data interpreted to be consistent with CST for weak barriers and sufficiently high temperatures, which was explained by an additional transport channel for strong interaction.

Against this background, it is desirable to have an unbiased method to compute the conductance without restricting from the beginning—by physical intuition—which physical processes are dominant. The fRG provides this with the only restriction that it is perturbative in the *renormalized* interaction but contains contributions of all orders in the bare interaction U. It confirms the UST picture but in addition allows to vary all parameters to see exactly at which temperature, barrier strength, dot size etc. the universal scaling sets in, if at all. While the justification of the fRG was weak-coupling, we reproduce one-parameter scaling for the single barrier at $U = 2$ very accurately [MAMSS 2003], and our results for the double barrier qualitatively agree with the QMC data ($U = \sqrt{3}$), indicating that the fRG is reliable up to this interaction strength.

5.2.1 Results

The fRG has been used before to compute the conductance through a single impurity at zero temperature [Meden&Schollwöck 2003a, Meden&Schollwöck 2003b, MAMSS 2003]. After having developed and implemented the finite-temperature fRG, I have obtained results for transport through a double barrier, symmetric or asymmetric, at or off resonance, with weak or strong barriers, enclosing small or large dots, for repulsive interaction (see also [MEAMS 2005, EMABMS 2005]). I will report

my findings for several interesting regions in this large parameter space, showing agreement with known results as well as providing clarification of a contentious issue.

I first present results for a strong symmetric double barrier, $V_{L,R} = 10$, enclosing a dot of $N_{\mathrm{dot}} = 6$ sites. The interacting system size is taken to be $N = 10^4$, in agreement with the size of realistic samples of carbon nanotubes. As the gate voltage V_G is varied across the band, there are six resonance peaks with level spacing roughly Δ_{dot} (figure 5.8). In non-interacting systems the peaks have a finite width even at

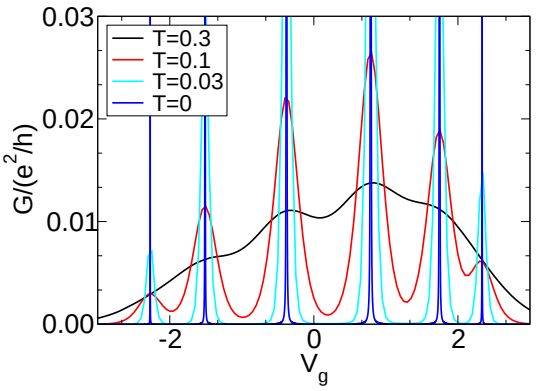


Figure 5.8: *The conductance $G(V_G)$ as a function of gate voltage V_G for $N_{dot} = 6$, $U = 0.5$, $V_{L,R} = 10$, $N = 10^4$ and different T. One observes N_{dot} resonance peaks which are widened with increasing temperature.*

$T = 0$, depending on the shape of the barrier and the local density of states of the leads at the barrier. Repulsive interaction has a strong influence on the line shape of the resonance peaks: they become infinitely sharp in the asymptotic limit ($N \to \infty$, $T \to 0$) but perfect transmission e^2/h is still possible for symmetric barriers. As the temperature is increased the peaks become wider and lower. The peak conductance $G_{\mathrm{p}}(T)$ as a function of temperature shows several different power laws for appropriately chosen dot parameters. All the peaks in figure 5.8 have a different shape and size due to band effects, however $G_{\mathrm{p}}(T)$ behaves similarly for each peak, and in the following I will always consider the peak closest to $V_G = 0$.

Figure 5.9 shows the peak conductance $G_{\mathrm{p}}(T)$ for three different dot sizes N_{dot} in the upper panel, while in the lower panel the logarithmic derivative is plotted. For temperatures larger than the bandwidth, the conductance scales as $G_{\mathrm{p}}(T) \sim T^{-1}$. This is because $f'(\epsilon)$ and the transmission in equation (4.39) vary only very little over the band, but $f'(\epsilon)$ decreases with increasing temperature as $1/T$. For temperatures below the dot level spacing Δ_{dot} (indicated by the arrows), the peak conductance decreases as $G_{\mathrm{p}}(T) \sim T^{\alpha_B - 1}$ (UST). This exponent is marked in the lower panel by the dashed line. In the UST regime the conductance integral is dominated by a single

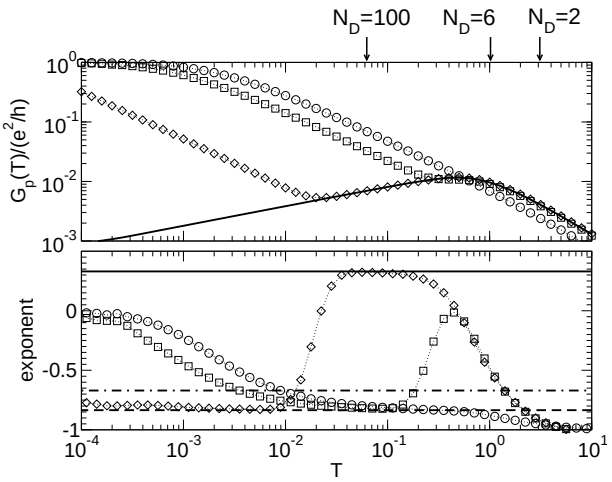


Figure 5.9: *The resonant peak conductance $G_p(T)$ for different dot sizes.* Upper panel: $N_{dot} = 2$ *(circles),* 6 *(squares), and* 100 *(diamonds), with the respective level spacing Δ_{dot} indicated by the arrows. $U = 0.5$, $N = 10^4$, $V_{L,R} = 10$. The solid curve shows $G(T)/2$ for a single barrier.* Lower panel: *Logarithmic derivative of $G_p(T)$. Solid line: $2\alpha_B$; dashed line: $\alpha_B - 1$; dash-dotted line: $2\alpha_B - 1$.*

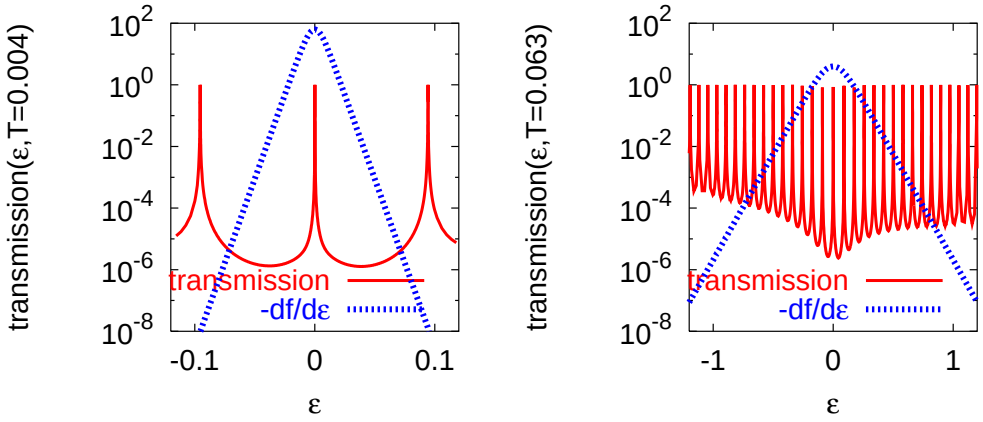


Figure 5.10: *Transmission $\mathcal{T}(\epsilon, T)$ for several temperatures:* left panel $T = 0.004$, right panel $T = 0.063$. *The dashed line is the derivative of the Fermi function at the respective temperature. The dot parameters are $N_{dot} = 100$, $U = 1$, $N = 10^4$ and $V_{L,R} = 10$. This shows that for low temperatures (*UST*), a single transmission peak determines the conductance, while for higher temperatures (Kirchhoff) many peaks contribute.*

peak in the transmission $\mathcal{T}(\epsilon, T)$ with a width $\Gamma < T$ (cf. figure 5.10, left panel). As the temperature is lowered, the UST regime extends down to T^* where $T = \Gamma$. In $G(V_G)$ the peaks are well separated and have a width $w(T) \sim T$.

For the above parameters and dots with $N_{\text{dot}} \geq 4$, the conductance shows a

third regime for $\Delta_{\rm dot} \lesssim T \lesssim 1$. In this region, the conductance increases with increasing temperature, leading to a non-monotonic overall T dependence. For large dots $N_{\rm dot} \gtrsim 30$, the conductance increases according to the power law $G_{\rm p}(T) \sim T^{2\alpha_B}$, indicated by the solid line in the lower panel of figure 5.9. Many peaks in the transmission $\mathcal{T}(\epsilon, T)$ contribute to the conductance (cf. figure 5.10, right panel). This regime is most clearly seen for strong barriers $V_{L,R} \gg 1$ and large dots $N_{\rm dot} \gg 1$.

If we add the resistances of both barriers separately according to Kirchhoff's law, $1/G = 1/G_L + 1/G_R$, we obtain the solid curve in the upper panel of figure 5.9. As our data lie on this curve for $T \gtrsim \Delta_{\rm dot}$, we suggest the following interpretation: the electrons first tunnel through one barrier with a certain probability, then incoherently through the next. Only as the temperature is lowered to $T \approx \Delta_{\rm dot}$, the electron "sees" both barriers coherently and tunnels resonantly, such that the conductance increases towards e^2/h as $T \to 0$.

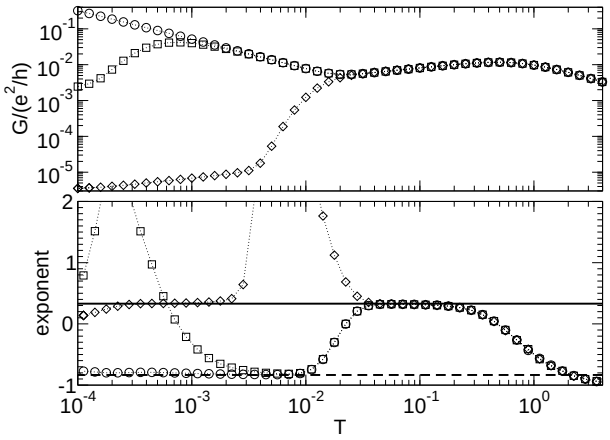


Figure 5.11: *On- and off-resonance conductance.* Upper panel: $G(T)$ *for* $U = 0.5$, $N = 10^4$, $V_{L,R} = 10$, *and* $N_{dot} = 100$. *On resonance* $\Delta V_G = 0$ *(circles), near resonance* $|\Delta V_G| = 0.001$ *(squares), and in a conductance minimum with* $|\Delta V_G| = 0.04$ *(diamonds). The off-resonance curves lie on the resonance curve for* $T \gtrsim |\Delta V_G|$, *then cross over to decay as* $G_p(T) \sim T^{2\alpha_B}$. Lower panel: *Logarithmic derivative of* $G(T)$. *Solid line:* $2\alpha_B$*; dashed line:* $\alpha_B - 1$. *At low temperature the double barrier off resonance behaves like a single impurity.*

It is thus only in the low-temperature range where it makes a difference whether V_G is tuned to resonance or not (cf. figure 5.11). If the gate voltage is slightly off resonance, $\Delta V_G \neq 0$ and $|\delta V_G| \ll \Delta_{\rm dot}$, the conductance is identical to the resonant case for $T \gtrsim \Delta V_G$, while for lower temperatures the double barrier acts as a single impurity of strength $|\Delta V_G|$, hence the conductance scales as $G(T) \sim T^{2\alpha_B}$.

Up to this point, we have presented conductance data for the weak interaction

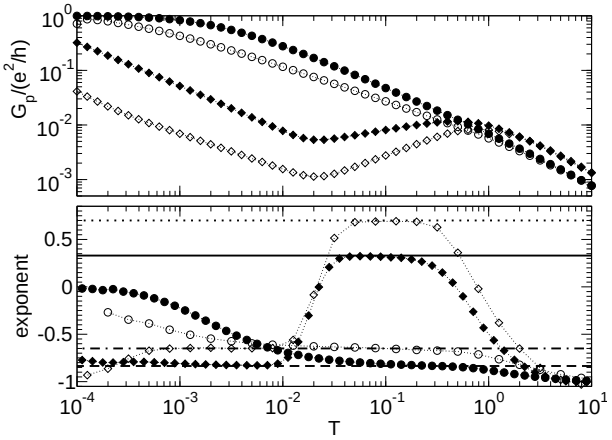


Figure 5.12: *Conductance for different interaction strength.* Upper panel: *Peak conductance $G_p(T)$ for $U = 0.5$ (full symbols) and $U = 1$ (open symbols). Curves are shown for dot sizes $N_{dot} = 2$ (red) and $N_{dot} = 100$ (blue).* Lower panel: *Logarithmic derivative of $G(T)$. The dependence of the exponents on the interaction strength support the claim that the exponents are $\alpha_B - 1$ and $2\alpha_B$, respectively.*

strength $U = 0.5$ ($\alpha_B = 0.165$). The numerical exponent of -0.835 in the UST regime was identified with $\alpha_B - 1$, and the exponent 0.330 in the Kirchhoff regime with $2\alpha_B$. Figure 5.12 shows the exponents for a different value of U: at $U = 1$ ($\alpha_B = 0.35$), the exponents -0.65 and 0.70 can be read off, confirming this identification within the numerical accuracy. A comparison of the exponents for strong and weak barriers can be found in [EMABMS 2005].

For strong barriers, large dot size and weak interaction, there is no indication of a power law with exponent $2\alpha_B - 1$ claimed by [TGCPD 2002, TEG 2004, Hügle&Egger 2004]. Consider, therefore, a dot with parameters as close as possible to those in [Hügle&Egger 2004]: weak to intermediate barriers, intermediate dot size and larger U (cf. figure 5.13). For a small dot $N_{\mathrm{dot}} = 10$ (circles), neither the exponent $\alpha_B - 1$ (dashed line) nor $2\alpha_B$ (solid line) is clearly developed. For larger dots $N_{\mathrm{dot}} = 30$ (squares) and $N_{\mathrm{dot}} = 50$ (diamonds), the $\alpha_B - 1$ exponent (UST) is clearly visible, but the Kirchhoff exponent $2\alpha_B$ is still not reached. In the QMC data [Hügle&Egger 2004] the conductance is fitted to a slope of 1/3 in a log-log plot, which is interpreted as scaling with exponent $2\alpha_B - 1$ (CST) for $\alpha_B = 2/3$. Our data shows the conductance curve with a slope of $0.3 \ldots 0.7$, depending on the dot parameters, but no fixed scaling exponent. Therefore, we interpret this as *non-universal* behavior.

Figure 5.14 shows the resonant peak conductance for strongly *asymmetric barriers*. The Kirchhoff regime is unchanged qualitatively as both barriers are very strong. For lower temperatures one observes a UST regime which crosses over into single-impurity

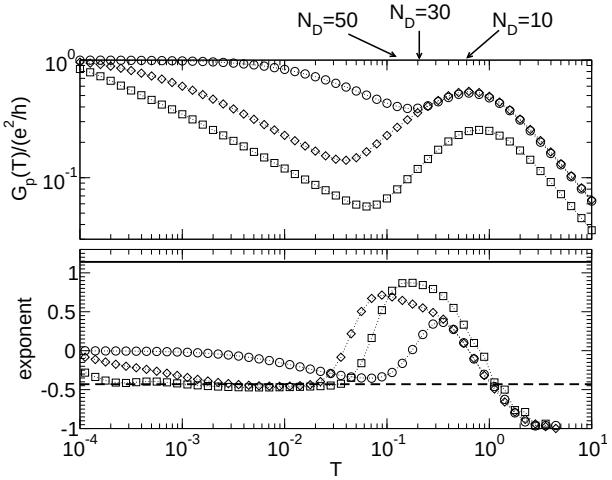


Figure 5.13: *Weak barriers,* Upper panel: $G_p(T)$ *for* $U = 1.5$, $N = 10^4$, $N_{dot} = 10$ *with* $V_{L,R} = 0.8$ *(circles),* $N_{dot} = 30$ *with* $V_{L,R} = 1.5$ *(squares), and* $N_{dot} = 50$ *with* $V_{L,R} = 0.8$ *(diamonds). The arrows indicate* Δ_{dot} *for the different dot sizes.* Lower panel: *Logarithmic derivative of* $G_p(T)$*. Solid line:* $2\alpha_B$*; dashed line:* $\alpha_B - 1$*. For small dots, the* $2\alpha_B$ *power law is not clearly developed; however the conductance agrees with the* QMC *data [Hügle&Egger 2004].*

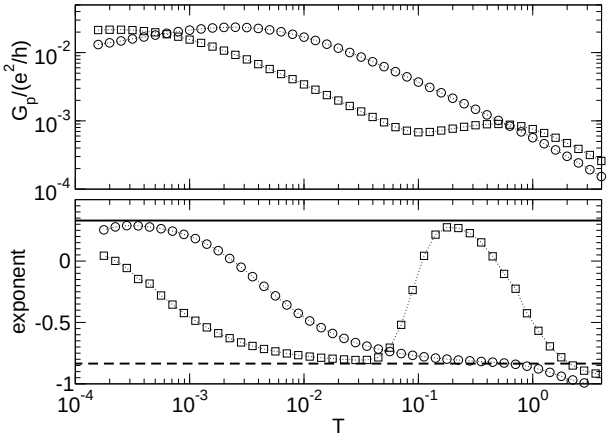


Figure 5.14: *Strongly asymmetric barriers,* Upper panel: $G_p(T)$ *for* $V_L = 5$, $V_R = 50$, $U = 0.5$, $N = 10^4$, $N_{dot} = 2$ *(circles) and* $N_{dot} = 20$ *(squares).* Lower panel: *Logarithmic derivative of* $G_p(T)$*. Solid line:* $2\alpha_B$*; dashed line:* $\alpha_B - 1$*.*

scaling $G_{\rm p}(T) \sim T^{2\alpha_B}$ for small dots at very low temperatures.

For a small dot ($N_{\rm dot} = 1$) with weak barriers the conductance approaches the perfect value e^2/h according to the power law [Kane&Fisher 1992b, Furusaki&Nagaosa 1993] (cf. figure 5.15)

$$\frac{e^2}{h} - G_{\rm p}(T) \sim T^{2K}.$$

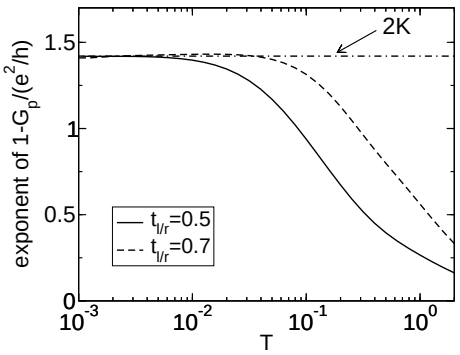


Figure 5.15: *Effective exponent of* $1 - G_p(T)/(e^2/h)$ *for a small dot with* $N_{dot} = 1$, $U = 1$, $N = 10^4$, *and intermediate to weak hopping barriers* $t_{l,r}$. *Dash-dotted line:* $2K$.

Thus, our method yields up to four different power laws within the same framework.

5.3 Summary

I have demonstrated that the fRG is a powerful method for multi-scale problems. As applications I have studied Friedel oscillations off an impurity or boundary in an interacting wire, and transport through a double barrier. Both problems were previously investigated using effective field-theoretical models; in the cases where exact results for such models are known I have obtained quantitative agreement for weak to intermediate interactions $1/2 \leq K \leq 1$. For the Friedel oscillations at $T = 0$, I observed the exponent K at large distances and $2K - 1$ for weak impurities at short distances [AEMMSS 2004].

For resonant tunneling, depending on the parameters of the quantum dot, I found several temperature regimes with power-law scaling as well as non-universal behavior (cf. figure 5.16) [MEAMS 2005, EMABMS 2005]. All these temperature regimes are obtained within the same approximation scheme. The crossover between the regimes can be studied in detail. For parameters for which a comparison is possible the results agree with the ones obtained in lowest-order perturbation theory in the barrier height and inverse barrier height. I did not find any indications of a CST regime with the exponent $2\alpha_B - 1$ predicted from an approximate Master-equation approach, and seemingly supported by QMC data. If it were present, our method should be able to reveal such a regime since its scaling exponent differs from the UST exponent already at leading order in the interaction.

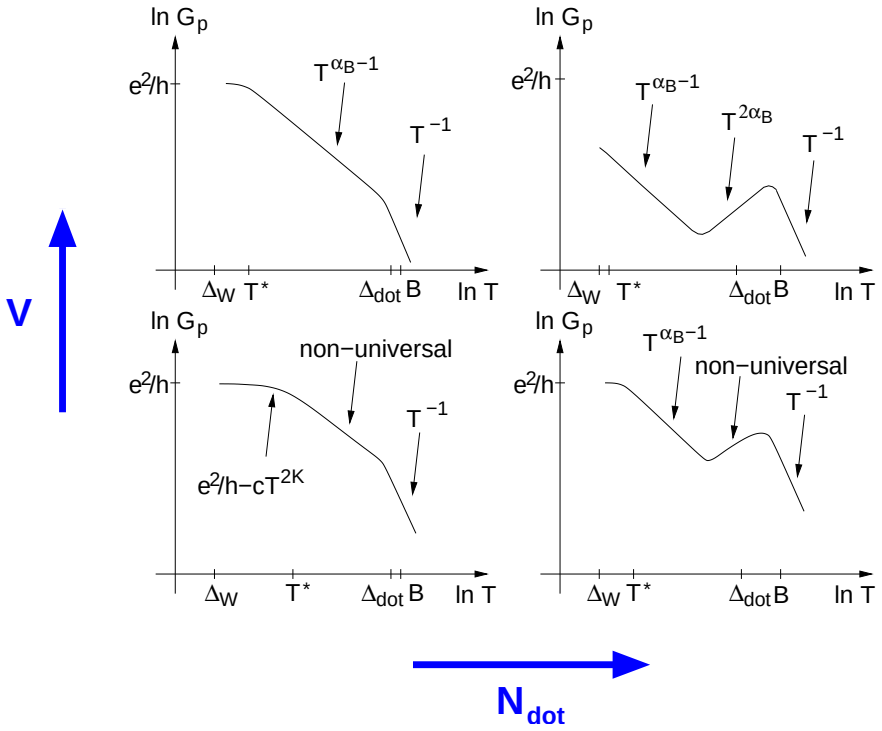


Figure 5.16: *Schematic plot of the different regimes for the scaling of the conductance $G_p(T)$ at resonance for symmetric barriers found using our method. The upper panels have higher barriers than the lower ones; the right panels have larger dot sizes than the left ones. $\Delta_W = \pi v_F/N$ is the energy scale of the interacting wire.*

6 Conclusions and outlook

In this thesis I investigate the role of symmetries and conservation laws in the functional renormalization-group formalism, and study specifically Friedel oscillations and transport in 1D correlated electron systems.

In the *functional renormalization group* (fRG) method an energy cutoff scale is introduced in the bare propagator as a flow parameter (Chapter 2). By solving coupled differential flow equations for the Green functions, the effective behavior on all energy scales can be computed for a given microscopic model. Because the full flow-equation hierarchy can be solved exactly only in a few special cases, for instance the Luttinger model [SBK 2004], in most practical applications one has to truncate the hierarchy by setting the flow of, say, the three-particle and higher Green functions to zero. This approximation is justified perturbatively in the renormalized interaction or some other small parameter. For applications such as the 2D Hubbard model and 1D impurity problems, different basis sets of Green functions have proven to be particularly useful.

The presence of continuous *symmetries* in the bare action leads by the Noether theorem to conservation laws and Ward identities relating Green and response functions (Chapter 3). The solution of the infinite flow-equation hierarchy preserves the symmetry once the cutoff is removed. The truncated flow equations with a momentum cutoff, however, generally violate the Ward identities. After discussing previous results from the high-energy physics literature, I show that if a manifestly gauge-invariant construction is possible as, for instance, in the temperature-flow scheme, the Ward identities between Green and response functions can be satisfied exactly despite truncations.

The related property of *self-consistency* is satisfied by construction in the conserving approximations [Baym&Kadanoff 1961], and it would be desirable if it were also satisfied in truncated fRG flows. However, I show that the commonly used truncations generally violate self-consistency. For special reduced models it has been shown that truncated flow equations can be modified to satisfy self-consistency and even yield the exact mean-field solution [Katanin 2004, SHML 2004], so the hope remains that this may be generalized to arbitrary interaction. However, in the 1D lattice model of the Luttinger liquid, the truncated fRG is surprisingly successful and self-consistency does not appear to play an important role on the level of our approximation.

Correlated electron systems in one dimension show *Luttinger-liquid* behavior with a strong interplay between interaction and impurities. The fRG method is particularly apt to compute the single-particle and transport properties of a lattice model of spinless fermions with one or two impurities at all energy scales (Chapter 4). For systems with up to 1000 sites the results agree well with the numerically exact DMRG. For large systems the fRG reproduces the asymptotic, universal power laws known from thermodynamic Bethe ansatz and bosonization, as well as various field-theoretical methods, and in addition indicates the onset of and crossover between different power-law regimes.

I have concentrated on two *observables*: the spatial density profile for Friedel oscillations and the conductance. In the exact solution the density profile can be obtained from the full propagator; within our approximation it is much more accurate to instead treat the density-response vertex as a separately flowing composite operator. On the other hand, the conductance is completely determined by the full propagator because current-vertex corrections do not arise in our approximation in accordance with Ward identities. The practical usefulness of the method relies on the fast computation of loop integrals (appendix B); a little-known mathematical trick is used to develop a new algorithm linear instead of quadratic in the system size which allows to treat lattices as large as 10^7 sites very accurately.

The Friedel oscillations off an impurity or boundary (Chapter 5) obey the characteristic power laws and show a crossover to the linear-response regime, both for repulsive and attractive interaction. The measured exponents agree with the exact values to linear order in the interaction; however the deviations are small up to $U \approx 1.5$ because we have incorporated the flow of the interaction vertex [AEMMSS 2004, Andergassen 2005]. A double barrier features several distinct power laws in the conductance as a function of temperature [MEAMS 2005, EMABMS 2005]. We reproduce the exponents for the limiting cases treated in earlier works but in addition observe non-universal behavior in the intermediate parameter and temperature regions. This serves to clarify a contentious issue in the literature where two different universal scaling laws have been claimed for a certain parameter range: our data agree qualitatively with the numerically exact QMC [Hügle&Egger 2004] but suggest an interpretation in terms of a non-universal crossover regime. In conclusion, it is remarkable that our simple approximation captures on an equal footing effects which originate from very different physical processes.

As an *outlook* there are several promising extensions of the current scheme. (i) The electron spin should be included to make the model more realistic [Andergassen 2005]. Preliminary results indicate that for the typical size of carbon nanotubes ($N \sim 10^4$), the results are even farther from the asymptotic behavior than in the spinless case, so the accurate treatment of the non-universal behavior is even more important.

(*ii*) X. Barnabé-Thériault studied junctions and rings pierced by a flux, and connected to several interacting leads [BSMS 2005a, BSMS 2005b]. He showed that the interpretation of the complicated behavior of such systems is greatly simplified if one considers not the (real) conductance but the (complex) Green function at the interfaces to the leads as the relevant observable: if plotted parametrically for different impurity strengths and energy scales, one arrives at a simple flow diagram in the complex plane. (*iii*) The investigation of non-equilibrium phenomena using a Keldysh variant of the fRG has been started [Jakobs 2004]. (*iv*) There are interesting Luttinger-liquid properties which appear only at two-loop order in the interaction, related to inelastic scattering. To take them into account one would need to include the frequency dependence of the interaction vertex or two-loop diagrams into the flow equation.

The fRG provides a powerful tool to compute properties of 1D lattice models where all microscopic parameters can be flexibly modeled. It captures the effects on many energy scales, yielding universal scaling as well as non-universal behavior.

A Heat equation

I hope to develop a better intuition of the formal procedures and transformations involved in the functional formalism by repeating them on a simple, well-known example: the heat equation in one dimension. Given a temperature distribution $u_0(x)$ at initial time $t = 0$, the heat flow governed by the equation

$$\partial_t\, u_t(x) = \partial_x^2\, u_t(x), \qquad\qquad u_{t=0}(x) = u_0(x), \tag{A.1}$$

determines the temperature distribution $u_t(x)$ at any later time $t \geq 0$.

In the left column below, we start with the solution of (A.1) in integral form, a convolution with the Green function, and transform it in several steps into the differential form. At the same time in the right column, we start with the functional integral definition (2.13) of the effective interaction $\mathcal{V}$ because the generating functional $e^{-\mathcal{V}}$ is the one formally most closely related to the temperature distribution $u_t(x)$ at fixed time $t = 1$:

$$\begin{aligned} u_t(x) &= \int_{-\infty}^{\infty} dy\, G_t(x-y)\, u_0(y) \\ &= \int_{-\infty}^{\infty} dy\, \frac{1}{\sqrt{4\pi t}}\, e^{-\frac{(x-y)^2}{4t}}\, u_0(y) \end{aligned} \qquad\qquad \begin{aligned} e^{-\mathcal{V}[\chi,\bar\chi]} &= e^{(\bar\chi, Q\chi) - \mathcal{G}[\eta = Q\chi, \bar\eta = Q^t\bar\chi]} \\ &= \frac{1}{Z_0} \int [d\psi\bar\psi]\, e^{\left([\bar\psi-\bar\chi], Q[\psi-\chi]\right)} \\ &\quad \times e^{-V_0[\psi,\bar\psi]} \end{aligned}$$

measure: $d\mu_t(x) = \mathcal{N} \cdot e^{-\frac{x^2}{4t}} dx, \int d\mu_t(x) = 1$

$$= \int d\mu_t(y-x)\, u_0(y) \qquad\qquad = \int d\mu_Q[\psi-\chi, \bar\psi-\bar\chi]\, e^{-V_0[\psi,\bar\psi]}$$

shift of variables:

$$\begin{aligned} &= \int d\mu_t(y)\, u_0(y+x) \\ &= u_0(\partial_s) \int d\mu_t(y)\, e^{(y+x)s}\Big|_{s=0} \end{aligned} \qquad\qquad \begin{aligned} &= \int d\mu_Q[\psi,\bar\psi]\, e^{-V_0[\psi+\chi,\bar\psi+\bar\chi]} \\ &= e^{-V_0[\delta_{\bar\varphi},\delta_\varphi]} \\ &\quad \times \int d\mu_Q[\psi,\bar\psi]\, e^{(\bar\varphi,\psi+\chi) - \left(\bar\psi+\bar\chi,\varphi\right)}\Big|_{\varphi=0} \end{aligned}$$

completing the square: $\mathcal{N}\int e^{-\frac{y^2}{4t}+ys}\,dy = e^{ts^2}$

$$
\begin{aligned}
&= u_0(\partial_s)\, e^{ts^2}\, e^{xs}\Big|_{s=0} && = e^{-V_0[\delta_{\bar\varphi},\delta_\varphi]}\, e^{(\bar\varphi, C\varphi)}\, e^{(\bar\varphi,\chi)-(\bar\chi,\varphi)}\Big|_0 \\
&= u_0(\partial_s)\, e^{t\partial_x^2}\, e^{xs}\Big|_{s=0} && = e^{-V_0[\delta_{\bar\varphi},\delta_\varphi]}\, e^{(\delta_\chi, C\delta_{\bar\chi})}\, e^{(\bar\varphi,\chi)-(\bar\chi,\varphi)}\Big|_0 \\
&= e^{t\Delta}\, u_0(x) && = e^{\Delta_C}\, e^{-V_0[\chi,\bar\chi]}\ .
\end{aligned}
$$

The solution of the heat equation is most conveniently formulated in Fourier space where the Laplacian $\Delta = -k^2$ is diagonal. However, on the field-theory side perturbation theory in the interaction V_0 leads to an expansion of e^{-V_0} in powers of χ, which corresponds to an expansion of $u_0(x)$ in powers of position x, not momentum k. Therefore, we will try to solve the heat equation in real space to make the analogy clearer. On the way we shall obtain a generalization of Hermite polynomials as basis functions and see how they are obtained from a generating function, the 1D analog of generating functionals. In the left column, we will first expand $u_0(x)$ in powers of x and then apply $e^{t\Delta}$ to it; in the right column, we proceed in the opposite order, first applying $e^{t\Delta}$ and then expanding in powers of x:

$$
\begin{aligned}
u_t(x) &= e^{t\Delta}\, u_0(x) && && \text{(A.2)}\\
&= e^{t\Delta}\Big[u_0(\partial_s)\, e^{xs}\Big]_{s=0} && = \Big[u_0(\partial_s)\, e^{ts^2+xs}\Big]_{s=0} && \text{(A.3)}\\
&= e^{t\Delta}\sum_{k=0}^{\infty}\tfrac{u_0^{(k)}(0)}{k!}\Big[\partial_s^k\, e^{xs}\Big]_0 && = \sum_{k=0}^{\infty}\tfrac{u_0^{(k)}(0)}{k!}\Big[\partial_s^k\, e^{ts^2+xs}\Big]_0 && \text{(A.4)}\\
&= \sum_{k=0}^{\infty}\tfrac{u_0^{(k)}(0)}{k!}\, e^{t\Delta}\, x^k && = \sum_{k=0}^{\infty}\tfrac{u_0^{(k)}(0)}{k!}\, H_k^t(x). && \text{(A.5)}
\end{aligned}
$$

In the last line, we have used "rescaled Hermite polynomials" $H_k^t(x)$ defined by

$$
H_k^t(x) = e^{t\partial_x^2}\, x^k, \qquad\qquad e^{ts^2+xs} = \sum_k \frac{1}{k!} H_k^t(x)\, s^k \qquad \text{(A.6)}
$$

which are related to (usual) Hermite polynomials $H_k(x)$,

$$
H_k(x) = e^{-\partial_x^2}\,(2x)^k, \qquad\qquad e^{-s^2+2xs} = \sum_k \frac{1}{k!} H_k(x)\, s^k \qquad \text{(A.7)}
$$

by

$$
H_k^t(x) = (-t)^{k/2} H_k(x/\sqrt{-4t}). \qquad \text{(A.8)}
$$

Thus, once we have expanded the initial condition into modes $u_0^{(k)}(0)$, they evolve in time independently of each other according to the t dependence of $H_k^t(x)$. As there are infinitely many modes in $u_0(x) \sim e^{-V_0[\chi,\bar\chi]}$, however, it turns out that other parametrizations are more efficient in our applications.

B Efficient computation of tridiagonal loops in O(N)

B.1 Propagator

For the frequency cutoff at $T = 0$ and $\Lambda < \Lambda_0 < \infty$ the flow equation for the self energy (4.24) can be written as

$$\partial_\Lambda \Sigma^\Lambda_{1',1} = -\frac{1}{2\pi} \sum_{2,2'} \Gamma^\Lambda_{1',2';1,2}\, 2\,\mathrm{Re}\left[\tilde{G}^\Lambda_{2,2'}(i\Lambda)\right] \ . \tag{B.1}$$

In order to compute its right-hand side, one needs to invert the tridiagonal matrix

$$T = G_0^{-1}(i\Lambda) - \Sigma^\Lambda \ , \tag{B.2}$$

where T is complex symmetric (*not* hermitean) with diagonal elements $a_i := i\Lambda + \mu - \Sigma^\Lambda_{i,i}$, $i = 1, \ldots, N$, and first off-diagonal elements $b_i := t - \Sigma^\Lambda_{i,i+1}$, $i = 1, \ldots, N-1$. Note that $\mathrm{Im}(a_i) = \Lambda > 0$ such that T is non-singular and its inverse well-defined.

The inverse $\tilde{G}^\Lambda(i\Lambda) = T^{-1}$ is not tridiagonal but a full matrix which can be computed by standard methods in $\mathcal{O}(N^2)$ time. However, for an interaction that does not extend beyond nearest neighbors on the lattice, only the tridiagonal part of $\tilde{G}$ is required, which can be computed in $\mathcal{O}(N)$ time, such that much larger lattices can be treated. We shall first explain how this is done and then present the resulting algorithm that can directly be incorporated into a computer program.

Under certain assumptions (see below), a matrix can be uniquely factorized into a lower unit triangular matrix L, a diagonal matrix D, and an upper unit triangular matrix U ("LDU factorization"): $T = LDU$ [PTVF 1986]. For a tridiagonal matrix T the unit triangular matrices L and U are in fact unit bidiagonal: their matrix elements are unity on the diagonal, and only the first off-diagonal is nonzero. Since our T is symmetric we have $L = U^T$. Thus we obtain a factorization of the form

$$T = U^{+T} D^+ U^+ = \begin{pmatrix} 1 & & & \\ U_1^+ & 1 & & \\ & U_2^+ & 1 & \\ & & \ddots & \ddots \end{pmatrix} \begin{pmatrix} D_1^+ & & & \\ & D_2^+ & & \\ & & D_3^+ & \\ & & & \ddots \end{pmatrix} \begin{pmatrix} 1 & U_1^+ & & \\ & 1 & U_2^+ & \\ & & 1 & \ddots \\ & & & \ddots \end{pmatrix}$$

where the label "+" distinguishes this factorization from another one used below. The prescription to compute the elements D_i^+ and U_i^+ is well known and can be

found for example in [PTVF 1986]. Starting in the upper left corner one proceeds to increasing row and column numbers until one arrives at the lower right corner of T:

$$D_1^+ := a_1, \quad U_i^+ := b_i/D_i^+, \quad D_{i+1}^+ := a_{i+1} - b_i U_i^+ \quad (i = 1, \ldots, N-1) \; . \quad \text{(B.3)}$$

This works well since in our case $\mathrm{Im}(D_i^+) \geq \Lambda > 0$, such that one never divides by zero.

To compute the inverse $\tilde{G} = T^{-1}$, one could directly calculate $(U^+)^{-1}(D^+)^{-1}(U^{+T})^{-1}$. It is however easier and more accurate to find the inverse by solving the linear system of equations $T\tilde{G} = \mathbf{1}$, where $\mathbf{1}$ is the identity matrix, by "back substitution". To be specific, consider the i^{th} column vector $\tilde{G}_{\cdot,i}$ of $\tilde{G}$:

$$e_i = T\tilde{G}_{\cdot,i} = U^{+T}(D^+U^+\tilde{G}_{\cdot,i}) = U^{+T}g_i, \quad U^+\tilde{G}_{\cdot,i} = (D^+)^{-1}g_i \quad \text{(B.4)}$$

where e_i is the i^{th} unit vector. The first step is to solve the linear system $U^{+T}g_i = e_i$ for g_i, and the second step to solve $U^+\tilde{G}_{\cdot,i} = (D^+)^{-1}g_i$ for $\tilde{G}_{\cdot,i}$. To solve a tridiagonal linear system for one vector takes $\mathcal{O}(N)$ time, so solving for the full inverse matrix $\tilde{G}$ takes $\mathcal{O}(N^2)$ time.

Now we shall derive an algorithm to compute the elements of g_i and $\tilde{G}_{\cdot,i}$. Begin with the last column $i = N$: $U^{+T}g_N = e_N$ can be solved from the first to the last row and gives $g_N = e_N$. Next $U^+\tilde{G}_{\cdot,N} = (D^+)^{-1}e_N$ can be solved starting from the last row, $\tilde{G}_{N,N} = 1/D_N^+$. From there one can work upwards by back substitution, $\tilde{G}_{j,N} = -U_j^+\tilde{G}_{j+1,N}$ $(j = 1, \ldots, N-1)$. For the other columns $i < N$, one cannot take the shortcut and has to solve both linear systems for g_i and $\tilde{G}_{\cdot,i}$. But it is now important to realize that for any column vector $\tilde{G}_{\cdot,i+1}$, if we somehow know the diagonal element $\tilde{G}_{i+1,i+1}$, the next element above the diagonal is

$$\tilde{G}_{i,i+1} = -U_i^+\tilde{G}_{i+1,i+1} \quad (i = 1, \ldots, N-1) \; . \quad \text{(B.5)}$$

Thus, we have a prescription how to go up one row in $\tilde{G}$. Together with the symmetry of $\tilde{G}$, i.e., $\tilde{G}_{i,i+1} = \tilde{G}_{i+1,i}$, which follows from the symmetry of T, we get the first off-diagonal element one column to the left *without* solving the two linear systems in (B.4). Hence, it is possible to compute directly the tridiagonal part of the inverse. However, there is another algorithm which is much more accurate for near-singular matrices at the end of the RG flow: the double factorization [Meurant 1992]. It does not rely on the symmetry of $\tilde{G}$ but uses the complementary "UDL" factorization

$$T = U^-D^-L^- = U^-D^-U^{-T} \; , \quad \text{(B.6)}$$

where the matrix elements are obtained as

$$D_N^- := a_N, \quad U_i^- := b_i/D_{i+1}^-, \quad D_i^- := a_i - b_i U_i^- \quad (i = N-1, \ldots, 1) \; . \quad \text{(B.7)}$$

We proceed as for the LDU factorization above and get

$$\tilde{G}_{1,1} = 1/D_1^- \tag{B.8}$$
$$\tilde{G}_{i,i+1} = -U_i^- \, \tilde{G}_{i,i} \; . \tag{B.9}$$

We can combine equations (B.5) and (B.9) to relate consecutive diagonal elements:

$$\tilde{G}_{i+1,i+1} = -\tilde{G}_{i,i+1}/U_i^+ = \tilde{G}_{i,i} \, U_i^-/U_i^+ = \tilde{G}_{i,i} \, D_i^+/D_{i+1}^- \; . \tag{B.10}$$

Thus, we start with (B.8) and use the $U^-D^-L^-$ decomposition to go one matrix element to the right in the inverse matrix, from the diagonal to the first off-diagonal (B.9), while the $L^+D^+U^+$ decomposition allows to go down by one, back to the next diagonal element (B.5). There is no need to compute the full inverse matrix.

One can implement the algorithm without knowing the derivation by using equations (B.3) and (B.7)–(B.10). One can further eliminate the U's using equations (B.3) and (B.7) and implement the algorithm such that only the input vectors a_i, b_i and the output vectors $\tilde{G}_{i,i}$, $\tilde{G}_{i,i+1}$ enter the temporary storage. This double factorization is numerically accurate to more than 10 significant digits (using double precision) even for large lattices (10^6 sites) and almost singular matrices with $|a_i| \sim 10^{-15}$ which appear at the end of the flow for half filling.

B.2 Bubble

Even the RHS of the flow equations (4.35) for the density-response vertex R^Λ and the flow of the self energy for $T > 0$ in equation (4.30) can be computed in $\mathcal{O}(N)$ time [Enss 2005]. In both cases the RHS of the flow has the form of a trace of a bubble with two vertices and two propagators,

$$\mathrm{tr}(UG_1TG_2) = \mathrm{tr}(UM) \tag{B.11}$$

where we have defined the product

$$M = G_1TG_2 \tag{B.12}$$

with U, T tridiagonal matrices ("vertices") and G_1, G_2 inverse tridiagonal matrices ("propagators"). In order to compute the trace in the end and also as a useful intermediate result in the flow equation, we need the tridiagonal part of M, i.e., M_{ii}, $M_{i,i+1}$ and $M_{i+1,i}$.

According to [Meurant 1992] the inverse of a tridiagonal matrix generally has the following structure: the upper triangle is spanned by two vectors x_i, y_i, while the

lower triangle is spanned by two vectors u_i, v_i:

$$G_{1;ik} = \begin{cases} u_{1i}v_{1k} & i \geq k \\ x_{1k}y_{1i} & i \leq k \\ \Delta_{1i} & i = k \end{cases} \qquad G_{2;kj} = \begin{cases} u_{2k}v_{2j} & k \geq j \quad \text{(lower triangle)} \\ x_{2j}y_{2k} & k \leq j \quad \text{(upper triangle)} \\ \Delta_{2k} & k = j \quad \text{(diagonal)} \end{cases} \tag{B.13}$$

On the diagonal, the upper and lower triangles agree, and we define an abbreviation $\Delta_i := x_i y_i = u_i v_i$ for it. The four vectors have the following interpretation: u_i (multiplied by v_1) is the first column, v_i (multiplied by u_N) the last row; x_i (multiplied by y_1) the first row, and y_i (multiplied by x_N) the last column. Each of these vectors can be computed via the $L^+D^+U^+$ and $U^-D^-L^-$ decompositions which relate one row or column to the next or previous:

$$\frac{u_{i+1}}{u_i} = -L_i^- \qquad \frac{v_i}{v_{i+1}} = -L_i^+ \tag{B.14}$$

$$\frac{x_{i+1}}{x_i} = -U_i^- \qquad \frac{y_i}{y_{i+1}} = -U_i^+ \tag{B.15}$$

Consider first the diagonal elements M_{ii}, then the off-diagonal elements $M_{i,i+1}$ and $M_{i+1,i}$ will be slight variations of it. The tridiagonal matrix $T = (a, b, c)$ has diagonal elements a_i, above the diagonal b_i and below the diagonal c_i:

$$\begin{aligned} M_{ii} &= \sum_k \left[G_{1;ik}a_k G_{2;ki} + G_{1;ik}b_k G_{2;k+1,i} + G_{1;i,k+1}c_k G_{2;ki}\right] \\ &= \Big\{\sum_{k\leq i} u_{1i}v_{1k}a_k y_{2k}x_{2i} - \Delta_{1i}a_i\Delta_{2i} + \sum_{k\geq i} y_{1i}x_{1k}a_k u_{2k}v_{2i}\Big\} \\ &+ \Big\{\sum_{k<i} u_{1i}v_{1k}b_k y_{2,k+1}x_{2i} \qquad\qquad + \sum_{k\geq i} y_{1i}x_{1k}b_k u_{2,k+1}v_{2i}\Big\} \\ &+ \Big\{\sum_{k<i} u_{1i}v_{1,k+1}c_k y_{2k}x_{2i} \qquad\qquad + \sum_{k\geq i} y_{1i}x_{1,k+1}c_k u_{2k}v_{2i}\Big\} \\ &= Q_i^+ - \Delta_{1i}a_i\Delta_{2i} + Q_i^- \end{aligned}$$

where Q_i^+ are the terms on the left side inside each curly bracket (lower k indices) and Q_i^- those on the right side (higher k indices), so up to now we have just split the terms in the k sum into two groups. The point of defining the Q's like this is the following: Q_{i+1}^+ can be computed from Q_i^+ in $\mathcal{O}(1)$ time and likewise Q_i^- from Q_{i+1}^-, so going from M_{ii} to $M_{i+1,i+1}$ is an $\mathcal{O}(1)$ operation. Thus we can compute the whole diagonal of M in $\mathcal{O}(N)$ time!

The recursion relation for Q_i^+ is read off from the above partition:

$$Q_i^+ = u_{1i}x_{2i}\sum_{k<i}\left(v_{1k}a_k y_{2k} + v_{1k}b_k y_{2,k+1} + v_{1,k+1}c_k y_{2k}\right) + \Delta_{1i}a_i\Delta_{2i}$$

$$
\begin{aligned}
Q^+_{i+1} &= u_{1,i+1}x_{2,i+1}\sum_{k<i+1}(v_{1k}a_k y_{2k} + v_{1k}b_k y_{2,k+1} + v_{1,k+1}c_k y_{2k}) + \Delta_{1,i+1}a_{i+1}\Delta_{2,i+1} \\
&= \frac{u_{1,i+1}}{u_{1i}}\frac{x_{2,i+1}}{x_{2i}}Q^+_i + u_{1,i+1}v_{1i}b_i y_{2,i+1}x_{2,i+1} + u_{1,i+1}v_{1,i+1}c_i y_{2i}x_{2,i+1} \\
&\quad + \Delta_{1,i+1}a_{i+1}\Delta_{2,i+1} \\
&= L^-_{1i}Q^+_i U^-_{2i} - L^-_{1i}\Delta_{1i}b_i\Delta_{2,i+1} - \Delta_{1,i+1}c_i\Delta_{2i}U^-_{2i} + \Delta_{1,i+1}a_{i+1}\Delta_{2,i+1}
\end{aligned}
$$

and likewise for Q^-_i:

$$
\begin{aligned}
Q^-_i &= y_{1i}v_{2i}\sum_{k\geq i}(x_{1k}a_k u_{2k} + x_{1k}b_k u_{2,k+1} + x_{1,k+1}c_k u_{2k}) \\
Q^-_i &= U^+_{1i}Q^-_{i+1}L^+_{2i} - \Delta_{1i}b_i\Delta_{2,i+1}L^+_{2i} - U^+_{1i}\Delta_{1,i+1}c_i\Delta_{2i} + \Delta_{1i}a_i\Delta_{2i}.
\end{aligned}
$$

In the same way the off-diagonal elements $M_{i,i+1}$ and $M_{i+1,i}$ are determined:

$$
\begin{aligned}
M_{i,i+1} &= \sum_k [G_{1;ik}a_k G_{2;k,i+1} + G_{1;ik}b_k G_{2;k+1,i+1} + G_{1;i,k+1}c_k G_{2;k,i+1}] \\
&= \Big\{\sum_{k\leq i} u_{1i}v_{1k}a_k y_{2k}x_{2,i+1} + \sum_{k>i} y_{1i}x_{1k}a_k u_{2k}v_{2,i+1}\Big\} \\
&+ \Big\{\sum_{k<i} u_{1i}v_{1k}b_k y_{2,k+1}x_{2,i+1} + u_{1i}v_{1i}b_i y_{2,i+1}x_{2,i+1} + \sum_{k>i} y_{1i}x_{1k}b_k u_{2,k+1}v_{2,i+1}\Big\} \\
&+ \Big\{\sum_{k<i} u_{1i}v_{1,k+1}c_k y_{2k}x_{2,i+1} + u_{1i}v_{1,i+1}c_i y_{2i}x_{2,i+1} + \sum_{k>i} y_{1i}x_{1,k+1}c_k u_{2k}v_{2,i+1}\Big\} \\
&= -Q^+_i U^-_{2i} + (\Delta_{1i}b_i\Delta_{2,i+1}) + (U^+_{1i}\Delta_{1,i+1}c_i\Delta_{2i}U^-_{2i}) - U^+_{1i}Q^-_{i+1}
\end{aligned}
$$

and

$$
\begin{aligned}
M_{i+1,i} &= \sum_k [G_{1;i+1,k}a_k G_{2;ki} + G_{1;i+1,k}b_k G_{2;k+1,i} + G_{1;i+1,k+1}c_k G_{2;ki}] \\
&= \Big\{\sum_{k\leq i} u_{1,i+1}v_{1k}a_k y_{2k}x_{2i} + \sum_{k>i} y_{1,i+1}x_{1k}a_k u_{2k}v_{2i}\Big\} \\
&+ \Big\{\sum_{k<i} u_{1,i+1}v_{1k}b_k y_{2,k+1}x_{2i} + u_{1,i+1}v_{1i}b_i y_{2,i+1}x_{2i} + \sum_{k>i} y_{1,i+1}x_{1k}b_k u_{2,k+1}v_{2i}\Big\} \\
&+ \Big\{\sum_{k<i} u_{1,i+1}v_{1,k+1}c_k y_{2k}x_{2i} + u_{1,i+1}v_{1,i+1}c_i y_{2i}x_{2i} + \sum_{k>i} y_{1,i+1}x_{1,k+1}c_k u_{2k}v_{2i}\Big\} \\
&= -L^-_{1i}Q^+_i + (L^-_{1i}\Delta_{1i}b_i\Delta_{2,i+1}L^+_{2i}) + (\Delta_{1,i+1}c_i\Delta_{2i}) - Q^-_{i+1}L^+_{2i}.
\end{aligned}
$$

After the full derivation, let us summarize the algorithm. We observe that certain combinations of terms appear frequently so we define the following abbreviations:

$$
A_i := \Delta_{1i}a_i\Delta_{2i} \tag{B.16}
$$

$$B_i := \Delta_{1i} b_i \Delta_{2,i+1} \tag{B.17}$$
$$C_i := \Delta_{1,i+1} c_i \Delta_{2i}. \tag{B.18}$$

At the beginning of the algorithm, Q_i^+ and Q_i^- need to be computed via the recursion formulas

$$Q_{i+1}^+ := L_{1i}^- Q_i^+ U_{2i}^- - L_{1i}^- B_i - C_i U_{2i}^- + A_{i+1} \tag{B.19}$$
$$Q_i^- := U_{1i}^+ Q_{i+1}^- L_{2i}^+ - B_i L_{2i}^+ - U_{1i}^+ C_i + A_i \tag{B.20}$$

with initial conditions

$$Q_1^+ = A_1 \tag{B.21}$$
$$Q_N^- = A_N. \tag{B.22}$$

Then the tridiagonal components of M can be computed in any order:

$$M_{i,i} := Q_i^+ - A_i + Q_i^- = Q_i^+ - B_i L_{2i}^+ - U_{1i}^+ C_i + U_{1i}^+ Q_{i+1}^- L_{2i}^+ \tag{B.23}$$
$$M_{i,i+1} := B_i - Q_i^+ U_{2i}^- - U_{1i}^+ Q_{i+1}^- + U_{1i}^+ C_i U_{2i}^- \tag{B.24}$$
$$M_{i+1,i} := C_i - L_{1i}^- Q_i^+ - Q_{i+1}^- L_{2i}^+ + L_{1i}^- B_i L_{2i}^+. \tag{B.25}$$

Finally, the trace (B.11) is

$$\mathrm{tr}(UM) := \sum_i (U_{ii} M_{ii} + U_{i+1,i} M_{i,i+1} + U_{i,i+1} M_{i+1,i}). \tag{B.26}$$

Bibliography

In the online PDF file, simply click on the journal references and `arXiv` numbers! After each citation appear the page numbers where it is referenced.

[AEMMSS 2004] Andergassen S, Enss T, Meden V, Metzner W, Schollwöck U, and Schönhammer K, *Functional renormalization group for Luttinger liquids with impurities*, Phys. Rev. B **70**, 075102 (2004), `cond-mat/0403517`. 10, 53, 57, 58, 59, 61, 68, 95, 98

[Andergassen 2005] Andergassen S, Ph.D. thesis, University of Stuttgart, Germany, 2005, in preparation. 58, 61, 80, 98

[Apel&Rice 1982] Apel W and Rice TM, *Combined effect of disorder and interaction on the conductance of a one-dimensional fermion system*, Phys. Rev. B **26**, 7063 (1982). 85

[BSMS 2005a] Barnabé-Thériault X, Sedeki A, Meden V, and Schönhammer K, *A junction of three quantum wires: restoring time-reversal symmetry by interaction*, Phys. Rev. Lett. (in press), 2005, `cond-mat/0411612`. 99

[BSMS 2005b] Barnabé-Thériault X, Sedeki A, Meden V, and Schönhammer K, *Junctions of one-dimensional quantum wires—correlation effects in transport*, 2005, `cond-mat/0501742`. 99

[Baym&Kadanoff 1961] Baym G and Kadanoff LP, *Conservation Laws and Correlation Functions*, Phys. Rev. **124**, 287 (1961). 45, 77, 97

[Baym 1962] Baym G, *Self-Consistent Approximations in Many-Body Sytems*, Phys. Rev. **127**, 1391 (1962). 45

[BDM 1993] Bonini M, D'Attanasio M, and Marchesini G, *Perturbative renormalization and infrared finiteness in the Wilson renormalization group: the massless scalar case*, Nucl. Phys. B **409**, 441 (1993), `hep-th/9301114`. 9, 21

[BDM 1994] Bonini M, D'Attanasio M, and Marchesini G, *Ward identities and Wilson renormalization group for QED*, Nucl. Phys. B **418**, 81 (1994), `hep-th/9307174`. 34

[Chamon&Wen 1993] Chamon CdeC and Wen XG, *Resonant tunneling in the fractional quantum Hall regime*, Phys. Rev. Lett. **70**, 2605 (1993). 84

[D'Attanasio&Morris 1996] D'Attanasio M and Morris TR, *Gauge Invariance, the Quantum Action Principle, and the Renormalization Group*, Phys. Lett. B **378**, 213 (1996), `hep-th/9602156`. 34

[Egger&Grabert 1995] Egger R and Grabert H, *Friedel Oscillations for Interacting Fermions in One Dimension*, Phys. Rev. Lett. **75**, 3505 (1995), `cond-mat/9509100`. 80, 81

[Ellwanger 1994] Ellwanger U, *Flow Equations and* BRS *Invariance for Yang-Mills Theories*, Phys. Lett. B **335**, 364 (1994), `hep-th/9402077`. 34

[EHW 1996] Ellwanger U, Hirsch M, and Weber A, *Flow equations for the relevant part of the pure Yang-Mills action*, Z. Phys. C **69**, 687 (1996), `hep-th/9506019`. 34

[Enss 2005] Enss T, *Loops of tridiagonal and inverse tridiagonal matrices in O(N)*, in preparation, 2005. 69, 105

[EMABMS 2005] Enss T, Meden V, Andergassen S, Barnabé-Thériault X, Metzner W, and Schönhammer K, *Impurity and correlation effects on transport in one-dimensional quantum wires*, Phys. Rev. B **71**, 155401 (2005), `cond-mat/0411310`. 89, 93, 95, 98

[Freire&Wetterich 1996] Freire F and Wetterich C, *Abelian Ward identity from the background field dependence of the effective action*, Phys. Lett. B **380**, 337 (1996), `hep-th/9601081`. 37

[Friedel 1958] Friedel J, *Metallic alloys*, Nuovo Cimento Suppl. **7**, 287 (1958). 80

[Furusaki&Nagaosa 1993] Furusaki A and Nagaosa N, *Resonant tunneling in a Luttinger liquid*, Phys. Rev. B **47**, 3827 (1993). 88, 89, 94

[Furusaki 1998] Furusaki A, *Resonant tunneling through a quantum dot weakly coupled to quantum wires or quantum Hall edge states*, Phys. Rev. B **57**, 7141 (1998), `cond-mat/9712054`. 88

[Giamarchi 2003] Giamarchi T, *Quantum Physics in One Dimension*, Oxford University Press, New York, 2003. 79

[GYL 2004] Grishin A, Yurkevich IV, and Lerner IV, *Functional integral bosonization for an impurity in a Luttinger liquid*, Phys. Rev. B **69**, 165108 (2004), `cond-mat/0307438`. 81

[Halboth&Metzner 2000] Halboth CJ and Metzner W, *Renormalization group analysis of the* 2D *Hubbard model*, Phys. Rev. B **61**, 7364 (2000), `cond-mat/9908471`. 10, 25

[Haldane 1980] Haldane FDM, *General Relation of Correlation Exponents and Spectral Properties of One-Dimensional Fermi Systems: Application to the Anisotropic $S = 1/2$ Heisenberg Chain*, Phys. Rev. Lett. **45**, 1358 (1980). 80

[Haldane 1981] Haldane FDM, *'Luttinger liquid theory' of one-dimensional quantum fluids. I. Properties of the Luttinger model and their extension to the general* 1D *interacting spinless Fermi gas*, J. Phys. C **14**, 2585 (1981). 79

[HMPS 2004] Hedden R, Meden V, Pruschke Th, and Schönhammer K, *Functional renormalization group approach to zero-dimensional interacting systems*, J. Phys.: Condens. Matter **16**, 5279 (2004), `cond-mat/0404711`. 50

[HSFR 2001] Honerkamp C, Salmhofer M, Furukawa N, and Rice TM, *Breakdown of the Landau-Fermi liquid in Two Dimensions due to Umklapp Scattering*, Phys. Rev. B **63**, 035109 (2001), `cond-mat/9912358`. 10

[Honerkamp&Salmhofer 2001] Honerkamp C and Salmhofer M, *The temperature-flow renormalization group and the competition between superconductivity and ferromagnetism*, Phys. Rev. B **64**, 184516 (2001), `cond-mat/0105218`. 16, 64, 65

[HRAE 2004] Honerkamp C, Rohe D, Andergassen S, and Enss T, *Interaction flow method for many-fermion systems*, Phys. Rev. B **70**, 235115 (2004), `cond-mat/0403633`. 16, 66

[Hügle&Egger 2004] Hügle S and Egger R, *Resonant tunneling in a Luttinger liquid for arbitrary barrier transmission*, Europhys. Lett. **66**, 565 (2004), `cond-mat/0304158`. 89, 93, 94, 98

[Itzykson&Zuber 1980] Itzykson C and Zuber J-B, *Quantum field theory*, McGraw-Hill, New York, 1980. 27

[Jakobs 2004] Jakobs S, *Nonlinear Transport through Quantum Wires: Functional Renormalization Group in Nonequilibrium*, talk at DPG-Tagung, Regensburg, 2004. 99

[Kane&Fisher 1992a] Kane CL and Fisher MPA, *Transport in a one-channel Luttinger liquid*, Phys. Rev. Lett. **68**, 1220 (1992). 79, 81, 83, 85

[Kane&Fisher 1992b] Kane CL and Fisher MPA, *Resonant tunneling in an interacting one-dimensional electron gas*, Phys. Rev. B **46**, 7268 (1992). 81, 94

[Kane&Fisher 1992c] Kane CL and Fisher MPA, *Transmission through barriers and resonant tunneling in an interacting one-dimensional electron gas*, Phys. Rev. B **46**, 15233 (1992). 79, 86

[Katanin 2004] Katanin AA, *Fulfillment of Ward identities in the functional renormalization group approach*, Phys. Rev. B **70**, 115109 (2004), `cond-mat/0402602`. 50, 97

[Keller&Kopper 1991] Keller G and Kopper C, *Perturbative renormalization of* QED *via flow equations*, Phys. Lett. B **273**, 323 (1991). 34

[KKS 1992] Keller G, Kopper C, and Salmhofer M, *Perturbative renormalization and effective Lagrangians in φ^4 in four dimensions*, Helv. Phys. Acta **65**, 32 (1992). 9

[Keller&Kopper 1996] Keller G and Kopper C, *Renormalizability proof for* QED *based on flow equations*, Commun. Math. Phys. **176**, 193 (1996). 34

[Komnik&Gogolin 2003] Komnik A and Gogolin AO, *Resonant Tunneling between Luttinger Liquids: A Solvable Case*, Phys. Rev. Lett. **90**, 246403 (2003), `cond-mat/0211474`. 89

[Kopietz&Busche 2001] Kopietz P and Busche T, *Exact renormalization group flow equations for nonrelativistic fermions: Scaling toward the Fermi surface*, Phys. Rev. B **64**, 155101 (2001), `cond-mat/0103633`. 9

[LLS 1996] Leclair A, Lesage F, and Saleur H, *Exact Friedel oscillations in the $g = 1/2$ Luttinger liquid*, Phys. Rev. B **54**, 13597 (1996), `cond-mat/9606124`. 81

[Luther&Peschel 1974a] Luther A and Peschel I, *Single-particle states, Kohn anomaly, and pairing fluctuations in one dimension*, Phys. Rev. B **9**, 2911 (1974). 79

[Luther&Peschel 1974b] Luther A and Peschel I, *Fluctuation Conductivity and Lattice Stability in One Dimension*, Phys. Rev. Lett. **32**, 992 (1974). 85

[Luttinger 1963] Luttinger JM, *An exactly soluble model of a many-fermion system*, J. Math. Phys. **4**, 1154 (1963). 79

[Luttinger 1964] Luttinger JM, *Theory of Thermal Transport Coefficients*, Phys. Rev. **135**, A1505 (1964). 72

[Mahan 2000] Mahan GD, *Many-particle physics*, 3. ed., Kluwer Academic, Plenum Publisher, New York, 2000. 71, 74

[Mattis&Lieb 1965] Mattis DC and Lieb EH, *Exact solution of a many-fermion system and its associated boson field*, J. Math. Phys. **6**, 304 (1965). 79

[Mattis 1974] Mattis DC, *New wave-operator identity applied to the study of persistent currents in* 1D, J. Math. Phys. **15**, 609 (1974). 79

[MYG 1993] Matveev KA, Yue D, and Glazman LI, *Tunneling in one-dimensional non-Luttinger electron liquid*, Phys. Rev. Lett. **71**, 3351 (1993), `cond-mat/9306041`. 81, 89

[MMSS 2002a] Meden V, Metzner W, Schollwöck U, and Schönhammer K, *Scaling behavior of impurities in mesoscopic Luttinger liquids*, Phys. Rev. B **65**, 045318 (2002), `cond-mat/0104336`. 10, 83

[MMSS 2002b] Meden V, Metzner W, Schollwöck U, and Schönhammer K, *A single impurity in a Luttinger liquid: How it "cuts" the chain*, J. Low Temp. Phys. **126**, 1147 (2002), `cond-mat/0109013`. 10, 83

[MAMSS 2003] Meden V, Andergassen S, Metzner W, Schollwöck U, and Schönhammer K, *Scaling of the conductance in a quantum wire*, Europhys. Lett. **64**, 769 (2003), `cond-mat/0303460`. 86, 89

[Meden&Schollwöck 2003a] Meden V and Schollwöck U, *Persistent currents in mesoscopic rings: A numerical and renormalization group study*, Phys. Rev. B **67**, 035106 (2003), `cond-mat/0209588`. 72, 89

[Meden&Schollwöck 2003b] Meden V and Schollwöck U, *The conductance of interacting nano-wires*, Phys. Rev. B **67**, 193303 (2003), `cond-mat/0210515`. 72, 89

[MEAMS 2005] Meden V, Enss T, Andergassen S, Metzner W, and Schönhammer K, *Correlation effects on resonant tunneling in one-dimensional quantum wires*, Phys. Rev. B **71**, 041302(R) (2005), `cond-mat/0403655`. 89, 95, 98

[Meurant 1992] Meurant G, *A review on the inverse of tridiagonal and block tridiagonal symmetric matrices*, SIAM J. Matrix Anal. Appl. **13**, 707 (1992). 104, 105

[Morris 1994] Morris TR, *The Exact Renormalisation Group and Approximate Solutions*, Int. J. Mod. Phys. A **9**, 2411 (1994), `hep-ph/9308265`. 9, 21

[Nazarov&Glazman 2003] Nazarov YV and Glazman LI, *Resonant Tunneling of Interacting Electrons in a One-Dimensional Wire*, Phys. Rev. Lett. **91**, 126804 (2003), `cond-mat/0209090`. 89

[Nicoll&Chang 1977] Nicoll JF and Chang TS, *An exact one-particle-irreducible renormalization-group generator for critical phenomena*, Phys. Lett. A **62**, 287 (1977). 9, 21

[Oguri 2001] Oguri A, *Transmission Probability for Interacting Electrons Connected to Reservoirs*, J. Phys. Soc. Japan **70**, 2666 (2001), `cond-mat/0106033`. 76

[Polchinski 1984] Polchinski J, *Renormalization and effective lagrangians*, Nucl. Phys. B **231**, 269 (1984). 9, 22

[Polyakov&Gornyi 2003] Polyakov DG and Gornyi IV, *Transport of interacting electrons through a double barrier in quantum wires*, Phys. Rev. B **68**, 035421 (2003), `cond-mat/0212355`. 89

[PTYGD 2001] Postma HWC, Teepen T, Yao Z, Grifoni M, and Dekker C, *Carbon Nanotube Single-Electron Transistors at Room Temperature*, Science **293**, 76 (2001). 71, 84, 88

[PTVF 1986] Press WH, Teukolsky SA, Vetterling WT, and Flannery BP, *Numerical Recipes in Fortran 77*, Cambridge Univ. Press, 1986. 54, 103, 104

[Reuter&Wetterich 1994] Reuter M and Wetterich C, *Exact evolution equation for scalar electrodynamics*, Nucl. Phys. B **427**, 291 (1994). 37, 38

[Rohe&Metzner 2005] Rohe D and Metzner W, *Pseudogap at hot spots in the two-dimensional Hubbard model at weak coupling*, Phys. Rev. B **71**, 115116 (2005), `cond-mat/0406164`. 25

[Salmhofer 1998] Salmhofer M, *Continuous Renormalization for Fermions and Fermi Liquid Theory*, Commun. Math. Phys. **194**, 249 (1998), `cond-mat/9706188`. 9, 24

[Salmhofer 1999] Salmhofer M, *Renormalization. An Introduction*, Springer, Berlin, 1999. 9, 24

[Salmhofer&Honerkamp 2001] Salmhofer M and Honerkamp C, *Fermionic renormalization group flows: Technique and theory*, Prog. Theor. Phys. **105**, 1 (2001). 9, 21, 24

[SHML 2004] Salmhofer M, Honerkamp C, Metzner W, and Lauscher O, *Renormalization group flows into phases with broken symmetry*, Prog. Theor. Phys. **112**, 943 (2004), `cond-mat/0409725`. 50, 97

[SBK 2004] Schütz F, Bartosch L, and Kopietz P, *Collective fields in the functional renormalization group for fermions, Ward identities, and the exact solution of the Tomonaga-Luttinger model*, 2004, `cond-mat/0409404`. 50, 97

[TGCPD 2002] Thorwart M, Grifoni M, Cuniberti G, Postma HWC, and Dekker C, *Correlated Tunneling in Intramolecular Carbon Nanotube Quantum Dots*, Phys. Rev. Lett. **89**, 196402 (2002), `cond-mat/0210511`. 88, 93

[TEG 2004] Thorwart M, Egger R, and Grifoni M, *Correlated sequential tunneling through a double barrier for interacting one-dimensional electrons*, 2004, `cond-mat/0407751`. 88, 93

[Tomonaga 1950] Tomonaga S, *Remarks on Blochs method of sound waves applied to many-fermion problems*, Prog. Theor. Phys. **5**, 544 (1950). 79

[Tüttő&Zawadowski 1985] Tüttő I and Zawadowski A, *Quantum theory of local perturbation of the charge-density wave by an impurity: Friedel oscillations*, Phys. Rev. B **32**, 2449 (1985). 80

[Voit 1995] Voit J, *One-Dimensional Fermi liquids*, Rep. Prog. Phys. **58**, 977 (1995), `cond-mat/9510014`. 79, 81

[Ward 1950] Ward JC, *An Identity in Quantum Electrodynamics*, Phys. Rev. **78**, 182 (1950). 27

[Wegner&Houghton 1973] Wegner FJ and Houghton A, *Renormalization Group Equation for Critical Phenomena*, Phys. Rev. A **8**, 401 (1973). 9

[Weinberg 1976] Weinberg S, *Critical phenomena for field theorists*, Erice Subnucl. Phys. 1 (1976). 9, 21

[Wetterich 1993] Wetterich C, *Exact evolution equation for the effective potential*, Phys. Lett. B **301**, 90 (1993). 9, 21

[Wetterich 2002] Wetterich C, *Bosonic effective action for interacting fermions*, 2002, `cond-mat/0208361`. 50

[Wieczerkowski 1988] Wieczerkowski C, *Symanzik improved actions from the viewpoint of the renormalization-group*, Commun. Math. Phys. **120**, 149 (1988). 9, 24

[Wilson 1971] Wilson KG, *Renormalization Group and Critical Phenomena. II. Phase-Space Cell Analysis of Critical Behavior*, Phys. Rev. B **4**, 3184 (1971). 9

[Wilson&Kogut 1974] Wilson KG and Kogut J, *The renormalization group and the ϵ expansion*, Phys. Rep. **12**, 75 (1974). 9

[Yang&Yang 1966] Yang CN and Yang CP, *One-Dimensional Chain of Anisotropic Spin-Spin Interactions. I.+II.*, Phys. Rev. **150**, 321 (1966). 80

[YGM 1994] Yue D, Glazman LI, and Matveev KA, *Conduction of a weakly interacting one-dimensional electron gas through a single barrier*, Phys. Rev. B **49**, 1966 (1994). 89

[Zanchi&Schulz 1998] Zanchi D and Schulz HJ, *Weakly correlated electrons on a square lattice: A renormalization group theory*, Europhys. Lett. **44**, 235 (1998), `cond-mat/9703189`. 10

[Zanchi&Schulz 2000] Zanchi D and Schulz HJ, *Weakly correlated electrons on a square lattice: Renormalization group theory*, Phys. Rev. B **61**, 13609 (2000), `cond-mat/9812303`. 10

[Zinn-Justin 2002] Zinn-Justin J, *Quantum Field Theory and Critical Phenomena*, 4. ed., Clarendon Press, Oxford, 2002. 12, 14, 28, 29, 72

Publications

Parts of this thesis are contained in the following publications:

- Enss T, Meden V, Andergassen S, Barnabé-Thériault X, Metzner W, and Schönhammer K, *Impurity and correlation effects on transport in one-dimensional quantum wires*, Phys. Rev. B **71**, 155401 (2005), `cond-mat/0411310`.

- Meden V, Enss T, Andergassen S, Metzner W, and Schönhammer K, *Correlation effects on resonant tunneling in one-dimensional quantum wires*, Phys. Rev. B **71**, 041302(R) (2005), `cond-mat/0403655`.

- Honerkamp C, Rohe D, Andergassen S, and Enss T, *Interaction flow method for many-fermion systems*, Phys. Rev. B **70**, 235115 (2004), `cond-mat/0403633`.

- Andergassen S, Enss T, Meden V, Metzner W, Schollwöck U, and Schönhammer K, *Functional renormalization group for Luttinger liquids with impurities*, Phys. Rev. B **70**, 075102 (2004), `cond-mat/0403517`.

- Enss T, *Loops of tridiagonal and inverse tridiagonal matrices in O(N)*, in preparation, 2005.

Acknowledgments

First of all I am indebted to Walter Metzner for giving me the opportunity to write my Ph. D. thesis at the Max-Planck-Institut in Stuttgart. It has been a great pleasure to work in his theory group. I wish to thank Walter Metzner for proposing this intriguing and challenging subject, always having time for discussions, reading my notes quickly and very carefully, and for giving me the opportunity to travel to such interesting and far-away places as Brasília. I am grateful to Manfred Salmhofer for many discussions and suggestions on the more formal and mathematical aspects of the fRG. I wish to thank Siegfried Dietrich for co-examining the thesis.

The close work with Sabine Andergassen on the 1D systems has been a great pleasure indeed, with discussions on virtually every detail of the calculations. I am thankful for a quick proofreading of the manuscript.

I wish to thank Kurt Schönhammer and Volker Meden in Göttingen for encouragement and for being an inexhaustible fountain of interesting physical questions and parameter regions to investigate.

Xavier Barnabé-Thériault was a great source of motivation, fun and programming tricks, and had an admirable desire to understand the physics and not to get caught up in technical details. He met a sudden and untimely death by a tragic traffic accident on August 15, 2004.

Daniel Rohe always has new ideas for variations on the scheme and deserves my thanks for many discussions and quickly proofreading the whole manuscript.

I wish to thank Julius Reiß for insightful discussions on the foundations of different RG schemes, and for organizing the fine cineastic evenings in the institute.

Carsten Honerkamp proposed several worthwhile applications of our machinery and always conveys the fun of doing physics.

I am indebted to the computer service group under Armin Burkhardt, and Daniel Rohe for providing a very fine IT infrastructure and responding very quickly and flexibly to my individual wishes.

I extend my thanks to all the wonderful people in the theory group, Dmitry Aristov, Heinz Barentzen, Sergej Brener, Luca Dell'Anna, Martin Feldbacher, Roland Gersch,

Karsten Held, Peter Horsch, Andrej Katanin, Dirk Manske, Matthias Mayr, Hiroyuki Yamase, Yi-Feng Yang, and Roland Zeyher for support and stimulating discussions about physics and everything else, and to Mrs Knapp for help in all organizational matters.

I thank the ICCMP in Brasília and the Erwin-Schrödinger-Institut in Vienna for the hospitable environment where many discussions on this thesis took place.

Last but not least I am indebted to my wife Carmen for never-ending encouragement, motivation and typographical expertise.

Curriculum Vitae

Name	Tilman Enss
Nationality	German
Date of birth	8 October 1975
Place of birth	Bielefeld, Germany
Marital status	Married

Studies

02/2002 – 02/2005	Ph.D. — with distinction — Max-Planck-Institut für Festkörperforschung, Stuttgart *Renormalization, conservation laws and transport in correlated electron systems*, with Prof. Walter Metzner
10/2000 – 01/2002	Diploma — with distinction — Ludwig-Maximilians-Universität, Munich *Transfer-matrix renormalization group far from the statistical equilibrium*, with Dr. Ulrich Schollwöck
10/1999 – 07/2000	studies of physics, Hebrew University Jerusalem, Israel Conformal field theory, with Prof. Eliezer Rabinovici
10/1998 – 07/1999	studies of physics, Ludwig-Maximilians-Universität, Munich
02/1997 – 08/1998	three one-month research visits, Princeton University Magnetic resonance imaging, with Prof. Warren S. Warren
05/1998	"Vordiplom" degree in physics, grade 1.0
10/1996 – 07/1998	studies of physics, Friedrich-Schiller-Universität, Jena
07/1995 – 07/1996	civilian service, Diakoniepflegestation Aachen
06/1995	Abitur, Kaiser-Karls-Gymnasium Aachen

Scholarships

11/1999 – 01/2002	Studienstiftung des deutschen Volkes
10/1999 – 06/2000	DAAD scholarship for Israel